

Radiative corrections to decay branching ratios of the CP-odd Higgs boson in two Higgs doublet models

Masashi Aiko,^{1,*} Shinya Kanemura,^{2,†} and Kodai Sakurai^{3,‡}

¹*KEK Theory Center, High Energy Accelerator Research*

Organization (KEK), Tsukuba, Ibaraki, 305-0801, Japan

²*Department of Physics, Osaka University, Toyonaka, Osaka 560-0043, Japan*

³*Department of Physics, Tohoku University, Sendai, Miyagi 980-8578, Japan*

We calculate radiative corrections to decay rates of CP-odd Higgs boson A for various decay modes in the four types of two Higgs doublet models with the softly broken discrete Z_2 symmetry. The decay branching ratios are evaluated at the next-to-leading order for electroweak corrections and the next-to-next-to-leading order for QCD corrections. We comprehensively study the impact of the electroweak corrections on the decay rates and the branching ratios. We find that the radiative corrections can sizably modify the branching ratios, especially for the $A \rightarrow Zh$ decay mode in the nearly alignment scenario, where coupling constants of the SM-like Higgs boson h are close to those in the standard model. We also show correlations between the branching ratios of A and the scaling factor of the SM-like Higgs boson coupling including higher-order corrections. In addition, we show characteristic predictions on the decay pattern depending on the types of Yukawa interaction, by which we can discriminate the types of Yukawa interaction in future collider experiments.

*Electronic address: maiko@post.kek.jp

†Electronic address: kanemu@het.phys.sci.osaka-u.ac.jp

‡Electronic address: kodai.sakurai.e3@tohoku.ac.jp

Contents

I. Introduction	4
II. Two Higgs doublet model	6
A. Lagrangian	7
B. Constraints from experimental data	10
III. Decay rates with higher-order corrections	11
A. Form factors for vertex functions of the CP-odd Higgs boson	12
1. $A f \bar{f}$ vertex	12
2. $AV\phi$ vertex	13
3. AV_1V_2 vertex	15
B. Decay rates of $A \rightarrow f \bar{f}$	15
C. Decay rates of $A \rightarrow V\phi$	17
D. Decay rates of loop-induced processes	19
IV. Next-to-leading-order electroweak corrections	20
A. Branching ratios	20
B. Total decay width	24
C. Impact of NLO EW corrections to the decay rates	25
V. Decay pattern of the CP-odd Higgs boson in the nearly alignment scenario	29
A. Scenario A	32
B. Scenario B	35
C. Discrimination of Types of the Yukawa interaction in the 2HDMs	38
VI. Discussions and conclusions	39
Acknowledgments	40
A. Input parameters	41
B. Scalar couplings	41
C. Three-body decays of the CP-odd Higgs boson	43
1. $A \rightarrow t\bar{t}^* \rightarrow tbW$	43

2. $A \rightarrow \phi Z^* \rightarrow \phi f \bar{f}$	43
3. $A \rightarrow H^\pm W^{\mp*} \rightarrow H^\pm f \bar{f}'$	44
D. QCD corrections for $A \rightarrow \gamma\gamma$ and $A \rightarrow gg$	45
1. $A \rightarrow \gamma\gamma$	45
2. $A \rightarrow gg$	45
E. 1PI diagram contributions for $A f \bar{f}$ and $AV\phi$ vertices	46
1. $A f \bar{f}$ vertex	47
2. $AV\phi$ vertex	51
3. $AV_1 V_2$ vertex	53
F. Formulae for the real photon emissions	54
1. Decay rates of $A \rightarrow f \bar{f} \gamma$	54
2. Decay rate of $A \rightarrow H^\pm W^\mp \gamma$	55
G. Size of next-to-leading order electroweak corrections for fermionic decays	55
1. Scenario A	55
2. Scenario B	55
References	56

I. INTRODUCTION

After the discovery of the new particle with a mass of 125 GeV at the LHC in 2012 [1, 2], it has turned out that its properties are in agreement with those of the Higgs boson in the standard model (SM) under the current experimental and theoretical uncertainties. While no signal for new physics beyond the SM has been observed yet, there are phenomena that cannot be explained within the SM such as dark matter, baryon asymmetry of the universe and tiny neutrino masses. In addition to these phenomenological problems, there are theoretical problems in the SM such as the hierarchy problem, incomplete descriptions for the gauge coupling unification and the flavor structure, and so on. Therefore, the SM must be replaced by a more fundamental theory.

While the Higgs boson was found, the structure of the Higgs sector remains unknown. There is no theoretical principle to insist on the minimal structure of the Higgs sector as introduced in the SM. The possibility that the Higgs sector takes a non-minimal form is not excluded experimentally at all. Furthermore, such non-minimal Higgs sectors are often introduced in various new physics models, where the above-mentioned problems are tried to be solved. Therefore, unraveling the structure of the Higgs sector is one of the central interests of current and future high-energy physics. The direction of new physics can be determined by reconstructing the Higgs sector experimentally. Among various extended Higgs models, the two Higgs doublet model (2HDM) is a representative model that contains two CP-even Higgs bosons h/H , a CP-odd Higgs boson A and charged Higgs bosons H^\pm .

Current measurements of the discovered Higgs boson at the LHC show that its couplings with the SM particles are consistent with the SM [3, 4]. There are two distinctive scenarios to explain this observation in the 2HDM [5, 6]. The first one is the decoupling scenario, where masses of the additional Higgs bosons are sufficiently higher than the electroweak scale, and this leads to the SM-like Higgs boson couplings simultaneously. The second one is the alignment-without-decoupling scenario, where the couplings of the SM-like Higgs boson approximately take their SM values keeping masses of the additional Higgs bosons to be at the electroweak (EW) scale.

In Ref. [7], we have studied the testability of such SM-like scenarios at the HL-LHC and future lepton colliders. It was shown that the so-called Higgs-to-Higgs decays such as $A \rightarrow Zh$ and $H \rightarrow hh$ are quite important to investigate the 2HDM, especially in the nearly alignment scenario, where the SM-like Higgs boson couplings slightly deviate from those SM values. In the nearly alignment scenario, there is an upper bound for the typical mass scale of the additional Higgs bosons due to the theoretical constraints such as perturbative unitarity and vacuum stability. Thus,

measuring deviations in the SM-like Higgs boson couplings is also useful to investigate the 2HDM. Therefore, direct searches of the additional Higgs bosons and indirect studies of the property of the discovered Higgs boson are complementary, and the combined study is powerful to test the extended Higgs sector.

In the indirect study of extended Higgs sectors, the precision calculation for the decay branching ratios of the SM-like Higgs boson is important since the effect of higher-order corrections can be comparable with the precise measurements in the future collider experiments, such as the HL-LHC [8], the International Linear Collider (ILC) [9–12], the Future Circular Collider (FCC-ee) [13] and the Circular Electron Positron Collider (CEPC) [14]. In Refs. [15, 16], it has been pointed out that various extended Higgs models can be discriminated from the SM by comparing patterns of deviations in Higgs boson couplings at tree level analysis. This study then has been extended including one-loop corrections [17–24]. In the context of 2HDMs, many studies for EW corrections to the Higgs boson couplings and/or decays have been performed [17–19, 22, 23, 25–39]. Several numerical computation tools have been published, e.g., **H-COUP** [40, 41], **2HDECAY** [42] and **Prophecy4f** [43].

The study for direct searches of the additional Higgs bosons in Ref. [7] is performed at leading order (LO). This leads us to investigate the impact of higher-order corrections. This is because radiative corrections would change the size of partial decay widths significantly since the Higgs-to-Higgs decays are sensitive to the magnitude of deviations in the SM-like Higgs boson couplings. We have studied the radiative corrections for decays of the charged Higgs bosons in Ref. [44]. The authors in Ref. [45] have studied those for decays of the additional CP-even Higgs boson. In this paper, we study decays of the CP-odd Higgs boson including the higher-order corrections. The analytical results of decay rates of all the additional Higgs bosons will be implemented in a new version of our developing program **H-COUP v3** [46]. There are also important previous works done by several other groups for the higher-order corrections to decays of the additional Higgs bosons [39, 47–52]. For decays of the CP-odd Higgs boson, the possible size of the next-to-leading order (NLO) EW corrections are discussed in various renormalization schemes in Ref. [39]. However, its dependence on the model parameters has not been exhibited.

In this paper, we calculate the full set of decay rates of the CP-odd Higgs boson including the higher-order corrections in the 2HDMs with the softly broken Z_2 symmetry. We calculate NLO EW corrections to the decay rates of the CP-odd Higgs boson into a pair of quarks and leptons, Z and the neutral Higgs bosons, and W^\pm and the charged Higgs bosons. The one-loop induced decays, $A \rightarrow W^\pm W^\mp$, ZZ , $\gamma\gamma$, $Z\gamma$ and gg , are calculated at LO for EW corrections. We present

the explicit formulae for the decay rates with NLO EW corrections as well as QCD corrections. The former is written by the renormalized vertex functions for the CP-odd Higgs boson, and the analytical formulae are given in Appendix E. We comprehensively study the impact of the electroweak corrections on the partial decay widths and decay branching ratios. We find that the radiative corrections can sizably modify the branching ratios, especially for the $A \rightarrow Zh$ decay mode in the nearly alignment scenario. In addition, we have characteristic predictions on the decay pattern depending on the types of Yukawa interaction, by which we can discriminate the types of Yukawa interaction in future collider experiments.

What is new in this paper is the following. First, we provide analytic formulae for the NLO EW corrections to the various decay modes of the CP-odd Higgs boson based on the improved on-shell renormalization scheme [23]. Second, we have newly implemented these results in the H-COUP program [40, 41], and behaviors of the higher-order corrections are studied in detail. We clearly exhibit the dependence of the EW corrections for the decay rates as well as the decay branching ratios on the model parameters. In addition, we analyze the correlations between the branching ratios of A and the scaling factor of the hZZ coupling including higher-order corrections. We show that NLO EW corrections sizably modify theoretical predictions at LO. Finally, we discuss the discrimination of the types of the 2HDM by studying the correlations of the decay branching ratios of the CP-odd Higgs boson.

This paper is organized as follows. In Sec. II, we introduce Lagrangian of the 2HDM, and the constraints on model parameters are discussed. In Sec. III, we give formulae for the decay rates of the CP-odd Higgs boson in terms of the renormalized vertex functions. In Sec. IV, we examine the theoretical behaviors of NLO EW corrections to the decay rates and model parameter dependence on the branching ratios with NLO corrections. In Sec. V, we discuss the impact of NLO EW corrections on the branching ratios and the discrimination of four types of 2HDMs. Conclusions are given in VI. In Appendices, we give analytic expressions for scalar couplings, self-energies and vertex functions of the CP-odd Higgs boson, and decay rates with real photon emission.

II. TWO HIGGS DOUBLET MODEL

In this section, we define 2HDM Lagrangian to fix our notation. There are two $SU(2)_L$ doublet Higgs fields Φ_1 and Φ_2 with the hypercharge $Y = 1/2$. We impose a softly-broken Z_2 symmetry to prohibit tree-level flavor changing neutral currents [53, 54]. The Z_2 charge assignment is shown in Table I. In addition, we assume CP conservation in the Higgs potential for simplicity.

	Φ_1	Φ_2	Q_L	L_L	u_R	d_R	e_R	ζ_u	ζ_d	ζ_e
Type-I	+	-	+	+	-	-	-	$\cot \beta$	$\cot \beta$	$\cot \beta$
Type-II	+	-	+	+	-	+	+	$\cot \beta$	$-\tan \beta$	$-\tan \beta$
Type-X (lepton specific)	+	-	+	+	-	-	+	$\cot \beta$	$\cot \beta$	$-\tan \beta$
Type-Y (flipped)	+	-	+	+	-	+	-	$\cot \beta$	$-\tan \beta$	$\cot \beta$

TABLE I: Z_2 charge assignments and ζ_f ($f = u, d, e$) factors in four types of 2HDMs [15].

A. Lagrangian

The Higgs potential under the softly-broken Z_2 symmetry is given by

$$V = m_1^2 |\Phi_1|^2 + m_2^2 |\Phi_2|^2 - \left(m_3^2 \Phi_1^\dagger \Phi_2 + \text{h.c.} \right) + \frac{\lambda_1}{2} |\Phi_1|^4 + \frac{\lambda_2}{2} |\Phi_2|^4 + \lambda_3 |\Phi_1|^2 |\Phi_2|^2 + \lambda_4 \left| \Phi_1^\dagger \Phi_2 \right|^2 + \left[\frac{\lambda_5}{2} \left(\Phi_1^\dagger \Phi_2 \right)^2 + \text{h.c.} \right], \quad (\text{II.1})$$

where m_3^2 corresponds to the softly breaking parameter of the Z_2 symmetry. Since we assume CP conservation in the Higgs potential, m_3^2 and λ_5 are real. The Higgs doublets are parametrized as

$$\Phi_i = \begin{pmatrix} \omega_i^+ \\ \frac{1}{\sqrt{2}}(v_i + \varphi_i + iz_i) \end{pmatrix}, \quad (i = 1, 2), \quad (\text{II.2})$$

where v_1 and v_2 are the vacuum expectation values (VEVs) of Φ_1 and Φ_2 , and the electroweak VEV is given by $v = \sqrt{v_1^2 + v_2^2}$.

We introduce the Higgs basis [55], where only one of the Higgs doublets acquires its VEV,

$$\begin{pmatrix} \Phi_1 \\ \Phi_2 \end{pmatrix} = R(\beta) \begin{pmatrix} H_1 \\ H_2 \end{pmatrix} \quad \text{with} \quad R(\theta) = \begin{pmatrix} c_\theta & -s_\theta \\ s_\theta & c_\theta \end{pmatrix}, \quad (\text{II.3})$$

where $\tan \beta = v_2/v_1$ with $0 \leq \beta \leq \pi/2$, and s_θ (c_θ) is abbreviation of $\sin \theta$ ($\cos \theta$). The Higgs potential can be expressed as

$$V(H_1, H_2) = Y_1^2 H_1^\dagger H_1 + Y_2^2 H_2^\dagger H_2 - Y_3^2 (H_1^\dagger H_2 + H_2^\dagger H_1) + \frac{1}{2} Z_1 (H_1^\dagger H_1)^2 + \frac{1}{2} Z_2 (H_2^\dagger H_2)^2 + Z_3 (H_1^\dagger H_1) (H_2^\dagger H_2) + Z_4 (H_1^\dagger H_2) (H_2^\dagger H_1) + \left\{ \frac{1}{2} Z_5 (H_1^\dagger H_2)^2 + [Z_6 H_1^\dagger H_1 + Z_7 H_2^\dagger H_2] H_1^\dagger H_2 + \text{h.c.} \right\}, \quad (\text{II.4})$$

where Y_i^2 and Z_i are functions of m_i^2 and λ_i . We give the explicit formulae of them in terms of the masses and mixing angles of the Higgs bosons in Appendix B.

The Higgs doublets are parametrized as

$$H_1 = \begin{pmatrix} G^+ \\ \frac{1}{\sqrt{2}}(v + h_1 + iG^0) \end{pmatrix}, \quad H_2 = \begin{pmatrix} H^+ \\ \frac{1}{\sqrt{2}}(h_2 + iA) \end{pmatrix}, \quad (\text{II.5})$$

where G^\pm and G^0 are the Nambu-Goldstone bosons while H^\pm and A are the physical charged and CP-odd Higgs bosons. In the Higgs basis, the mass matrices of the charged and CP-odd states are diagonalized after imposing the stationary conditions,

$$Y_1^2 = -\frac{1}{2}Z_1v^2, \quad Y_3^2 = \frac{1}{2}Z_6v^2. \quad (\text{II.6})$$

The masses of H^\pm and A are given by

$$m_{H^\pm}^2 = Y_2^2 + \frac{1}{2}Z_3v^2, \quad (\text{II.7})$$

$$m_A^2 = Y_2^2 + \frac{1}{2}(Z_3 + Z_4 - Z_5)v^2. \quad (\text{II.8})$$

In general, the mass matrix of the CP-even states is not diagonalized on the Higgs basis,

$$\mathcal{M}^2 = \begin{pmatrix} Z_1v^2 & Z_6v^2 \\ Z_6v^2 & Y_2^2 + \frac{1}{2}Z_{345}v^2 \end{pmatrix}. \quad (\text{II.9})$$

We need further rotation to define the CP-even mass eigenstates h and H ,

$$\begin{pmatrix} h_1 \\ h_2 \end{pmatrix} = R(\alpha - \beta) \begin{pmatrix} H \\ h \end{pmatrix}. \quad (\text{II.10})$$

The masses of the CP-even Higgs bosons and the mixing angle $\beta - \alpha$ are given by

$$m_H^2 = \mathcal{M}_{11}^2 c_{\beta-\alpha}^2 + \mathcal{M}_{22}^2 s_{\beta-\alpha}^2 - \mathcal{M}_{12}^2 s_{2(\beta-\alpha)}, \quad (\text{II.11})$$

$$m_h^2 = \mathcal{M}_{11}^2 s_{\beta-\alpha}^2 + \mathcal{M}_{22}^2 c_{\beta-\alpha}^2 + \mathcal{M}_{12}^2 s_{2(\beta-\alpha)}, \quad (\text{II.12})$$

$$\tan 2(\beta - \alpha) = \frac{-2\mathcal{M}_{12}^2}{\mathcal{M}_{11}^2 - \mathcal{M}_{22}^2}. \quad (\text{II.13})$$

In this paper, we identify h and H as the observed Higgs boson with the mass 125 GeV and an additional CP-even Higgs boson, respectively.

The original eight parameters in the Higgs potential can be replaced by the physical parameters. While the mass of the discovered Higgs boson and the electroweak VEV are fixed, we have the following six parameters as inputs,

$$m_H, \quad m_A, \quad m_{H^\pm}, \quad M^2, \quad \tan \beta, \quad s_{\beta-\alpha}, \quad (\text{II.14})$$

where we have introduced a softly Z_2 breaking scale $\sqrt{M^2} = \sqrt{m_{12}^2/s_\beta c_\beta}$. These parameters are constrained by theoretical arguments such as perturbative unitarity [56–59], tree-level vacuum stability [60–64] and the true vacuum condition [65, 66]. In this paper, we take $M^2 \geq 0$ which ensures the true vacuum condition.

Under the Z_2 symmetry, 2HDM can be classified into four independent types of Yukawa interactions as given in Table. I [15, 67]. We call them Type-I, Type-II, Type-X and Type-Y, respectively. Yukawa Lagrangian is generally written in terms of Φ_1 and Φ_2 by

$$\mathcal{L}_Y = -Y_u \bar{Q}_L \tilde{\Phi}_u u_R - Y_d \bar{Q}_L \Phi_d d_R - Y_e \bar{L}_L \Phi_e e_R + \text{h.c.}, \quad (\text{II.15})$$

where $\tilde{\Phi}_u = i\sigma_2 \Phi_u^*$, and $\Phi_{u,d,e}$ are Φ_1 or Φ_2 depending on the types of 2HDMs.

In the mass eigenstate, the interaction terms among the gauge bosons and the CP-even scalars are given by,

$$\begin{aligned} \mathcal{L}_{\text{kin}} &= |D_\mu \Phi_1|^2 + |D_\mu \Phi_2|^2 \\ &\supset [s_{\beta-\alpha} h + c_{\beta-\alpha} H] \left(\frac{2m_W^2}{v} W^{+\mu} W_\mu^- + \frac{m_Z^2}{v} Z^\mu Z_\mu \right). \end{aligned} \quad (\text{II.16})$$

The Yukawa interaction terms among the fermions and the CP-even scalars are given by

$$\mathcal{L}_{\text{int}} = - \sum_{f=u,d,e} \frac{m_f}{v} \left(\zeta_h^f \bar{f} f h + \zeta_H^f \bar{f} f H \right), \quad (\text{II.17})$$

where

$$\zeta_h^f = s_{\beta-\alpha} + \zeta_f c_{\beta-\alpha}, \quad (\text{II.18})$$

$$\zeta_H^f = c_{\beta-\alpha} - \zeta_f s_{\beta-\alpha}, \quad (\text{II.19})$$

and ζ_f is the type-dependent parameter given in Table I. When $s_{\beta-\alpha} = 1$, the couplings of h with various SM particles become SM like. We call this SM-like limit as the alignment limit in this paper.

The alignment limit can be achieved in different two ways [5, 17]; (i) decoupling of the additional Higgs bosons, and (ii) alignment without decoupling. In the scenario (i), we take the decoupling limit, $M^2 \gg f(\lambda_i)v^2$. Then, we have

$$\tan 2(\beta - \alpha) \simeq \frac{-2Z_6 v^2}{-M^2} \simeq 0, \quad (\text{II.20})$$

where we have used that Z_6 does not depend on $\sqrt{M^2}$. Eq. (II.20) implies $s_{\beta-\alpha} = 1$, and the couplings of h become SM like. In the decoupling scenario, masses of the additional Higgs bosons

are close to $\sqrt{M^2}$, decoupling from electroweak physics. In scenario (ii), the off-diagonal component of the mass matrix for the CP-even states is equal to zero, $Z_6 = 0$. In this scenario, the additional Higgs bosons need not be decoupled, and their masses can be taken around the electroweak scale.

B. Constraints from experimental data

We here discuss experimental constraints on the 2HDMs. Although these experimental constraints have been discussed in Ref. [44], we dare to explain them here again for completeness.

- Electroweak precision tests

The constraint from the electroweak precision tests is imposed by the S and T parameters [68, 69]. The new physics contributions in the 2HDMs are defined by $\Delta S = S_{2\text{HDM}} - S_{\text{SM}}$ and $\Delta T = T_{2\text{HDM}} - T_{\text{SM}}$. The analytical formulae for ΔS and ΔT are given in Refs. [19, 70–72]. The experimental data are given in Ref. [73],

$$\Delta S = 0.04 \pm 0.08, \quad \Delta T = 0.08 \pm 0.07, \quad (\text{II.21})$$

where the U parameter is fixed to zero. The reference values of the masses of the SM Higgs boson and the top quark are $m_{h,\text{ref}} = 125$ GeV and $m_{t,\text{ref}} = 172.5$ GeV, respectively. The correlation coefficient in χ^2 analysis is +0.92. We require ΔS and ΔT to be within 95% CL.

- Signal strengths of the SM-like Higgs boson

Measurements of signal strengths for the SM-like Higgs boson constrain the parameter space of the 2HDMs. We evaluate the decay rates of the SM-like Higgs boson, $\Gamma(h \rightarrow XY)$, including the NLO EW and higher-order QCD corrections by using **H-COUP v2** [41]. The analytic expressions for $\Gamma(h \rightarrow XY)$ are given in Ref. [28]. We define the scaling factors at the one-loop level,

$$\kappa_X = \sqrt{\frac{\Gamma_{\text{LO+EW+QCD}}^{2\text{HDM}}(h \rightarrow XY)}{\Gamma_{\text{LO+QCD}}^{\text{SM}}(h \rightarrow XY)}}. \quad (\text{II.22})$$

We require that the scaling factors for $XY = bb, \tau\tau, \gamma\gamma, gg$ and ZZ^* to be consistent with the values presented in Table 11 (a) of Ref. [3] at 95 % CL.

- Direct searches of the additional Higgs bosons

In Ref. [7], constraints from direct searches of the additional Higgs bosons at the LHC 13 TeV with 36 fb^{-1} have been evaluated for the alignment limit and nearly alignment scenario for all the types of 2HDMs. The excluded regions at 95% CL are shown in Figs. 10 and 11 in Ref. [7].

In the alignment limit, $A \rightarrow \tau\tau$ gives the lower bound, $m_A \gtrsim 350$ GeV, depending on the value of $\tan\beta$ and the types of 2HDMs. For Type-I and Type-Y, $\tan\beta \lesssim 2$ and $\tan\beta \lesssim 1.2$ is excluded,

respectively. For Type-II, $\tan\beta \lesssim 2.3$ and $\tan\beta \gtrsim 8$ are excluded, while $\tan\beta \lesssim 8$ is excluded for Type-X. $H^+ \rightarrow t\bar{b}$ gives the lower bound, $m_{H^\pm} \gtrsim 650$ GeV, for $\tan\beta \lesssim 1$ for the all types of 2HDMs.

In the nearly alignment scenarios with $s_{\beta-\alpha} = 0.99$, $A \rightarrow Zh$ gives the lower bound on m_A , e.g., $m_A \gtrsim 950$ (1100) GeV for $\tan\beta = 1$ for Type-I (Type-II) and Type-X (Type-Y). For $s_{\beta-\alpha} = 0.995$, the lower bound on m_A is relaxed, and $m_A \gtrsim 350$ GeV for $\tan\beta = 5(2)$ for Type-I (Type-Y). For Type-II and Type-X with $s_{\beta-\alpha} = 0.995$, $A \rightarrow \tau\tau$ gives the almost same bound as in the alignment limit, and it is stronger than the bound by $A \rightarrow Zh$. For $s_{\beta-\alpha} = 0.995$, $H \rightarrow hh$ gives the lower bound on m_H , e.g., $m_H \gtrsim 950$ (1100) GeV for $\tan\beta = 1$ with $m_H = \sqrt{M^2}$ for Type-I (Type-II) and Type-X (Type-Y). We note that the partial decay width of $H \rightarrow hh$ depends on the value of $\sqrt{M^2}$, while the above-mentioned decay processes are independent of it at LO.

- Flavor constraints

The mass of the charged Higgs bosons is constrained by the B meson flavor violating decay, $B \rightarrow X_s \gamma$ [74, 75]. For Type-II and Type-Y, $m_{H^\pm} \lesssim 800$ GeV is excluded for $\tan\beta > 1$ [74, 75]. For Type-I and Type-X, the constraint is weaker than that for Type-II and Type-Y. The excluded regions are given in lower $\tan\beta$ regions, e.g., $m_{H^\pm} \lesssim 400$ (180) GeV for $\tan\beta = 1$ (1.5) [74]. For Type-II, high $\tan\beta$ regions are also constrained by the B meson rare leptonic decay, $B_s \rightarrow \mu^+ \mu^-$ [76]. For $m_{H^\pm} = 800$ GeV, the region with $\tan\beta \gtrsim 10$ is excluded [73]. Comprehensive studies for constraints from various flavor observables such as B meson decays, D meson decays and $B_0 - \bar{B}_0$ mixing, are performed in Refs. [73, 77].

III. DECAY RATES WITH HIGHER-ORDER CORRECTIONS

In this section, we first define the renormalized vertex functions of the CP-odd Higgs boson. The decay rates of $A \rightarrow f\bar{f}$, Zh/H and $W^\pm H^\mp$ including the NLO EW corrections are given in terms of the form factors of the vertex functions. We also give the decay rates of the loop-induced decays, $A \rightarrow W^+ W^-$, ZZ , $Z\gamma$, $\gamma\gamma$ and gg at LO EW. We include higher-order QCD corrections for the decays into a pair of quarks, photons and gluons.

We here give an overview of our calculation scheme of NLO EW corrections. In order to treat UV divergences, we employ the on-shell renormalization scheme, where external-leg corrections are absorbed into the field renormalization constant. For the gauge sector and the fermion sector, we follow the on-shell renormalization scheme developed in Ref. [78, 79]. For the renormalization of the Higgs sector, we employ the improved on-shell renormalization scheme developed in Ref. [23]. In the

improved on-shell renormalization scheme, the masses of the additional Higgs bosons, the mixing angles and the wave function renormalization constants are renormalized by imposing the on-shell conditions for the Higgs bosons in the mass eigenstates. The gauge dependences, which appear in the renormalization of mixing angles [80], are removed by applying the pinch technique [23, 50]. For the calculation of the decays of the CP-odd Higgs boson, we do not need to renormalize M^2 , while it can be renormalized by the minimal subtraction [17]. Among the various renormalization scheme discussed in Ref. [39], our renormalization scheme is essentially the same as the pOS^o scheme, where $\delta\beta$ is determined by the pinched self-energies of the CP-odd scalars [17, 23]. This scheme provides relatively stable numerical results compared with other renormalization schemes such as the $\overline{\text{MS}}$ scheme [39, 50]. We perform the calculation in the 't Hooft-Feynman gauge, i.e., $\xi = 1$, and implement the analytical formulae into H-COUP program [40, 41]. For numerical evaluations of the Passarino-Veltman functions [81], we use **LoopTools** [82].

We regularize the IR divergences, which appear in one-loop diagrams containing a virtual photon, by introducing the finite photon mass. The photon-mass dependence is canceled by adding the decay rate of the real-photon emission process. We confirm the cancellation of the photon-mass dependence numerically.

In the following calculation, the contribution of AZ mixing, which can arise in the amplitudes for A decays at loop level, vanishes due to the Slavnov-Taylor identity [83],

$$\hat{\Pi}_{AG^0}(m_A^2) + i\frac{m_A^2}{m_Z}\hat{\Pi}_{AZ}(m_A^2) = 0, \quad (\text{III.1})$$

where $\hat{\Pi}_{AG^0(AZ)}(q^2)$ denotes the renormalized self-energy for $AG^0(AZ)$ mixing. Since we impose the on-shell renormalization condition, $\hat{\Pi}_{AG^0}(m_A^2) = 0$, the contribution of AZ mixing vanishes in the decay amplitude.

A. Form factors for vertex functions of the CP-odd Higgs boson

1. $Af\bar{f}$ vertex

The renormalized $Af\bar{f}$ vertex functions can be expressed as

$$\begin{aligned} \hat{\Gamma}_{Af\bar{f}}(p_1, p_2, q) = & \hat{\Gamma}_{Af\bar{f}}^S + \gamma_5 \hat{\Gamma}_{Af\bar{f}}^P + \not{p}_1 \hat{\Gamma}_{Af\bar{f}}^{V_1} + \not{p}_2 \hat{\Gamma}_{Af\bar{f}}^{V_2} + \not{p}_1 \gamma_5 \hat{\Gamma}_{Af\bar{f}}^{A_1} + \not{p}_2 \gamma_5 \hat{\Gamma}_{Af\bar{f}}^{A_2} \\ & + \not{p}_1 \not{p}_2 \hat{\Gamma}_{Af\bar{f}}^T + \not{p}_1 \not{p}_2 \gamma_5 \hat{\Gamma}_{Af\bar{f}}^{PT}, \end{aligned} \quad (\text{III.2})$$

where p_1 (p_2) is the incoming four-momentum of the anti-fermion (fermion), and $q^\mu (= p_1 + p_2)$ is the outgoing four-momentum of the CP-odd Higgs boson (see Fig. 1).

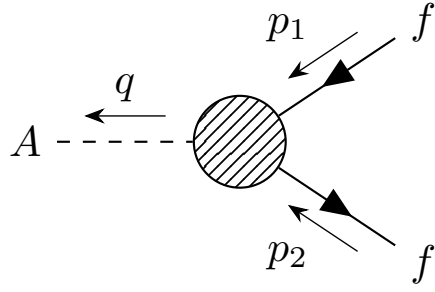


FIG. 1: Momentum assignment for the renormalized $Af\bar{f}$ vertex.

The renormalized form factors are composed of the tree-level and the one-loop parts as

$$\hat{\Gamma}_{Af\bar{f}}^X = \Gamma_{Af\bar{f}}^{X,\text{tree}} + \Gamma_{Af\bar{f}}^{X,\text{loop}}, \quad (X = S, P, V_1, V_2, A_1, A_2, T, PT), \quad (\text{III.3})$$

where the tree-level couplings for $Af\bar{f}$ vertex are given by

$$\Gamma_{Af\bar{f}}^{P,\text{tree}} = i2I_f \frac{m_f \zeta_f}{v}, \quad \Gamma_{Af\bar{f}}^{X,\text{tree}} = 0, \quad (X \neq P), \quad (\text{III.4})$$

where I_f is the third component of the iso-spin of fermions.

The one-loop parts are further decomposed into contributions from 1PI diagrams and counterterms,

$$\Gamma_{Af\bar{f}}^{X,\text{loop}} = \Gamma_{Af\bar{f}}^{X,1\text{PI}} + \delta\Gamma_{Af\bar{f}}^X. \quad (\text{III.5})$$

The 1PI diagrams contributions $\Gamma_{Af\bar{f}}^{X,1\text{PI}}$ are given in Appendix E. The counterterms $\delta\Gamma_{Af\bar{f}}^X$ are given by

$$\delta\Gamma_{Af\bar{f}}^P = \Gamma_{Af\bar{f}}^{P,\text{tree}} \left[\frac{\delta m_f}{m_f} - \frac{\delta v}{v} - \zeta_f \delta\beta_f + \delta Z_V^f + \frac{\delta Z_A}{2} + \frac{\delta C_A}{\zeta_f} - \left(\frac{1}{\zeta_f} + \zeta_f \right) \delta\beta^{\text{PT}} \right], \quad (\text{III.6})$$

$$\delta\Gamma_{Af\bar{f}}^X = 0, \quad (X \neq P). \quad (\text{III.7})$$

The analytic expressions for the counterterms in Eq. (III.6) are given in Refs. [23, 44].

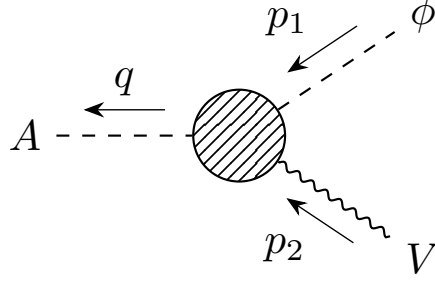
When we neglect the effects of the CP violation, the renormalized $Af\bar{f}$ vertex functions satisfy the following relations,

$$\hat{\Gamma}_{Af\bar{f}}^S = \hat{\Gamma}_{Af\bar{f}}^T = 0, \quad \hat{\Gamma}_{Af\bar{f}}^{V_1} = \hat{\Gamma}_{Af\bar{f}}^{V_2}, \quad \hat{\Gamma}_{Af\bar{f}}^{A_1} = \hat{\Gamma}_{Af\bar{f}}^{A_2}, \quad (q^2 = m_A^2, p_1^2 = p_2^2 = m_f^2). \quad (\text{III.8})$$

2. $AV\phi$ vertex

The renormalized $AV\phi$ vertex functions $(V, \phi) = (Z, h)$, (Z, H) and (W^\pm, H^\mp) can be expressed as

$$\hat{\Gamma}_{AV\phi}^\mu(p_1, p_2, q) = (p_1 + q)^\mu \hat{\Gamma}_{AV\phi}, \quad (\text{III.9})$$

FIG. 2: Momentum assignment for the renormalized $AV\phi$ vertex.

where p_1 and p_2 denote the incoming four-momentum of the scalar boson ϕ and the gauge boson V , respectively. The momentum q is the outgoing four-momentum of the CP-odd Higgs boson (see Fig. 2). Since we assume that the external gauge boson is on-shell, the term proportional to p_2 vanishes due to the orthogonality of the polarization vector. For the $A \rightarrow W^\pm H^\mp$ decays, we use the renormalized $H^\pm W^\mp A$ vertex function given in Ref. [44],

$$\hat{\Gamma}_{AW^\pm H^\mp}^\mu(p_1, p_2, q) = -(q + p_1)^\mu \hat{\Gamma}_{H^\pm W^\pm A}(q^2, p_2^2, p_1^2), \quad (\text{III.10})$$

where the additional minus sign comes from the change of momentum assignment.

The renormalized form factors are composed of the tree-level and the one-loop parts as

$$\hat{\Gamma}_{AV\phi} = \Gamma_{AV\phi}^{\text{tree}} + \Gamma_{AV\phi}^{\text{loop}}, \quad (\text{III.11})$$

where $\Gamma_{AZ\phi}^{\text{tree}}$ are given by

$$\Gamma_{AZh}^{\text{tree}} = i \frac{m_Z}{v} c_{\beta-\alpha}, \quad \Gamma_{AZH}^{\text{tree}} = -i \frac{m_Z}{v} s_{\beta-\alpha}, \quad \Gamma_{AW^\mp H^\pm}^{\text{tree}} = -i \frac{m_W}{v}. \quad (\text{III.12})$$

The one-loop parts are further decomposed into contributions from 1PI diagrams and counterterms,

$$\Gamma_{AV\phi}^{\text{loop}} = \Gamma_{AV\phi}^{\text{1PI}} + \delta\Gamma_{AV\phi}. \quad (\text{III.13})$$

The 1PI diagrams contributions $\Gamma_{AV\phi}^{\text{1PI}}$ are given in Appendix E. The counterterms $\delta\Gamma_{AZ\phi}$ vertices are given by

$$\begin{aligned} \delta\Gamma_{AZh} = \Gamma_{AZh}^{\text{tree}} & \left[\frac{\delta m_Z^2}{2m_Z^2} - \frac{\delta v}{v} + \frac{1}{2}(\delta Z_h + \delta Z_A + \delta Z_Z) \right. \\ & \left. + \tan(\beta - \alpha)(\delta C_A - \delta C_h - \delta\beta^{\text{PT}} + \delta\alpha^{\text{PT}}) \right], \end{aligned} \quad (\text{III.14})$$

$$\begin{aligned} \delta\Gamma_{AZH} = \Gamma_{AZH}^{\text{tree}} & \left[\frac{\delta m_Z^2}{2m_Z^2} - \frac{\delta v}{v} + \frac{1}{2}(\delta Z_H + \delta Z_A + \delta Z_Z) \right. \\ & \left. - \cot(\beta - \alpha)(\delta C_A + \delta C_h - \delta\beta^{\text{PT}} + \delta\alpha^{\text{PT}}) \right], \end{aligned} \quad (\text{III.15})$$

$$\delta\Gamma_{AW^\mp H^\pm} = \Gamma_{AW^\mp H^\pm}^{\text{tree}} \left[\frac{\delta m_W^2}{2m_W^2} - \frac{\delta v}{v} + \frac{1}{2}(\delta Z_{H^\pm} + \delta Z_A + \delta Z_W) \right]. \quad (\text{III.16})$$

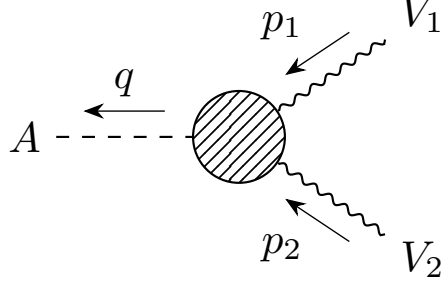


FIG. 3: Momentum assignment for the renormalized AV_1V_2 vertex.

The analytic expressions for the counterterms are given in Refs. [23, 44].

3. AV_1V_2 vertex

The AV_1V_2 vertex functions $(V_1, V_2) = (W^\pm, W^\mp), (Z, Z), (Z, \gamma)$ and (γ, γ) appear at one-loop level. They can be expressed as

$$\hat{\Gamma}_{AV_1V_2}^{\mu\nu}(p_1, p_2, q) = g^{\mu\nu}\Gamma_{AV_1V_2}^{1,1\text{PI}} + p_1^\nu p_2^\mu \Gamma_{AV_1V_2}^{2,1\text{PI}} + i\epsilon^{\mu\nu\rho\sigma} p_{1\rho} p_{2\sigma} \Gamma_{AV_1V_2}^{3,1\text{PI}}, \quad (\text{III.17})$$

where p_1 and p_2 denote the incoming four-momentum of the gauge bosons V_i ($i = 1, 2$), and q is the outgoing four-momentum of the CP-odd Higgs boson (see Fig. 3). We take $\epsilon^{0123} = +1$ and assume that the external gauge bosons are on-shell. When we neglect the effects of the CP violation, the 1PI vertices satisfy

$$\Gamma_{AV_1V_2}^{1,1\text{PI}} = \Gamma_{AV_1V_2}^{2,1\text{PI}} = 0. \quad (\text{III.18})$$

In the CP-conserving 2HDMs, radiative corrections consist of fermion loops only [84]. This is because the bosonic sector separately conserves P and C symmetries [85], and AV_1V_2 couplings are prohibited. On the other hand, the fermion sector breaks them, and $\Gamma_{AV_1V_2}^{3,1\text{PI}}$ is induced at the one-loop level. The 1PI diagrams contributions $\Gamma_{AV_1V_2}^{3,1\text{PI}}$ are given in Appendix E.

B. Decay rates of $A \rightarrow f\bar{f}$

The decay rates of the CP-odd Higgs boson into a pair of fermions with NLO EW and QCD corrections are given by

$$\Gamma(A \rightarrow f\bar{f}) = \Gamma_{\text{LO}}(A \rightarrow f\bar{f}) \left(1 + \Delta_{\text{EW}}^f + \Delta_{\text{QCD}}^f \right) + \Gamma(A \rightarrow f\bar{f}\gamma). \quad (\text{III.19})$$

The decay rate at LO is given by

$$\Gamma_{\text{LO}}(A \rightarrow f\bar{f}) = N_c^f \frac{m_A}{8\pi} \left| \Gamma_{A f \bar{f}}^{P, \text{tree}} \right|^2 \lambda^{1/2} \left(\frac{m_f^2}{m_A^2}, \frac{m_f^2}{m_A^2} \right), \quad (\text{III.20})$$

where N_c^f is the color factor, and the kinematical factor $\lambda(x, y)$ is given by

$$\lambda(x, y) = (1 - x - y)^2 - 4xy. \quad (\text{III.21})$$

For the decays into a pair of light quarks, $A \rightarrow q\bar{q}$ ($q \neq t$), we replace the quark mass in the Yukawa coupling to the running mass $\bar{m}_q(\mu)$ evaluated at $\mu = m_A$ [86–89]. Factors Δ_{EW}^f and Δ_{QCD}^f denote the EW and QCD corrections, respectively. Since the NLO EW correction includes the IR divergences, we regularize them by introducing the finite photon mass. The photon mass dependence is canceled by adding the decay rates of real photon emission $\Gamma(A \rightarrow f\bar{f}\gamma)$. The analytic expression of $\Gamma(A \rightarrow f\bar{f}\gamma)$ is given in Appendix F.

The EW correction Δ_{EW}^f is given by

$$\Delta_{\text{EW}}^f = \frac{2}{\left| \Gamma_{A f \bar{f}}^{P, \text{tree}} \right|^2} \text{Re} \left(\Gamma_{A f \bar{f}}^{P, \text{tree}} G_{A f \bar{f}}^{P, \text{loop}*} \right) - \Delta r, \quad (\text{III.22})$$

with

$$G_{A f \bar{f}}^{P, \text{loop}} = \Gamma_{A f \bar{f}}^{P, \text{loop}} - 2m_f \Gamma_{A f \bar{f}}^{A_1, \text{loop}} + m_A^2 \left(1 - \frac{3m_f^2}{m_A^2} \right) \Gamma_{A f \bar{f}}^{PT, \text{loop}}, \quad (\text{III.23})$$

where we have used Eq. (III.8). The one-loop weak correction to the muon decay, Δr , is introduced by the resummation of universal leading higher-order corrections [90, 91].

For $A \rightarrow q\bar{q}$, we apply the QCD corrections at NNLO in the $\overline{\text{MS}}$ scheme. The QCD correction is given by

$$\Delta_{\text{QCD}}^q = \Delta_{qq} + \Delta_A. \quad (\text{III.24})$$

The correction Δ_{qq} is evaluated in the chiral limit, $m_A \gg m_q$, and it is the same for CP-odd and CP-even particles. The NLO correction is given in Refs. [86–89], while the NNLO correction is given in Refs. [92, 93].

$$\Delta_{qq} = \frac{\alpha_s(m_A)}{\pi} \frac{17}{4} C_F + \left(\frac{\alpha_s(m_A)}{\pi} \right)^2 \left[\frac{10801}{144} - \frac{39}{2} \zeta(3) - \left(\frac{65}{24} - \frac{2}{3} \zeta(3) \right) N_f - \pi^2 \left(\frac{19}{12} - \frac{1}{18} N_f \right) \right], \quad (\text{III.25})$$

with the color factor $C_F = 4/3$ and the Riemann zeta function $\zeta(n)$. We take the number of active flavors N_f as $N_f = 5$ for $m_A \leq m_t$, while $N_f = 6$ for $m_A > m_t$. The correction Δ_A includes the

logarithms of the light-quarks and top-quark masses. In the heavy top-mass limit, $m_t \gg m_A$, and $\mu = m_A$, it is given by [94, 95]

$$\Delta_A = \left(\frac{\alpha_s(m_A)}{\pi} \right)^2 \left(3.83 + \ln \frac{m_t^2}{m_A^2} + \frac{1}{6} \ln^2 \frac{\bar{m}_q^2(m_A)}{m_A^2} \right). \quad (\text{III.26})$$

For the decay into the top-quark pair, the effects of the top-quark mass in the QCD corrections are significant near the threshold region. The QCD correction in the on-shell scheme is given by [96, 97]

$$\Delta_{\text{QCD}}^t = \frac{\alpha_s(\mu)}{\pi} C_F \left[\frac{L(\beta_t)}{\beta_t} - \frac{1}{16\beta_t} (19 + 2\beta_t^2 + 3\beta_t^4) \ln \rho_t + \frac{3}{8} (7 - \beta_t^2) \right], \quad (\text{III.27})$$

with $\beta_t = \lambda^{1/2}(m_t^2/m_A^2, m_t^2/m_A^2)$ and $\rho_t = (1 - \beta_t)/(1 + \beta_t)$. The function $L(\beta_t)$ is given by

$$\begin{aligned} L(\beta_t) = (1 + \beta_t^2) & \left[4\text{Li}_2(\rho_t) + 2\text{Li}_2(-\rho_t) + 3 \ln \rho_t \ln \frac{2}{1 + \beta_t} + 2 \ln \rho_t \ln \beta_t \right] \\ & - 3\beta_t \ln \frac{4}{1 - \beta_t^2} - 4\beta_t \ln \beta_t, \end{aligned} \quad (\text{III.28})$$

where $\text{Li}_2(x)$ is the dilog function. When $m_A \gg m_t$, we can treat the top-quark as massless, and apply the QCD corrections in the $\overline{\text{MS}}$ scheme. In order to treat the transition between the two regions, we use linear interpolation for the QCD corrections to $A \rightarrow t\bar{t}$ as discussed in Ref. [98].

$$\begin{aligned} \Gamma(A \rightarrow t\bar{t}) = R^2 \Gamma_{\text{LO}}^{\text{pole}}(A \rightarrow t\bar{t}) (1 + \Delta_{\text{QCD}}^t) & + (1 - R^2) \Gamma_{\text{LO}}^{\overline{\text{MS}}}(A \rightarrow t\bar{t}) (1 + \Delta_{\text{QCD}}^{t, \overline{\text{MS}}}) \\ & + \Gamma_{\text{LO}}^{\text{pole}}(A \rightarrow t\bar{t}) \Delta_{\text{EW}}^t + \Gamma(A \rightarrow t\bar{t}\gamma), \end{aligned} \quad (\text{III.29})$$

with $R = 2m_t/m_A$. In the evaluation of $\Gamma_{\text{LO}}^{\text{pole}}(A \rightarrow t\bar{t})$, we use the top-quark pole mass for the Yukawa coupling, while the running mass is used for $\Gamma_{\text{LO}}^{\overline{\text{MS}}}(A \rightarrow t\bar{t})$. The QCD correction in the $\overline{\text{MS}}$ scheme $\Delta_{\text{QCD}}^{t, \overline{\text{MS}}}$ is evaluated as similar to the decays into the light quarks.

When $m_t + m_W \leq m_A < 2m_t$, the CP-odd Higgs boson decays into a pair of on-shell and off-shell top quarks, $A \rightarrow t t^* \rightarrow t b W$. We calculate the decay rate at the tree level and give the analytic expressions in Appendix C.

C. Decay rates of $A \rightarrow V\phi$

The decay rate for the CP-odd Higgs boson decays into a Z boson and a CP-even Higgs boson ϕ ($\phi = h, H$) with NLO EW corrections is given by

$$\Gamma(A \rightarrow Z\phi) = \Gamma_{\text{LO}}(A \rightarrow Z\phi) \left(1 + \Delta_{\text{EW}}^\phi \right). \quad (\text{III.30})$$

The decay rate at LO is given by

$$\Gamma_{\text{LO}}(A \rightarrow Z\phi) = \frac{|\Gamma_{AZ\phi}^{\text{tree}}|^2}{16\pi} \frac{m_A^3}{m_Z^2} \lambda^{3/2} \left(\frac{m_\phi^2}{m_A^2}, \frac{m_Z^2}{m_A^2} \right). \quad (\text{III.31})$$

The EW correction Δ_{EW}^ϕ is given by

$$\Delta_{\text{EW}}^\phi = \frac{2 \text{Re} \left(\Gamma_{AZ\phi}^{\text{tree}} \Gamma_{AZ\phi}^{\text{loop}*} \right)}{|\Gamma_{AZ\phi}^{\text{tree}}|^2} - \Delta r - \text{Re} \hat{\Pi}'_{ZZ}(m_Z^2). \quad (\text{III.32})$$

The term $\hat{\Pi}'_{ZZ}(m_Z^2)$ is included since the residue of renormalized Z boson's propagator is not unity [78, 79].

The decay rate for the CP-odd Higgs boson decays into a W^\pm boson and a charged Higgs boson H^\pm with NLO EW corrections is given by

$$\Gamma(A \rightarrow W^\pm H^\mp) = \Gamma_{\text{LO}}(A \rightarrow W^\pm H^\mp) \left(1 + \Delta_{\text{EW}}^{H^\pm} \right) + \Gamma(A \rightarrow H^\pm W^\mp \gamma). \quad (\text{III.33})$$

The decay rate at LO is given by

$$\Gamma_{\text{LO}}(A \rightarrow W^\pm H^\mp) = \frac{|\Gamma_{AW^\mp H^\pm}^{\text{tree}}|^2}{8\pi} \frac{m_A^3}{m_W^2} \lambda^{3/2} \left(\frac{m_{H^\pm}^2}{m_A^2}, \frac{m_W^2}{m_A^2} \right). \quad (\text{III.34})$$

The EW correction $\Delta_{\text{EW}}^{H^\pm}$ is given by

$$\Delta_{\text{EW}}^{H^\pm} = \frac{2 \text{Re} \left(\Gamma_{AW^\mp H^\pm}^{\text{tree}} \Gamma_{AW^\mp H^\pm}^{\text{loop}*} \right)}{|\Gamma_{AW^\mp H^\pm}^{\text{tree}}|^2} - \Delta r - \text{Re} \hat{\Pi}'_{WW}(m_W^2). \quad (\text{III.35})$$

The term $\hat{\Pi}'_{WW}(m_W^2)$ is included since the residue of renormalized W^\pm bosons propagator is not unity. The IR divergences in the NLO EW correction are regularized by introducing the finite photon mass. The photon mass dependence is removed by including the decay rates of real photon emission $A \rightarrow H^\pm W^\mp \gamma$ as similar to $A \rightarrow f\bar{f}$. The analytic expression of $\Gamma(A \rightarrow H^\pm W^\mp \gamma)$ is given in Appendix F.

When $m_\phi \leq m_A < m_\phi + m_Z$, the CP-odd Higgs boson decays into a pair of on-shell CP-even Higgs boson ϕ and off-shell Z boson, $A \rightarrow \phi Z^* \rightarrow \phi f\bar{f}$. In addition, when $m_{H^\pm} \leq m_A < m_{H^\pm} + m_W$, the CP-odd Higgs boson decays into a pair of on-shell charged Higgs bosons H^\pm and off-shell W^\pm bosons, $A \rightarrow H^\pm W^{\mp*} \rightarrow H^\pm f\bar{f}'$. We calculate these decay rates at the tree level and give the analytic expressions in Appendix C.

D. Decay rates of loop-induced processes

We calculate the decay rates of $A \rightarrow W^+W^-$, ZZ and $Z\gamma$ at LO, while higher-order QCD corrections are included for the decay rates of $\gamma\gamma$ and gg . The decay rates for the $A \rightarrow W^+W^-$, ZZ and $Z\gamma$ are given by

$$\Gamma(A \rightarrow V_i V_j) = \frac{m_A^3}{32\pi(1 + \delta_{ij})} \lambda^{3/2} \left(\frac{m_{V_i}^2}{m_A^2}, \frac{m_{V_j}^2}{m_A^2} \right) \left| \Gamma_{AV_i V_j}^3 \right|^2. \quad (\text{III.36})$$

The decay rate for the CP-odd Higgs boson into a pair of photons is given by

$$\begin{aligned} \Gamma(A \rightarrow \gamma\gamma) = & \frac{G_F \alpha_{\text{em}}^2 m_A^3}{128\sqrt{2}\pi^3} \left| \sum_{\ell} Q_{\ell}^2 \kappa_{\ell}^A I_F^A(\tau_{\ell}) \right. \\ & \left. + \sum_q N_c^q Q_q^2 \kappa_q^A I_F^A(\tau_q) \left[1 + \frac{\alpha_s(m_A)}{\pi} \left(C_1^A(\tau_q) + C_2^A(\tau_q) \ln \frac{4\tau_q \mu^2}{m_A^2} \right) \right] \right|^2, \end{aligned} \quad (\text{III.37})$$

where $\kappa_f^A = -2iI_f \zeta_f$, $\tau_f = m_A^2/(4m_f^2)$ and Q_f is the electric charge of the fermion. The terms in the first line correspond to the contributions from the charged leptons, while the terms in the second line are those from the quarks. The loop function $I_F^A(\tau_f)$ is given by

$$I_F^A(\tau_f) = \frac{2}{\tau_f} f(\tau_f), \quad (\text{III.38})$$

with

$$f(\tau) = \begin{cases} \arcsin^2(\sqrt{\tau}) & (\tau \leq 1), \\ -\frac{1}{4} \left[\ln \frac{1 + \sqrt{1 - \tau^{-1}}}{1 - \sqrt{1 - \tau^{-1}}} - i\pi \right]^2 & (\tau > 1). \end{cases} \quad (\text{III.39})$$

The NLO QCD correction in the $\overline{\text{MS}}$ scheme is given in Refs. [99, 100]. The analytic expressions for QCD corrections are given in Appendix D.

The decay rate of the CP-odd Higgs boson into a pair of gluons is given by

$$\Gamma(A \rightarrow gg) = \Gamma_{\text{LO}}(A \rightarrow gg) \left[1 + \frac{\alpha_s(m_A)}{\pi} E_A^{(1)} + \left(\frac{\alpha_s(m_A)}{\pi} \right)^2 E_A^{(2)} \right], \quad (\text{III.40})$$

where the decay rate at LO is given by

$$\Gamma_{\text{LO}}(A \rightarrow gg) = \frac{\sqrt{2} G_F \alpha_s^2 m_A^3}{128\pi^3} \left| \sum_q \kappa_q^A I_F^A(\tau_q) \right|^2, \quad (\text{III.41})$$

with the loop function $I_F^A(\tau)$ defined in Eq. (III.38). The NLO QCD correction $E_A^{(1)}$ is given in Refs. [99, 100], while the NNLO QCD correction $E_A^{(2)}$ in heavy top-mass limit is given in Ref. [101]. The analytic expressions for QCD corrections are given in Appendix D.

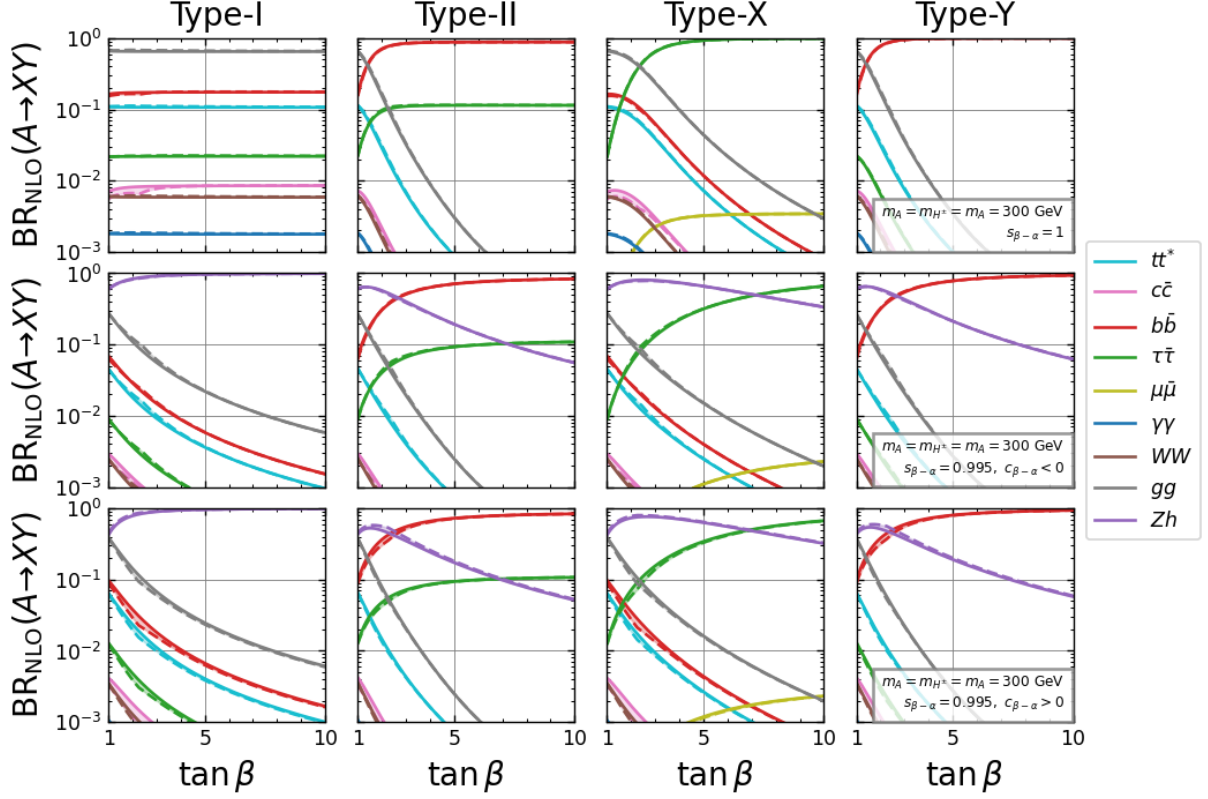


FIG. 4: $\text{BR}(A \rightarrow XY)$ as a function of $\tan\beta$ in the alignment limit $s_{\beta-\alpha} = 1$ (first row) and in the nearly alignment case $s_{\beta-\alpha} = 0.995$ with $c_{\beta-\alpha} < 0$ (second row) and $c_{\beta-\alpha} > 0$ (third row) including the higher-order EW and QCD corrections. The masses of the additional Higgs bosons are degenerate and taken to be $m_\Phi = 300$ GeV. Each decay mode is specified by color as given in the legend. The solid and dashed lines correspond to the results with $\sqrt{M^2} = M_{\text{max}}$ and M_{min} , respectively, where M_{max} (M_{min}) is a maximum (minimum) value of $\sqrt{M^2}$ satisfying the theoretical constraints and S and T parameters.

IV. NEXT-TO-LEADING-ORDER ELECTROWEAK CORRECTIONS

A. Branching ratios

In this subsection, we examine the decay branching ratios of the CP-odd Higgs boson including the higher-order corrections in the four types of 2HDMs. The qualitative behavior does not change from those at LO, while the size of higher-order corrections can reach several dozens of percent. Therefore, we first discuss their behavior and summarize the dominant decay modes in each type of 2HDMs. Since $\text{BR}(A \rightarrow Zh)$ can be negative near $s_{\beta-\alpha} = 1$, we include the contribution of the square of the NLO amplitude. We discuss this point at the end of this subsection. The magnitude of the higher-order corrections will be examined in the next subsection.

In Fig. 4, we show $\text{BR}(A \rightarrow XY)$ including the higher-order corrections as a function of $\tan \beta$. We have assumed that the masses of additional Higgs bosons are degenerate, i.e., $m_\Phi \equiv m_A = m_H = m_{H^\pm}$ and $m_\Phi = 300$ GeV, where the CP-odd Higgs boson cannot decay into a pair of top-quarks. However, the magnitude of the three-body decay width of $A \rightarrow tt^*$ is not negligible, and we include it at LO. We have scanned $\sqrt{M^2}$ for $0 < \sqrt{M^2} < m_A + 500$ GeV under the theoretical constraints and the S and T parameters. M_{\max} (M_{\min}) denotes the maximum (minimum) value of $\sqrt{M^2}$. In order to discuss the theoretical behavior of NLO EW corrections, we dare to omit the constraint from the direct and indirect search and flavor experiment. The results in Type-I, Type-II, Type-X and Type-Y are shown from the first to fourth columns in order. The results in the alignment limit are shown in the first row, while those in the nearly alignment scenario with $c_{\beta-\alpha} < 0$ and $c_{\beta-\alpha} > 0$ are shown in the second and third rows, respectively.

In the alignment limit, the CP-odd Higgs boson mainly decays into a pair of fermions and gluons. Since $\kappa_f = \cot \beta$ in Type-I, the partial decay widths of $A \rightarrow f\bar{f}$ and $A \rightarrow gg$ monotonically decrease as $\tan \beta$ increases. Therefore, the decay branching ratios are almost constant in Type-I. On the other hand, there is $\tan \beta$ enhancement in either or both decays into a pair of down-type quarks and leptons in the other types of 2HDMs. In Type-II, both $A \rightarrow b\bar{b}$ and $A \rightarrow \tau\bar{\tau}$ can be dominant with large $\tan \beta$, while $A \rightarrow \tau\bar{\tau}$ ($A \rightarrow b\bar{b}$) can be dominant in Type-X (Type-Y).

In the nearly alignment case with $c_{\beta-\alpha} < 0$, the CP-odd Higgs boson decays into the Z boson and the SM-like Higgs boson. Since the tree-level hAZ vertex is independent of $\tan \beta$, the partial decay width of $A \rightarrow hZ$ is almost constant in all types of 2HDMs. In Type-I, the other decay modes monotonically decrease as $\tan \beta$ becomes large, and $A \rightarrow Zh$ can be the dominant decay mode despite the tree-level vertex being small in the nearly alignment case. In the other types of 2HDMs, $A \rightarrow b\bar{b}$ or $A \rightarrow \tau\bar{\tau}$ is enhanced with large $\tan \beta$, but the decay branching ratio of $A \rightarrow Zh$ is still several percent with $\tan \beta = 10$. The results with $c_{\beta-\alpha} > 0$ are similar to those with $c_{\beta-\alpha} < 0$.

In Fig. 5, we show $\text{BR}(A \rightarrow XY)$ with $m_\Phi = 600$ GeV, where the CP-odd Higgs boson can decay into a pair of top quarks. While $\text{BR}(A \rightarrow t\bar{t})$ monotonically decreases as $\tan \beta$ becomes large, it is the dominant decay mode for all of the types of 2HDMs due to the large top Yukawa coupling. In the alignment limit, the CP-odd Higgs boson mainly decays into a pair of fermions. In Type-I, $A \rightarrow t\bar{t}$ is dominant, and the decay branching ratios are almost constant similar to the case with $m_\Phi = 300$ GeV. In Type-II, both $A \rightarrow b\bar{b}$ and $A \rightarrow \tau\bar{\tau}$ are enhanced with large $\tan \beta$, and they are comparable with $A \rightarrow t\bar{t}$. In Type-X and Type-Y, $A \rightarrow \tau\bar{\tau}$ and $A \rightarrow b\bar{b}$ are enhanced, respectively, and they are comparable with $A \rightarrow t\bar{t}$.

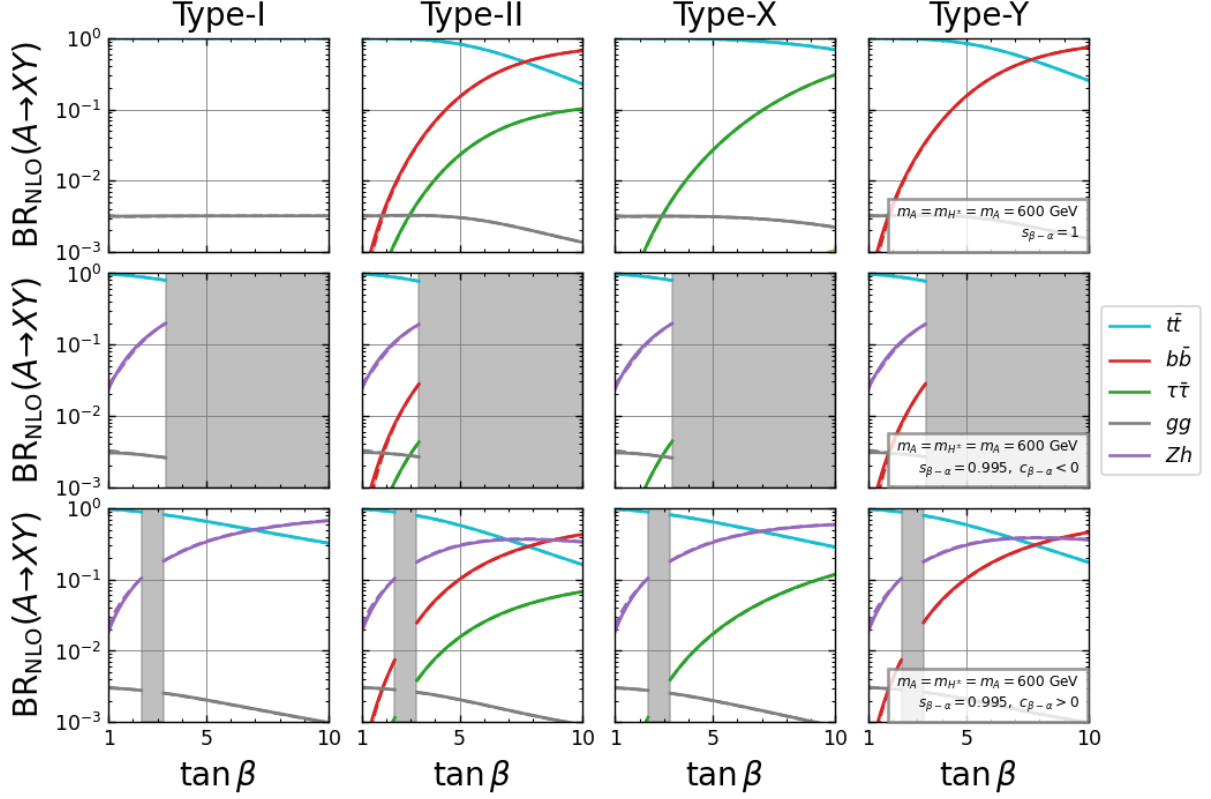


FIG. 5: $\text{BR}(A \rightarrow XY)$ as a function of $\tan \beta$ in the alignment limit $s_{\beta-\alpha} = 1$ (first row) and in the nearly alignment case $s_{\beta-\alpha} = 0.995$ with $c_{\beta-\alpha} < 0$ (second row) and $c_{\beta-\alpha} > 0$ (third row) including the higher-order EW and QCD corrections. The masses of the additional Higgs bosons are degenerate and taken to be $m_\Phi = 600$ GeV. Each decay mode is specified by color as given in the legend. The solid and dashed lines correspond to the results with $\sqrt{M^2} = M_{\text{max}}$ and M_{min} , respectively. The gray-shaded region is excluded by the theoretical constraints.

In the nearly alignment case with $s_{\beta-\alpha} = 0.995$ and $m_\Phi = 600$ GeV, the unitarity and vacuum stability bounds exclude the shaded regions. In the case with $c_{\beta-\alpha} < 0$, $A \rightarrow t\bar{t}$ is dominant in all types of 2HDMs since the possible value of the $\tan \beta$ is not enough large. On the other hand, in the case with $c_{\beta-\alpha} < 0$, there are parameter regions with large $\tan \beta$, where $A \rightarrow Zh$ and $A \rightarrow b\bar{b}$ can be dominant.

As we have mentioned, the partial decay width and the decay branching ratio of $A \rightarrow Zh$ can be negative if we truncate the perturbation up to NLO. In Fig. 6, we show $\text{BR}(A \rightarrow Zh)$ including the higher-order corrections with $\tan \beta = 2$ (red), 3 (blue) and 5 (green). We assume that the masses of additional Higgs bosons are degenerate and $m_\Phi = 300$ GeV. The plots in the left (right) column show the results without (with) partial NNLO EW corrections. The first and second

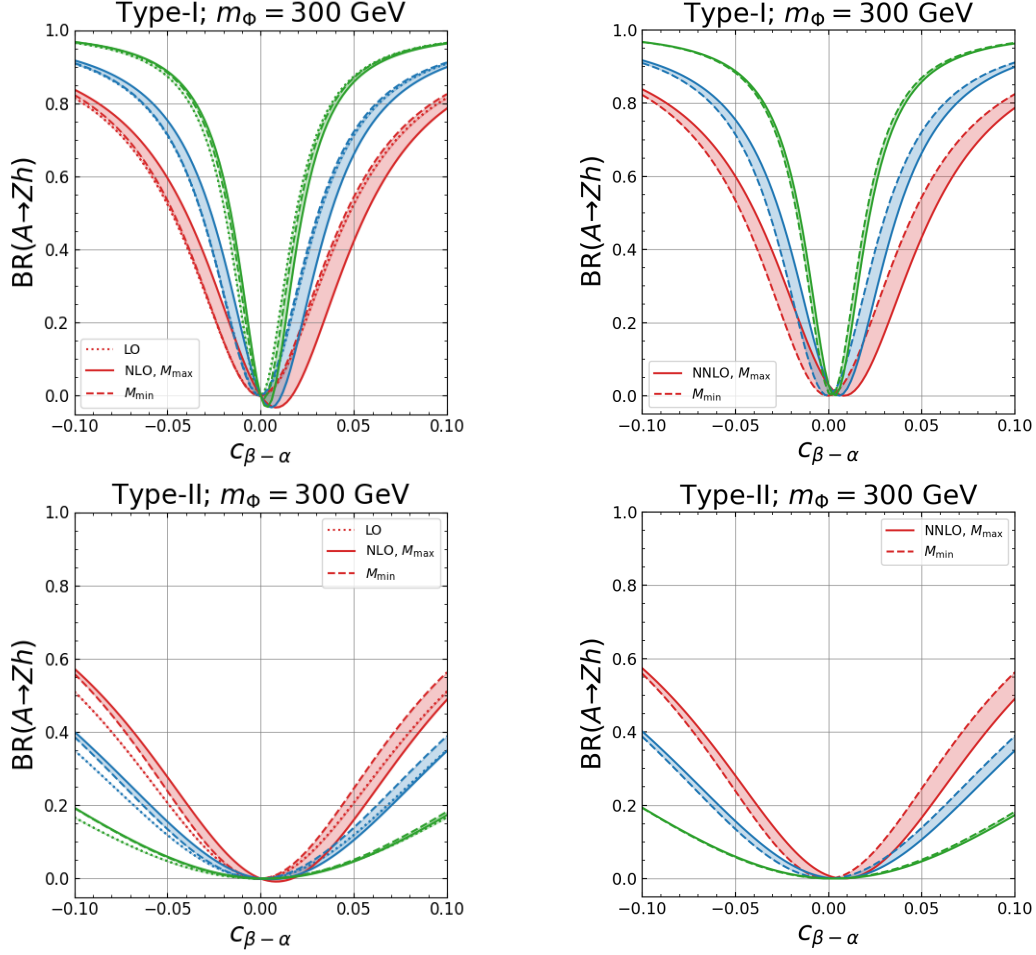


FIG. 6: $\text{BR}(A \rightarrow Zh)$ including the higher-order corrections with $m_\Phi = 300$ GeV, and $\tan\beta=2$ (red), 3 (blue) and 5 (green). We take the masses of additional Higgs bosons to be degenerate. The plots in the left (right) column show the results without (with) partial NNLO EW corrections. The first (second) row shows the results in Type-I (Type-II) 2HDM. M_{\max} (M_{\min}) denotes the maximum (minimum) value of $\sqrt{M^2}$.

rows correspond to the results in Type-I and Type-II 2HDMs, respectively. When we truncate the square of the one-loop amplitude, which corresponds to the two-loop order, the decay branching ratio becomes negative near $c_{\beta-\alpha} = 0$. This is because the tree-level amplitude is proportional to $c_{\beta-\alpha}$, and the LO contribution can be smaller than the NLO contribution. Since the partial decay width must be positive, the calculation up to NLO is not valid near $c_{\beta-\alpha} = 0$.

This problem can be solved by including the square of the NLO amplitude. As shown in the right column of Fig. 6, the decay branching ratio becomes positive even with $c_{\beta-\alpha} \simeq 0$, and it gives a physically meaningful result. Since we have no infrared divergence in the NLO amplitude of $A \rightarrow Zh$, we can safely include the square of the NLO amplitude¹.

¹ In the Higgs-to-Higgs decays of the other additional Higgs bosons, such as $H^\pm \rightarrow W^\pm h$ and $H \rightarrow W^\pm W^\mp$, there

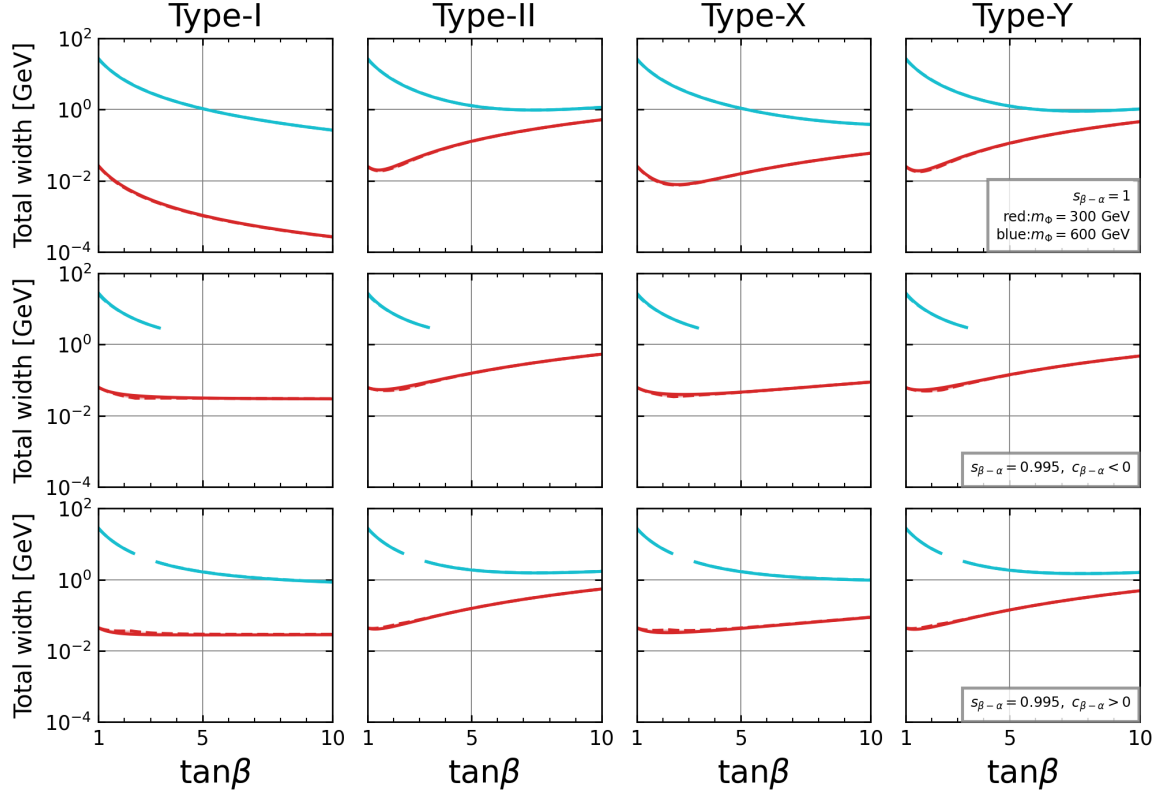


FIG. 7: Total decay width as a function of $\tan\beta$ in the alignment limit $s_{\beta-\alpha} = 1$ (first row) and in the nearly alignment case $s_{\beta-\alpha} = 0.995$ with $c_{\beta-\alpha} < 0$ (second row) and $c_{\beta-\alpha} > 0$ (third row) including the higher-order EW and QCD corrections. The masses of the additional Higgs bosons are degenerate and taken to be $m_\Phi = 300$ GeV (red) and 600 GeV (blue). The solid and dashed lines correspond to the results with $\sqrt{M^2} = M_{\max}$ and M_{\min} , respectively. The lines with $m_\Phi = 600$ GeV are terminated when $c_{\beta-\alpha} < 0$ and they are discontinuous when $c_{\beta-\alpha} > 0$ due to the unitarity and vacuum stability bounds.

B. Total decay width

In this subsection, we discuss the total decay width of the CP-odd Higgs boson including the higher-order corrections in the four types of 2HDMs. Similar to the decay branching ratio, the qualitative behavior does not change from those at LO.

In Fig. 7, we show the total decay width of the CP-odd Higgs boson including the higher-order corrections as a function of $\tan\beta$. We assume that the masses of additional Higgs bosons are degenerate, and the red and blue lines correspond to $m_\Phi = 300$ and 600 GeV, respectively. As

are infrared divergences in the NLO amplitude. In order to make the partial decay widths of these decay processes positive even when $c_{\beta-\alpha}$ closes to zero, we need to take into account higher-order corrections to real photon emission.

similar to the Figs. 4 and 5, we have scanned $\sqrt{M^2}$ under the theoretical constraints and S and T parameters.

In Type-I with the alignment limit, the total decay width monotonically decreases as $\tan \beta$ becomes large because the partial decay widths of $A \rightarrow f\bar{f}$ and $A \rightarrow gg$ are proportional to $\cot^2 \beta$. On the other hand, the total decay width increases as $\tan \beta$ becomes large in the other types of 2HDMs since either or both $A \rightarrow b\bar{b}$ and $A \rightarrow \tau\bar{\tau}$ are enhanced, especially with $m_\Phi = 300$ GeV. Above the top-quark threshold, $A \rightarrow t\bar{t}$ is dominant, and we cannot see sizable enhancement in the total decay width below $\tan \beta = 10$.

In the nearly alignment scenario with $m_\Phi = 300$ GeV, the total decay width behaves as almost constant in Type-I, since the dominant $A \rightarrow Zh$ is independent of $\tan \beta$ at the LO. In the other types of 2HDMs, $A \rightarrow b\bar{b}$ or $A \rightarrow \tau\bar{\tau}$ is enhanced as $\tan \beta$ becomes large, and they increase the total decay width. Above the top-quark thresholds, $A \rightarrow t\bar{t}$ is dominant, and the behavior is almost the same as that in the alignment limit. Since the unitarity and vacuum stability bounds exclude the parameter regions as shown in Fig. 5, the lines with $m_\Phi = 600$ GeV are terminated when $c_{\beta-\alpha} < 0$ and they are discontinuous when $c_{\beta-\alpha} > 0$.

C. Impact of NLO EW corrections to the decay rates

In this subsection, we examine the impact of NLO EW corrections on the decay rates of the CP-odd Higgs boson in Type-I and Type-II. We do not show the results in Type-X and Type-Y since they are almost similar to those in Type-I or Type-II. We introduce the following quantity to parametrize the NLO EW corrections.

$$\Delta_{\text{EW}}(A \rightarrow XY) = \frac{\Gamma_{\text{LO+EW}}(A \rightarrow XY)}{\Gamma_{\text{LO}}(A \rightarrow XY)} - 1, \quad (\text{IV.1})$$

where $\Gamma_{\text{LO+EW}}(A \rightarrow XY)$ is the decay rate of $A \rightarrow XY$ including the NLO EW correction but no QCD correction. For the calculation of decay rates at LO, $\Gamma_{\text{LO}}(A \rightarrow XY)$, we employ the quark pole masses, instead of the running masses. The NLO EW corrections on the total decay width are parameterized by

$$\Delta_{\text{EW}}^{\text{tot}} = \frac{\Gamma_{\text{LO+EW}}^{\text{tot}}}{\Gamma_{\text{LO}}^{\text{tot}}} - 1, \quad (\text{IV.2})$$

where $\Gamma_{\text{LO+EW}}^{\text{tot}}$ is the total decay width of the CP-odd Higgs boson including the NLO EW corrections but no QCD correction. As similar to $\Delta_{\text{EW}}(A \rightarrow XY)$, we use the quark pole masses in the calculation of total decay width at LO, $\Gamma_{\text{LO}}^{\text{tot}}$.

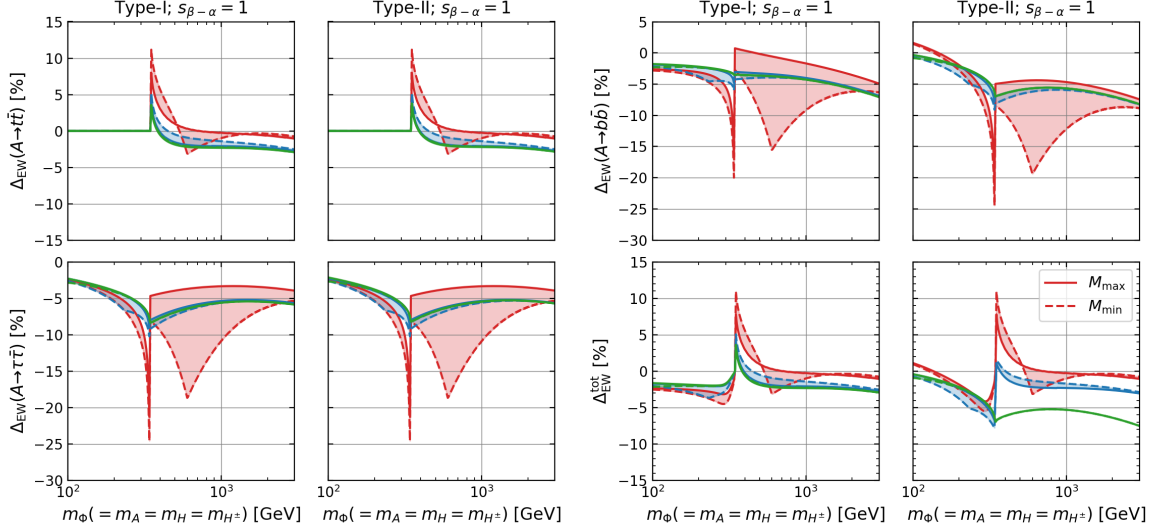


FIG. 8: NLO EW corrections to the partial decay widths of the CP-odd Higgs boson with $s_{\beta-\alpha} = 1$ and $\tan \beta = 1$ (red), 3 (blue), 10 (green). Masses of additional Higgs bosons are degenerate, $m_{\Phi} = m_{H^{\pm}} = m_A = m_H$. $M_{max}(M_{min})$ denotes the maximum (minimum) value of $\sqrt{M^2}$ satisfying the theoretical constraints and S, T parameters.

We evaluate $\Delta_{EW}(A \rightarrow XY)$ and Δ_{EW}^{tot} in the alignment limit, $s_{\beta-\alpha} = 1$, and the nearly alignment scenario, $s_{\beta-\alpha} = 0.995$ with $c_{\beta-\alpha} < 0$ and $c_{\beta-\alpha} > 0$. We assume that the masses of additional Higgs bosons are degenerate. For each scenario, we take $\tan \beta = 1, 3$, and 10, and scan $\sqrt{M^2}$ under the constraints of perturbative unitarity, vacuum stability and S and T parameters. In order to discuss the theoretical behavior of NLO EW corrections, we dare to omit the constraint from the direct and indirect search and flavor experiment.

In Fig. 8, we show $\Delta_{EW}(A \rightarrow XY)$ as a function of m_{Φ} with $s_{\beta-\alpha} = 1$. The red, blue, and green colored regions correspond to $\tan \beta = 1, 3$, and 10, respectively. The solid and dashed lines correspond to the results with maximum and minimum values of $\sqrt{M^2}$ under the constraints, respectively.

For $\tan \beta = 1$, there are two kinks at $m_{\Phi} \simeq 350$ GeV and $m_{\Phi} \simeq 600$ GeV. The kink at $m_{\Phi} \simeq 350$ GeV is the threshold of the top quark. For $A \rightarrow t\bar{t}$, threshold effects appear both in 1PI triangle diagrams and top-quark loop diagrams in the two-point function of the neutral Higgs bosons. The latter contributions also appear in $A \rightarrow b\bar{b}$ and $A \rightarrow \tau\bar{\tau}$. The kink at $m_{\Phi} \simeq 600$ GeV corresponds to the point where the minimum value of $\sqrt{M^2}$ changes from zero to non-zero due to the theoretical bounds. At this point, the scalar couplings take maximal value under the constraints, especially from perturbative unitarity, and the non-decoupling effects of scalar loops

become dominant. The behaviors of $\Delta_{\text{EW}}(A \rightarrow t\bar{t})$ and $\Delta_{\text{EW}}(A \rightarrow \tau\bar{\tau})$ in Type-I are almost the same as those in Type-II. The size of non-decoupling effects for $\Delta_{\text{EW}}(A \rightarrow t\bar{t})$ reaches about -3% , while that for $\Delta_{\text{EW}}(A \rightarrow \tau\bar{\tau})$ reaches about -19% . On the other hand, the behavior of $\Delta_{\text{EW}}(A \rightarrow b\bar{b})$ in Type-I is different from that in Type-II. This is because of the contributions from 1PI diagrams including the virtual G^\pm, H^\pm and W^\pm bosons, that proportional to $\zeta_t\zeta_b$. Due to the large top Yukawa coupling and the type dependence of $\zeta_t\zeta_b$, the behavior of $\Delta_{\text{EW}}(A \rightarrow b\bar{b})$ depends on the types of 2HDMs. The size of non-decoupling effects for $\Delta_{\text{EW}}(A \rightarrow b\bar{b})$ reaches about -15% and -20% in Type-I and Type-II, respectively.

For $\tan\beta = 3$ and 10 , $\sqrt{M^2}$ is almost degenerate with m_Φ due to the theoretical constraints. $\Delta_{\text{EW}}(A \rightarrow t\bar{t})$ is almost constant above the top threshold, and it is about -2% for $m_\Phi = 1$ TeV. The size of $\Delta_{\text{EW}}(A \rightarrow b\bar{b})$ is about -4% (-6%) for Type-I (Type-II) with $m_\Phi = 1$ TeV, while that of $\Delta_{\text{EW}}(A \rightarrow \tau\bar{\tau})$ is about -5% both in Type-I and Type-II.

The behavior of $\Delta_{\text{EW}}^{\text{tot}}$ in Type-I is different from that in Type-II, especially with $\tan\beta = 10$. In Type-I, it is almost the same as $\Delta_{\text{EW}}(A \rightarrow t\bar{t})$, and $\Delta_{\text{EW}}^{\text{tot}}$ is about -2% for $m_\Phi = 1$ TeV with $\tan\beta = 10$. On the other hand, $\Delta_{\text{EW}}^{\text{tot}}$ is about -5% for $m_\Phi = 1$ TeV with $\tan\beta = 10$ in Type-II. This is because of $\tan\beta$ enhancement of $\text{BR}(A \rightarrow b\bar{b})$ in Type-II. Above the top-quark threshold, $\Delta_{\text{EW}}^{\text{tot}}$ can be expanded as

$$\Delta_{\text{EW}}^{\text{tot}} = \Delta_{\text{EW}}(A \rightarrow t\bar{t})\text{BR}_{\text{LO}}(A \rightarrow t\bar{t}) + \Delta_{\text{EW}}(A \rightarrow b\bar{b})\text{BR}_{\text{LO}}(A \rightarrow b\bar{b}) + \text{other channels.} \quad (\text{IV.3})$$

As we can see from Fig. 5, $\text{BR}(A \rightarrow t\bar{t}) \approx 1$ in Type-I, and $\Delta_{\text{EW}}^{\text{tot}} \approx \Delta_{\text{EW}}(A \rightarrow t\bar{t})$. On the other hand, $\text{BR}(A \rightarrow b\bar{b})$ is also dominant in Type-II with large $\tan\beta$. Therefore, $\Delta_{\text{EW}}(A \rightarrow b\bar{b})$ also contributes to $\Delta_{\text{EW}}^{\text{tot}}$.

In Fig. 9, we show $\Delta_{\text{EW}}(A \rightarrow XY)$ and $\Delta_{\text{EW}}^{\text{tot}}$ as a function of m_Φ with $s_{\beta-\alpha} = 0.995$ and $c_{\beta-\alpha} < 0$. The main differences between the case with $s_{\beta-\alpha} = 1$ and $s_{\beta-\alpha} \neq 1$ are upper bound on m_Φ and the new decay mode $A \rightarrow Zh$. Since we cannot take the decoupling limit keeping $s_{\beta-\alpha} \neq 1$, there is an upper bound on m_Φ , and it should be below 1 TeV with $s_{\beta-\alpha} = 0.995$ and $\tan\beta = 1$ under the theoretical constraints, especially perturbative unitarity. Since the deviation from the alignment limit is small, the qualitative behavior of $\Delta_{\text{EW}}(A \rightarrow f\bar{f})$ is almost unchanged, except for the region with large m_Φ .

The behavior of $\Delta_{\text{EW}}(A \rightarrow Zh)$ in Type-I is almost the same as that in Type-II. There are two kinks at $m_\Phi \simeq 200$ GeV and 350 GeV. The first one corresponds to the threshold effects of Zh , and the second one corresponds to those of the top quark. Near the top-quark threshold, the magnitude of the NLO EW correction is above 50%, while it decreases as m_Φ becomes large.

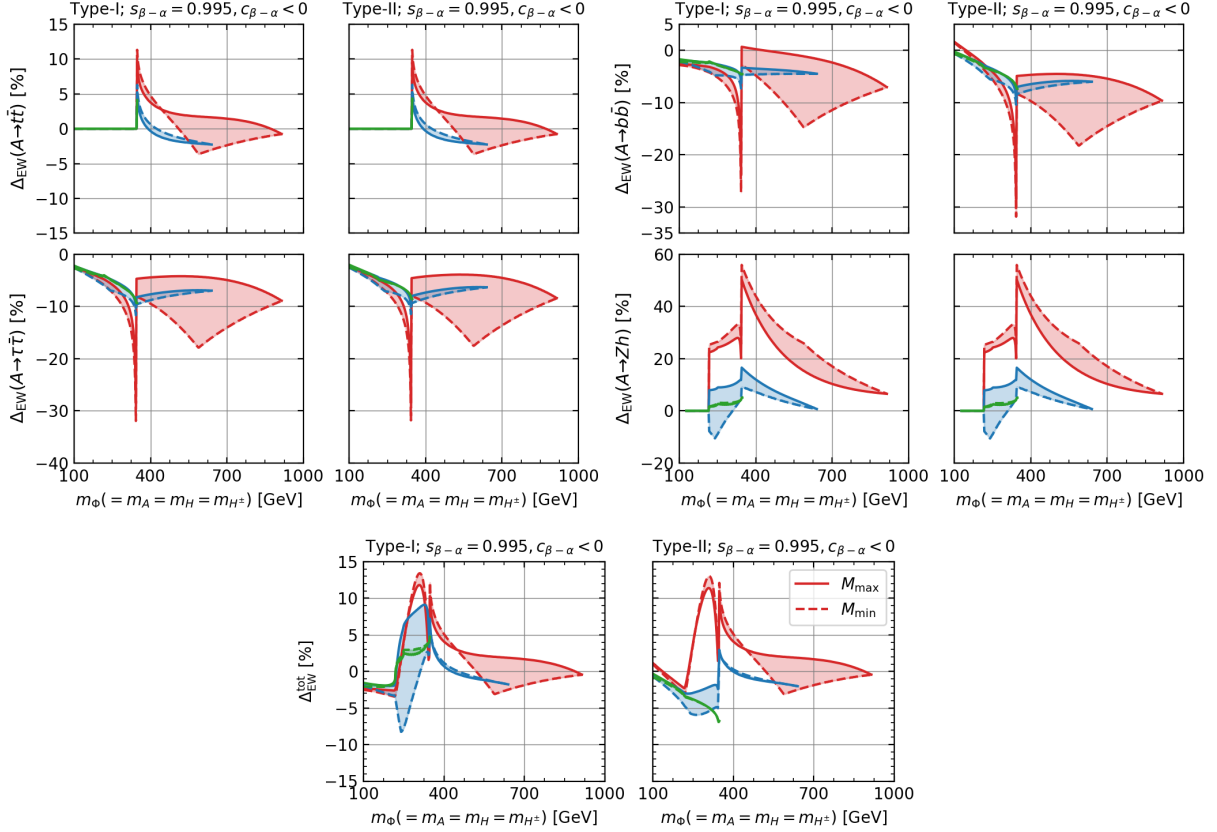


FIG. 9: NLO corrections for the decay widths of the CP-odd Higgs boson with $s_{\beta-\alpha} = 0.995$, $c_{\beta-\alpha} < 0$ and $\tan \beta = 1$ (red), 3 (blue), 10 (green).

When $\tan \beta = 1$, $\Delta_{\text{EW}}(A \rightarrow Zh)$ is positive, and non-decoupling effects of scalar loops enhance its magnitude. On the other hand, non-decoupling effects decrease the size of $\Delta_{\text{EW}}(A \rightarrow Zh)$ when $\tan \beta = 3$, and it can be negative for $m_\Phi \lesssim 300$ GeV.

The behavior of $\Delta_{\text{EW}}^{\text{tot}}$ can be understood by Eq. (IV.3), while we have an additional contribution from $A \rightarrow Zh$. When $\tan \beta = 1$, the behavior of $\Delta_{\text{EW}}^{\text{tot}}$ in Type-I is almost the same as that in Type-II, except for below the Zh threshold. Below the Zh threshold, $A \rightarrow b\bar{b}$ and $A \rightarrow gg$ are the main decay modes, and $\Delta_{\text{EW}}(A \rightarrow b\bar{b})$ causes the difference between Type-I and Type-II. Above the Zh threshold, $A \rightarrow Zh$ and $A \rightarrow gg$ are the main decay modes, while $A \rightarrow t\bar{t}$ also contribute to the decay branching ratio, especially for $m_\Phi \lesssim 2m_t$. Above the top-quark threshold, $A \rightarrow t\bar{t}$ mainly determine $\Delta_{\text{EW}}^{\text{tot}}$. When $\tan \beta = 10$, $A \rightarrow t\bar{t}$ is suppressed by $\cot \beta$, and $A \rightarrow Zh$ can be dominant, while $A \rightarrow b\bar{b}$ also contributes to $\Delta_{\text{EW}}^{\text{tot}}$ in Type-II.

In Fig. 10, we show $\Delta_{\text{EW}}(A \rightarrow XY)$ and $\Delta_{\text{EW}}^{\text{tot}}$ as a function of m_Φ with $s_{\beta-\alpha} = 0.995$ and $c_{\beta-\alpha} > 0$. The main differences from the case with $c_{\beta-\alpha} < 0$ are the possible value of $\tan \beta$ and

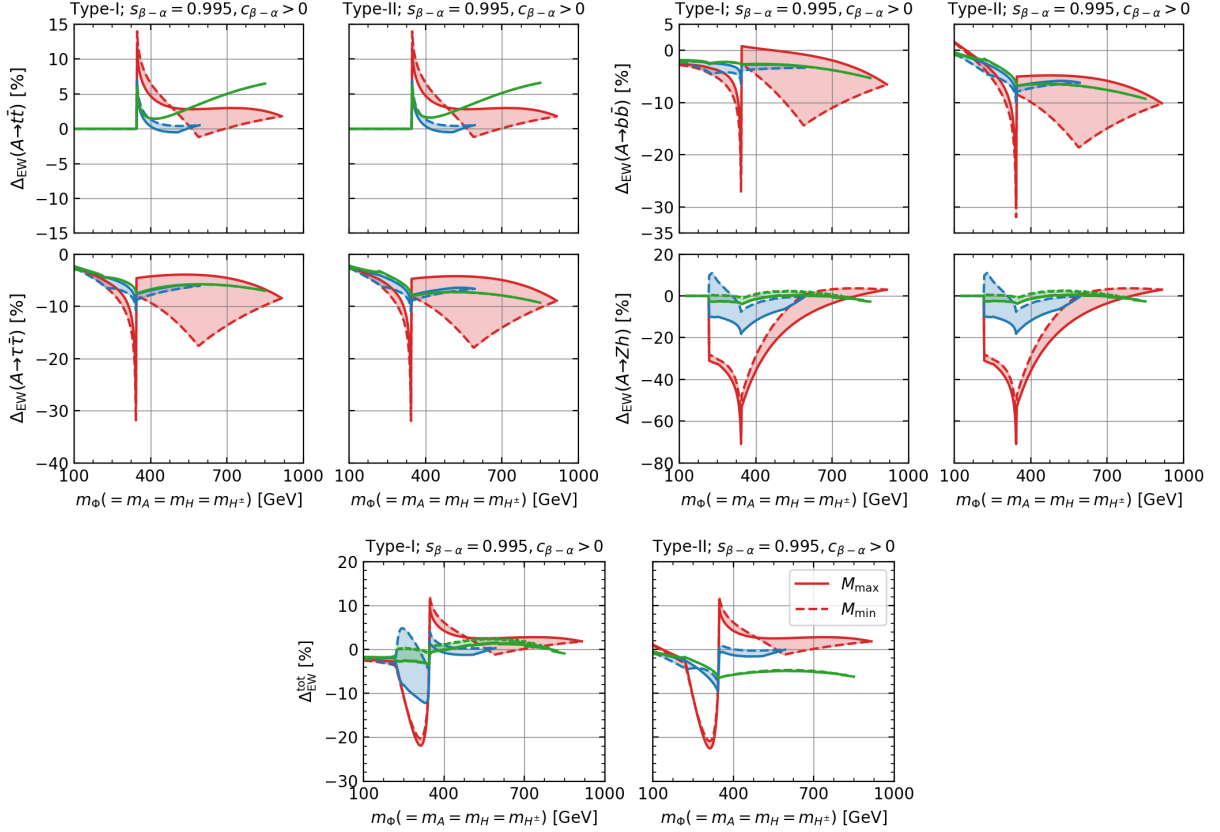


FIG. 10: NLO corrections for the decay widths of the CP-odd Higgs boson with $s_{\beta-\alpha} = 0.995$, $c_{\beta-\alpha} > 0$ and $\tan\beta=1$ (red), 3 (blue), 10 (green).

the sign of $\Delta_{\text{EW}}(A \rightarrow Zh)$. The allowed regions for $\tan\beta = 10$ are broader than those in $c_{\beta-\alpha} < 0$, and the upper bound on m_Φ is about 850 GeV. The sign of the NLO EW corrections to $A \rightarrow Zh$ is opposite to those in $c_{\beta-\alpha} < 0$, and higher-order corrections mainly decrease the partial decay width. Above the top-threshold, the behavior of $\Delta_{\text{EW}}^{\text{tot}}$ is mainly determined by $A \rightarrow t\bar{t}$ and $A \rightarrow Zh$ in Type-I similar to the case with $c_{\beta-\alpha} < 0$, while $A \rightarrow b\bar{b}$ also contributes to $\Delta_{\text{EW}}^{\text{tot}}$ when $\tan\beta$ is large in Type-II.

V. DECAY PATTERN OF THE CP-ODD HIGGS BOSON IN THE NEARLY ALIGNMENT SCENARIO

In this section, we discuss the decay pattern of the CP-odd Higgs boson in the nearly alignment scenario including the higher-order corrections. In addition to the theoretical constraints, we take into account the constraint from the S and T parameters, the signal strength of the SM-like Higgs boson, the direct searches of the additional Higgs bosons, and flavor experiments explained in

Sec. II B. Although there are constraints from the direct searches for $A \rightarrow Zh$ and $H \rightarrow hh$ at the LHC, they are quite sensitive to the value of $s_{\beta-\alpha}$, and the excluded region would be changed when we include the higher-order corrections. Therefore, we dare to omit the constraint from the Higgs-to-Higgs decay modes in this paper. We will study how the higher-order corrections modify the constraints from the direct searches for the additional Higgs bosons elsewhere.

We consider the following two scenarios for the mass spectrum of the additional Higgs bosons.

$$\text{Scenario A : } m_A = m_{H^\pm} = 300 \text{ GeV}, \quad m_A \leq m_H, \quad (\text{V.1})$$

$$\text{Scenario B : } m_A = m_{H^\pm} = 800 \text{ GeV}, \quad m_H \leq m_A - m_Z. \quad (\text{V.2})$$

In order to avoid the constraint from the T parameter, we assume that the Higgs potential respects the custodial symmetry² [105], and the masses of the CP-odd and charged Higgs bosons are degenerate, $m_A = m_{H^\pm}$. In Scenario A, $A \rightarrow t\bar{t}$ does not open, and the CP-odd Higgs boson mainly decays into Zh , $t\bar{t}^*$, $b\bar{b}$, $\tau\bar{\tau}$ and gg as shown in Fig. 4. In Scenario B, the CP-odd Higgs boson mainly decays into Zh , ZH , $t\bar{t}$, $b\bar{b}$ and $\tau\bar{\tau}$ as shown in Fig. 5.

For Scenario A, we study Type-I because Type-II and Type-Y are excluded by the flavor constraints [73], and Type-X is also excluded by the constraint from $A \rightarrow \tau\bar{\tau}$ [7]. We take $\tan\beta = 2$ and 5. The mass of the additional CP-even Higgs boson is scanned as

$$m_A \leq m_H \leq m_A + 500 \text{ GeV}. \quad (\text{V.3})$$

The remaining parameters are scanned as

$$0.995 \leq s_{\beta-\alpha} \leq 1, \quad 0 \leq \sqrt{M^2} \leq m_A + 500 \text{ GeV}, \quad (\text{V.4})$$

with both of $c_{\beta-\alpha} < 0$ and $c_{\beta-\alpha} > 0$. The lower bound on $\tan\beta$ comes from the constraint of $B_d \rightarrow \mu\mu$ [73]. In addition, the region with $\tan\beta \lesssim 2$ is excluded by the direct searches for $A \rightarrow \tau\bar{\tau}$ and $H^\pm \rightarrow tb$ [7].

For Scenario B, we study all types of 2HDMs. We scan $\tan\beta$ as

$$2 < \tan\beta < 10. \quad (\text{V.5})$$

For $m_{H^\pm} = 800 \text{ GeV}$, the region with $\tan\beta \lesssim 1.2$ is excluded for all types of 2HDM by $B_d \rightarrow \mu\mu$ [73]. While there are allowed parameter regions with $\tan\beta \leq 2$, we take $\tan\beta = 2$ as a minimum

² We can also consider the scenario with the twisted-custodial symmetry [102–104], which requires $m_H = m_{H^\pm} = \sqrt{M^2}$ and $s_{\beta-\alpha} = 1$. In this scenario, the Higgs-to-Higgs decays are prohibited.

value conservatively. We also scan the mass of the additional CP-even Higgs bosons as

$$m_A - 500 \text{ GeV} < m_H < m_A - m_Z. \quad (\text{V.6})$$

The scan regions of the remaining parameters are the same as those in Eqs. (V.3) and (V.4).

In order to study the size of the NLO EW corrections on the decay branching ratios, we define $\Delta_{\text{EW}}^{\text{BR}}(A \rightarrow XY)$ as

$$\Delta_{\text{EW}}^{\text{BR}}(A \rightarrow XY) = \frac{\text{BR}_{\text{LO+EW+QCD}}(A \rightarrow XY)}{\text{BR}_{\text{LO+QCD}}(A \rightarrow XY)} - 1, \quad (\text{V.7})$$

where $\text{BR}_{\text{LO+EW+QCD}}(A \rightarrow XY)$ includes the NLO EW and the higher-order QCD corrections, while $\text{BR}_{\text{LO+QCD}}(A \rightarrow XY)$ includes only the higher-order QCD corrections. We employ the running quark masses for the evaluation of the LO parts. At the one-loop level, we can approximate $\Delta_{\text{EW}}^{\text{BR}}(A \rightarrow XY)$ as

$$\Delta_{\text{EW}}^{\text{BR}}(A \rightarrow XY) \approx \bar{\Delta}_{\text{EW}}(A \rightarrow XY) - \bar{\Delta}_{\text{EW}}^{\text{tot}}, \quad (\text{V.8})$$

where $\bar{\Delta}_{\text{EW}}(A \rightarrow XY)$ and $\bar{\Delta}_{\text{EW}}^{\text{tot}}$ are given by

$$\bar{\Delta}_{\text{EW}}(A \rightarrow XY) = \frac{\Gamma_{\text{LO+EW+QCD}}(A \rightarrow XY)}{\Gamma_{\text{LO+QCD}}(A \rightarrow XY)} - 1, \quad (\text{V.9})$$

$$\bar{\Delta}_{\text{EW}}^{\text{tot}} = \frac{\Gamma_{\text{LO+EW+QCD}}^{\text{tot}}}{\Gamma_{\text{LO+QCD}}^{\text{tot}}} - 1. \quad (\text{V.10})$$

For the decays into a pair of quarks, we can approximate $\bar{\Delta}_{\text{EW}}(A \rightarrow Q\bar{Q})$ ($Q = q, t$) as

$$\bar{\Delta}_{\text{EW}}(A \rightarrow Q\bar{Q}) \approx \frac{m_Q^2}{\bar{m}_Q^2(m_A)} \Delta_{\text{EW}}(A \rightarrow Q\bar{Q}), \quad (\text{V.11})$$

where $\Delta_{\text{EW}}(A \rightarrow XY)$ given in Eq. (IV.1). The ratio of the pole and running mass of the quarks enhances the size of $\bar{\Delta}_{\text{EW}}(A \rightarrow Q\bar{Q})$. For instance, $m_b/\bar{m}_b(m_A) \approx 2$ for $m_A = 500 \text{ GeV}$, and the size of $\bar{\Delta}_{\text{EW}}(A \rightarrow b\bar{b})$ becomes four times larger than $\Delta_{\text{EW}}(A \rightarrow b\bar{b})$. For $A \rightarrow \ell\bar{\ell}$ and $A \rightarrow V\phi$, $\bar{\Delta}_{\text{EW}}(A \rightarrow XY) = \Delta_{\text{EW}}(A \rightarrow XY)$ because we have no QCD correction at the one-loop level.

In order to study the deviation in the SM-like Higgs boson coupling, we define $\Delta\kappa_Z$ as

$$\Delta\kappa_Z = \kappa_Z - 1, \quad (\text{V.12})$$

where κ_Z is defined in Eq. (II.22) with the partial decay rate of $h \rightarrow ZZ^*$. In the 2HDM, $\Delta\kappa_Z$ is mostly negative independently of the sign of $c_{\beta-\alpha}$ [27]. On the other hand, allowed parameter regions depend on the sign of $c_{\beta-\alpha}$. Therefore, we take $\text{Sign}(c_{\beta-\alpha})|\Delta\kappa_Z|$ as the horizontal axis in some figures shown below to clearly exhibit the difference due to the sign of the $c_{\beta-\alpha}$.

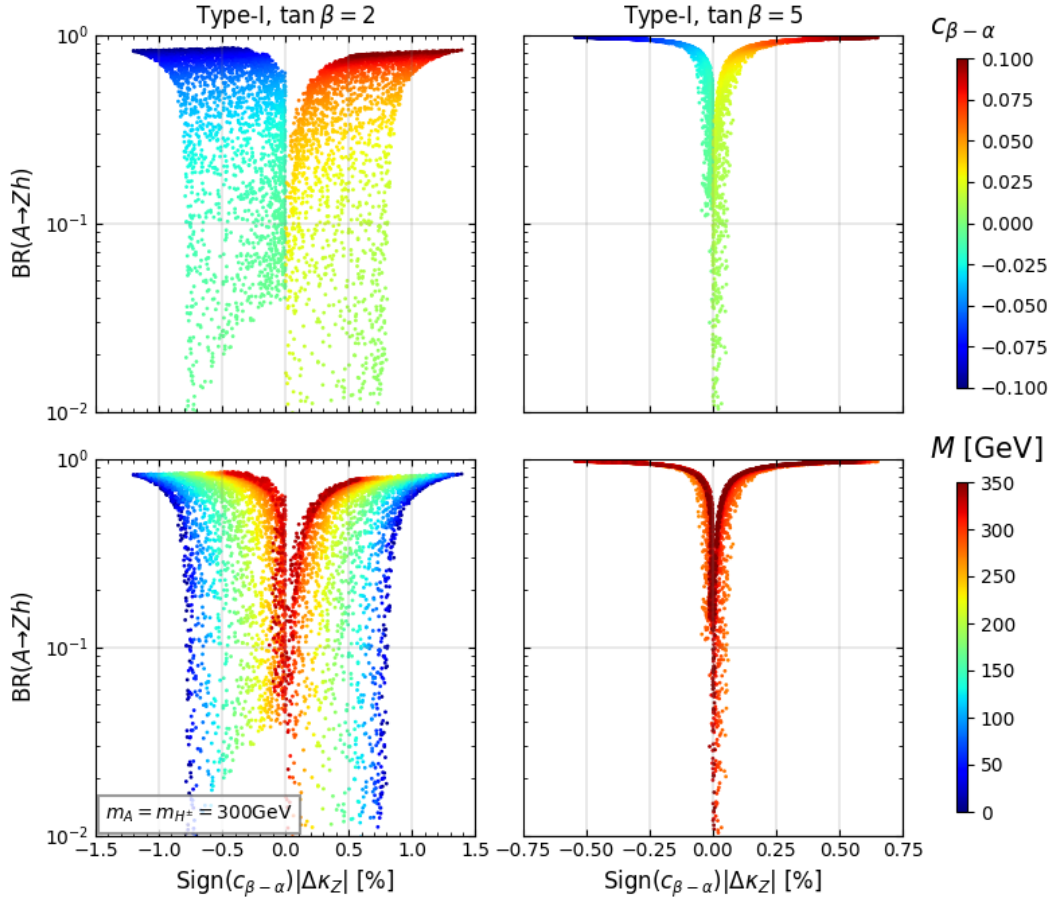


FIG. 11: Decay branching ratios of $A \rightarrow Zh$ in Type-I 2HDM in Scenario A. The color differences correspond to the values of $c_{\beta-\alpha}$ and $\sqrt{M^2}$, in the top and bottom panels, respectively.

A. Scenario A

In Fig. 11, we show the branching ratio of $A \rightarrow Zh$ including the NLO EW corrections in Type-I for Scenario A. The plots in the first column are the results with $\tan \beta = 2$, while those in the second column are the results with $\tan \beta = 5$. The color differences correspond to the values of $c_{\beta-\alpha}$ and $\sqrt{M^2}$ in the top and bottom panels, respectively. When $c_{\beta-\alpha} \simeq 0.1$, $\text{BR}(A \rightarrow Zh)$ reaches almost 80% (100%) for $\tan \beta = 2$ (5). Since $\Delta\kappa_Z$ is proportional to $|c_{\beta-\alpha}|$ at LO, we expect that $\text{BR}(A \rightarrow Zh)$ becomes large when $\Delta\kappa_Z$ is large. However, this is not necessarily true when we include NLO corrections. When $\tan \beta = 2$, we have the parameter points, where $\Delta\kappa_Z$ sizably deviates from the SM value, while the $\text{BR}(A \rightarrow Zh)$ is small. This is because of the non-decoupling scalar-loop effects in $\Delta\kappa_Z$. When $\sqrt{M^2} \approx 0$, the non-decoupling effects make $\Delta\kappa_Z$ large even with $c_{\beta-\alpha} \approx 0$. When $\tan \beta = 5$, $\sqrt{M^2}$ is almost degenerate with m_A due to perturbative unitarity

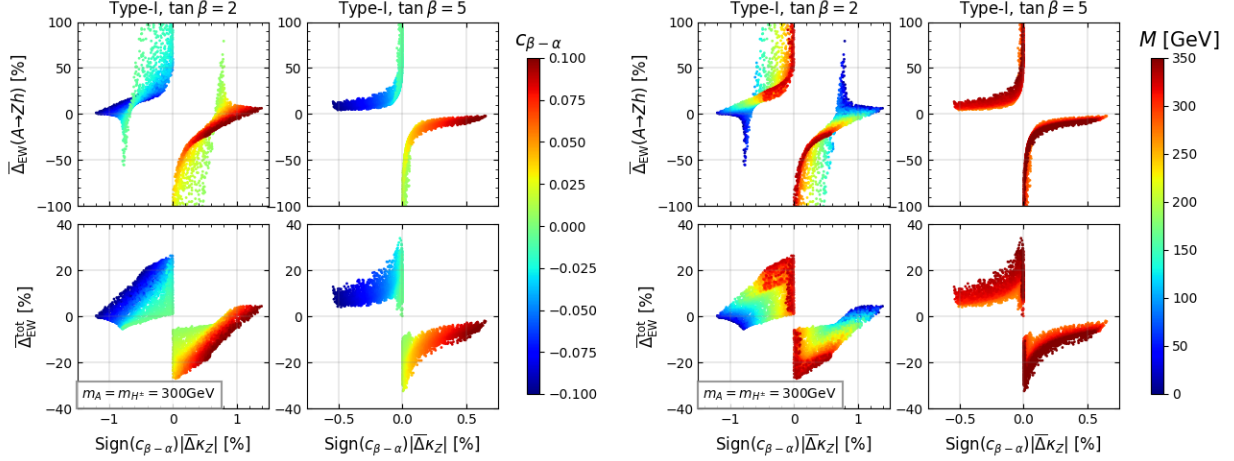


FIG. 12: NLO corrections to the decay rates of $A \rightarrow Zh$ and the total decay width of the CP-odd Higgs boson in Type-I 2HDM in Scenario A. The color differences correspond to the values of $c_{\beta-\alpha}$ and $\sqrt{M^2}$, in the left and right panels, respectively.

and vacuum stability, and the size of the higher-order corrections is smaller than the tree-level contributions. Therefore, the correlation between $\text{BR}(A \rightarrow Zh)$ and $\Delta\kappa_Z$ follows the expectation at LO. We note that $\text{BR}(A \rightarrow Zh)$ can reach about 100% even with $\Delta\kappa_Z \leq 0.6$, where it is difficult to observe the deviation in the hZZ coupling at the ILC250 [106]. In this sense, $A \rightarrow Zh$ is useful to explore the nearly alignment scenario.

In Fig. 12, we show the size of NLO EW corrections to the decay rates $\overline{\Delta}_{\text{EW}}(A \rightarrow Zh)$ and the total decay width $\overline{\Delta}_{\text{EW}}^{\text{tot}}$. The plots in the first and third columns are the results with $\tan\beta = 2$, while those in the second and fourth columns are the results with $\tan\beta = 5$. The color differences correspond to the values of $c_{\beta-\alpha}$ and $\sqrt{M^2}$ in the left and right panels, respectively. The sign of $\overline{\Delta}_{\text{EW}}(A \rightarrow Zh)$ is opposite with the sign of $c_{\beta-\alpha}$, except for $\sqrt{M^2} \lesssim 150$ GeV with $\tan\beta = 2$. The size of $\overline{\Delta}_{\text{EW}}(A \rightarrow Zh)$ becomes quite large when $c_{\beta-\alpha} \simeq 0$ since the LO contribution is close to zero. We note that such large $\overline{\Delta}_{\text{EW}}(A \rightarrow Zh)$ does not mean a breakdown of the perturbation, since it is caused by the smallness of the tree-level coupling. When $\sqrt{M^2} \lesssim 150$ GeV with $\tan\beta = 2$, the non-decoupling effects of scalar loops change the sign of $\overline{\Delta}_{\text{EW}}(A \rightarrow Zh)$ as shown Figs. 9 and 10. In addition, $\overline{\Delta}_{\text{EW}}(A \rightarrow Zh)$ becomes large due to the smallness of the LO contribution, while $\Delta\kappa_Z$ takes large value even if $c_{\beta-\alpha} \simeq 0$ due to the non-decoupling effects. Therefore, we have two kinks around $|\kappa_Z| \simeq 0.8$ with $c_{\beta-\alpha} \simeq 0$.

As similar to Eq. (IV.3), we can expand $\overline{\Delta}_{\text{EW}}^{\text{tot}}$ as

$$\overline{\Delta}_{\text{EW}}^{\text{tot}} = \overline{\Delta}_{\text{EW}}(A \rightarrow b\bar{b})\text{BR}_{\text{LO}}(A \rightarrow b\bar{b}) + \overline{\Delta}_{\text{EW}}(A \rightarrow Zh)\text{BR}_{\text{LO}}(A \rightarrow Zh)$$

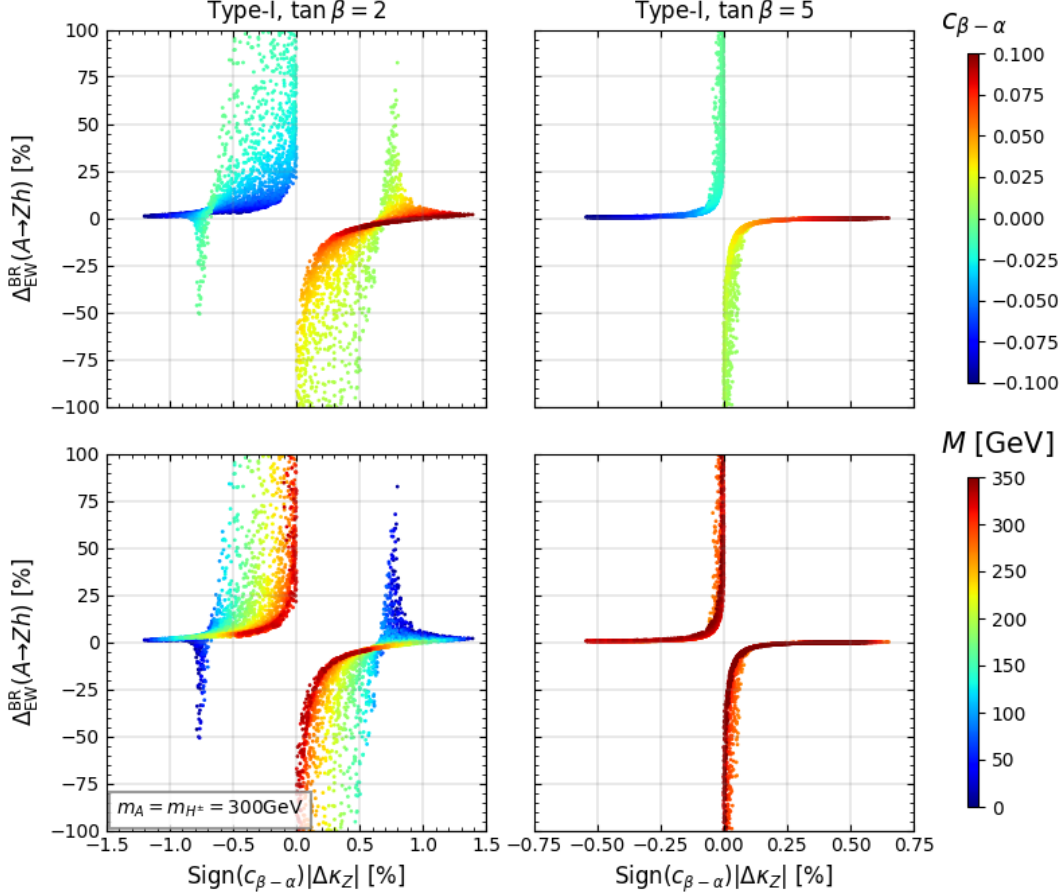


FIG. 13: NLO corrections to the decay branching ratios of the CP-odd Higgs boson in Type-I 2HDM in Scenario A. The color differences correspond to the values of $c_{\beta-\alpha}$ and $\sqrt{M^2}$, in the top and bottom panels, respectively.

$$+ \text{ other channels.} \quad (\text{V.13})$$

When $c_{\beta-\alpha} \simeq 0.1$, the behavior of $\overline{\Delta}_{\text{EW}}^{\text{tot}}$ is mainly determined by $\overline{\Delta}_{\text{EW}}(A \rightarrow Zh)$ since $\text{BR}_{\text{LO}}(A \rightarrow Zh)$ is dominant. On the other hand, when $c_{\beta-\alpha} \simeq 0$, both $\overline{\Delta}_{\text{EW}}(A \rightarrow b\bar{b})$ and $\overline{\Delta}_{\text{EW}}(A \rightarrow Zh)$ contribute to $\overline{\Delta}_{\text{EW}}^{\text{tot}}$. While $\overline{\Delta}_{\text{EW}}(A \rightarrow Zh)$ takes quite large value with $c_{\beta-\alpha} \simeq 0$, $\text{BR}_{\text{LO}}(A \rightarrow Zh)$ is close to zero. Therefore, we have no singular behavior on $\overline{\Delta}_{\text{EW}}^{\text{tot}}$ even at $|\Delta\kappa_Z| \simeq 0$.

In Fig. 13, we show the size of NLO EW corrections to the decay branching ratios $\Delta_{\text{EW}}^{\text{BR}}(A \rightarrow Zh)$. The behavior of $\Delta_{\text{EW}}^{\text{BR}}(A \rightarrow Zh)$ can be understood from $\overline{\Delta}_{\text{EW}}(A \rightarrow Zh)$ and $\overline{\Delta}_{\text{EW}}^{\text{tot}}$ as shown in Eq. (V.8). When $c_{\beta-\alpha} \simeq 0.1$, $\text{BR}_{\text{LO}}(A \rightarrow Zh) \simeq 1$ and $\Delta_{\text{EW}}^{\text{tot}} \simeq \Delta_{\text{EW}}(A \rightarrow Zh)$. Therefore, $\overline{\Delta}_{\text{EW}}(A \rightarrow Zh)$ and $\overline{\Delta}_{\text{EW}}^{\text{tot}}$ are canceled out, and $\Delta_{\text{EW}}^{\text{BR}}(A \rightarrow XY)$ is close to zero. When $c_{\beta-\alpha} \simeq 0$, $\text{BR}_{\text{LO}}(A \rightarrow Zh) \simeq 0$ and $\Delta_{\text{EW}}^{\text{BR}}(A \rightarrow Zh)$ can be larger than 100%.

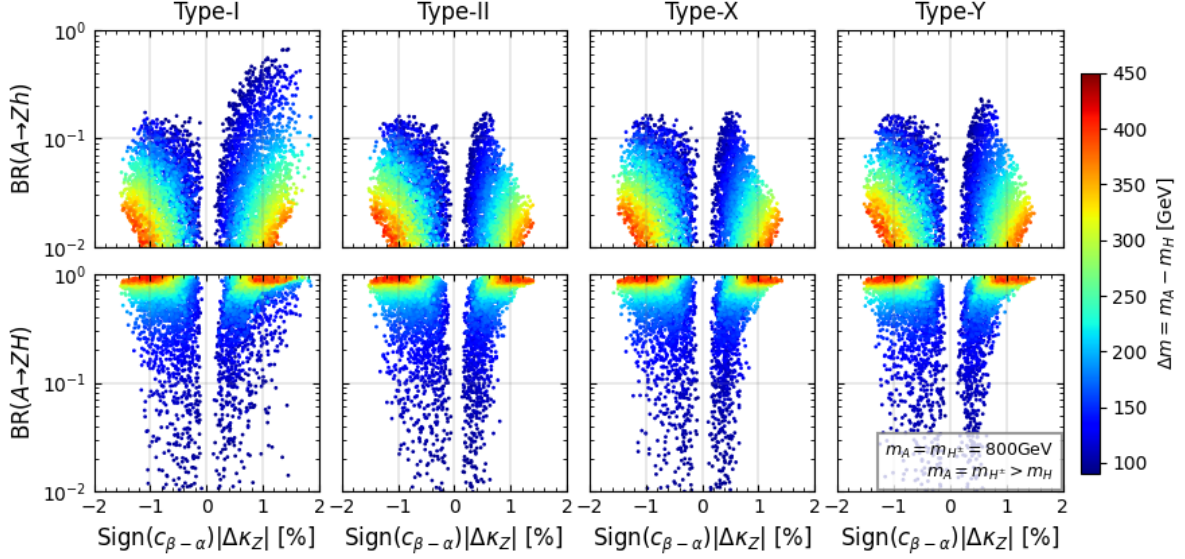


FIG. 14: Decay branching ratios of the CP-odd Higgs boson in Scenario B. Predictions on Type-I, Type-II, Type-X and Type-Y are shown from the left to the right panels in order. The color differences correspond to the values of $\Delta m = m_A - m_H$.

B. Scenario B

In Fig. 14, we show the branching ratios of the CP-odd Higgs boson including the NLO EW corrections in Scenario B. The results in Type-I, Type-II, Type-X and Type-Y are shown from the left to the right panels in order. The color differences correspond to the values of $\Delta m = m_A - m_H$. In Scenario B, $A \rightarrow ZH$ is open in addition to $A \rightarrow Zh$, $t\bar{t}$, $b\bar{b}$ and $\tau\bar{\tau}$, and it can be the dominant decay mode depending on Δm . The value of $\tan \beta$ is approximately 2 independently of the types of 2HDM for both $c_{\beta-\alpha} > 0$ and $c_{\beta-\alpha} < 0$. The exceptional regions, where $\tan \beta$ can be large are $c_{\beta-\alpha} \simeq 0$ in all types of 2HDMs and $c_{\beta-\alpha} > 0$ in Type-I. The value of $\sqrt{M^2}$ is almost degenerate with m_H . As similar to Scenario A with $\tan \beta = 2$, we have parameter regions where non-decoupling effects enlarge $\Delta\kappa_Z$ even with $c_{\beta-\alpha} \simeq 0$ in all types of 2HDMs. The maximal size of $\Delta\kappa_Z$ with $c_{\beta-\alpha} \simeq 0$ is about 1%. On the other hand, $\Delta\kappa_Z$ can be larger than 1% if $c_{\beta-\alpha} \neq 0$, and $\Delta\kappa_Z$ reaches about 1.5% independently of the types of 2HDM for both $c_{\beta-\alpha} > 0$ and $c_{\beta-\alpha} < 0$.

For $A \rightarrow Zh$, the branching ratio reaches about 80% (20%) in Type-I with $c_{\beta-\alpha} > 0$ ($c_{\beta-\alpha} < 0$). In Type-II, Type-X, and Type-Y, it reaches about 20% independently of the sign of $c_{\beta-\alpha}$. The branching ratio of $A \rightarrow ZH$ reaches about 100% independently of the types of 2HDMs when $\Delta m \gtrsim 300$ GeV. Since the tree-level AZH coupling is proportional to $s_{\beta-\alpha}$, we expect that $\text{BR}(A \rightarrow ZH)$ can be large with $\Delta\kappa_Z \simeq 0$. However, $\text{BR}(A \rightarrow ZH)$ tends to be small when

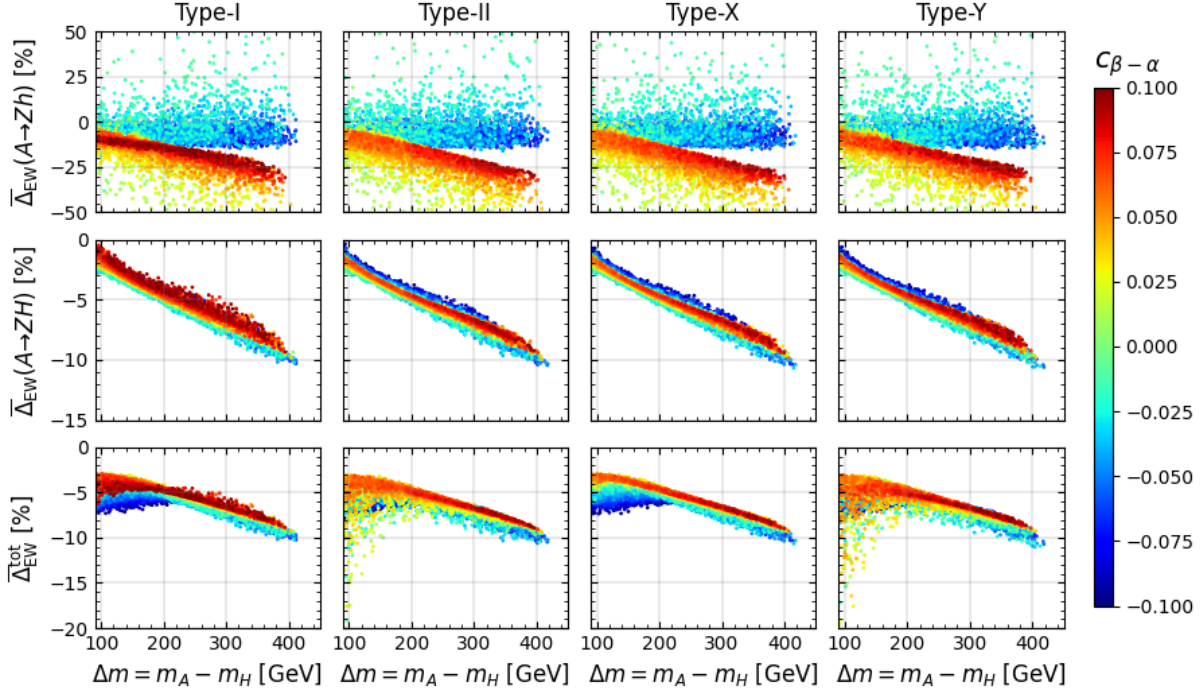


FIG. 15: NLO corrections to the decay rates and the total decay width of the CP-odd Higgs boson as a function of $m_A - m_H$ in Scenario B. Predictions on Type-I, Type-II, Type-X and Type-Y are shown from the left to the right panels in order. The color differences correspond to the values of $c_{\beta-\alpha}$.

$\Delta\kappa_Z \simeq 0$. This is because of the theoretical bounds such as perturbative unitary and vacuum stability. If Δm is so large that $\text{BR}(A \rightarrow ZH) \simeq 1$, $c_{\beta-\alpha} \neq 0$ is favored by the theoretical bounds, and $\Delta\kappa_Z$ becomes large due to the both of tree-level mixing and the non-decoupling effects.

In Fig. 15, we show the size of $\overline{\Delta}_{\text{EW}}(A \rightarrow XY)$ and $\overline{\Delta}_{\text{EW}}^{\text{tot}}$ as a function of Δm . The color differences correspond to the values of $c_{\beta-\alpha}$. We find that both $\overline{\Delta}_{\text{EW}}(A \rightarrow Zh)$ and $\overline{\Delta}_{\text{EW}}(A \rightarrow ZH)$ are the almost same among all types of 2HDMs, while $\overline{\Delta}_{\text{EW}}^{\text{tot}}$ shows type-dependent behavior, especially for $\Delta m \lesssim 200$ GeV. When $c_{\beta-\alpha} < 0$, the magnitude of $\overline{\Delta}_{\text{EW}}(A \rightarrow Zh)$ is almost independent of Δm . On the other hand, it monotonically increases as Δm becomes large when $c_{\beta-\alpha} > 0$. We note that $\overline{\Delta}_{\text{EW}}(A \rightarrow Zh)$ can be larger than 100% if $c_{\beta-\alpha}$ is quite small, while we take the range of $\overline{\Delta}_{\text{EW}}(A \rightarrow Zh)$ as $[-50, 50]\%$ for the illustration purpose. The magnitude of $\overline{\Delta}_{\text{EW}}(A \rightarrow ZH)$ increases as Δm becomes large due to the non-decoupling effects of scalar loops. When $\Delta m \gtrsim 200$ GeV, $\overline{\Delta}_{\text{EW}}^{\text{tot}}$ is mainly determined by $A \rightarrow ZH$, and its magnitude increases as Δm becomes large in all types of 2HDMs. In Type-II and Type-Y, $A \rightarrow b\bar{b}$ contributes to $\overline{\Delta}_{\text{EW}}^{\text{tot}}$ when $\Delta m \lesssim 200$ GeV with large $\tan\beta$, and $\overline{\Delta}_{\text{EW}}^{\text{tot}}$ reaches about -20% .

In Fig. 16, we show the size of $\Delta_{\text{EW}}^{\text{BR}}(A \rightarrow XY)$ as a function of Δm . The color differences

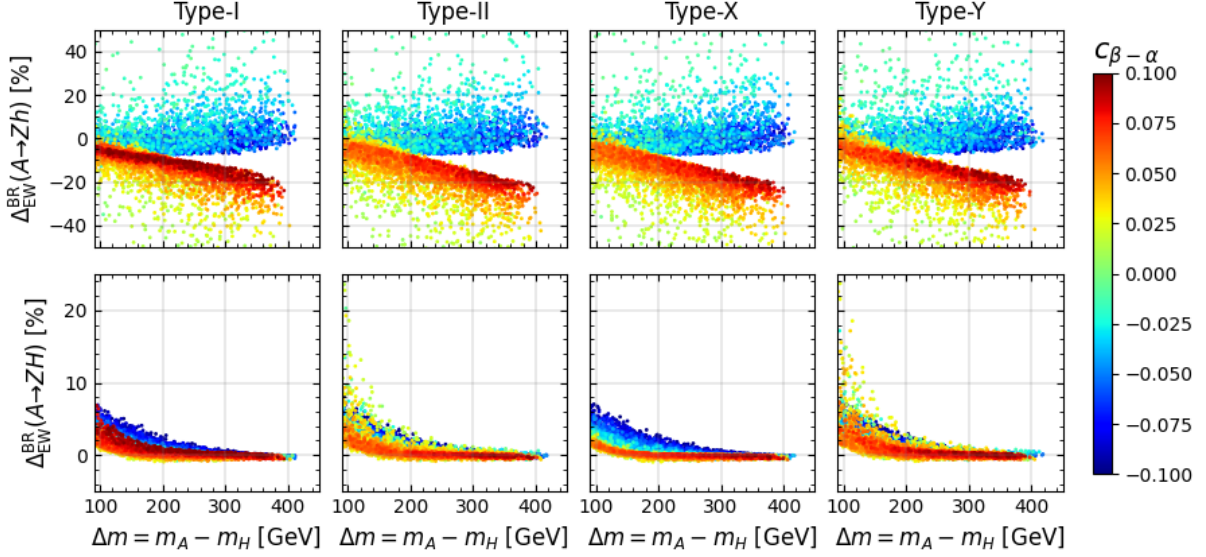


FIG. 16: NLO corrections to the decay branching ratios for the CP-odd Higgs boson as a function of $m_A - m_H$ in Scenario B. Predictions on Type-I, Type-II, Type-X and Type-Y are shown from the left to the right panels in order. The color differences correspond to the values of $c_{\beta-\alpha}$.

correspond to the values of $c_{\beta-\alpha}$. $\Delta_{\text{EW}}^{\text{BR}}(A \rightarrow Zh)$ is negative when $c_{\beta-\alpha} > 0$, while it can be positive when $c_{\beta-\alpha} < 0$ due to the contribution of $\overline{\Delta}_{\text{EW}}^{\text{tot}}$. $\Delta_{\text{EW}}^{\text{BR}}(A \rightarrow ZH)$ is close to zero in large Δm region due to the cancellation between $\overline{\Delta}_{\text{EW}}(A \rightarrow ZH)$ and $\Delta_{\text{EW}}^{\text{tot}}$. When $\Delta m \lesssim 150$ GeV and $c_{\beta-\alpha} \simeq 0$, $\Delta_{\text{EW}}^{\text{BR}}(A \rightarrow ZH)$ becomes large in Type-II and Type-Y, where $A \rightarrow b\bar{b}$ contributes to $\overline{\Delta}_{\text{EW}}^{\text{tot}}$.

Finally, we would like to comment on the difference between our results and those in Ref. [39]. We have compared the maximum value of $\Delta_{\text{EW}}^{\text{BR}}(A \rightarrow XY)$ with those in Table 13 in Ref. [39], and it was found that our results for $\Delta_{\text{EW}}^{\text{BR}}(A \rightarrow t\bar{t})$ and $\Delta_{\text{EW}}^{\text{BR}}(A \rightarrow b\bar{b})$ take larger values. For example, $\Delta_{\text{EW}}^{\text{BR}}(A \rightarrow b\bar{b})$ reaches -40% in Scenario B, while the maximum value is about 20% in Ref. [39] (See the discussion in Appendix G). This difference might be understood by the treatment of the running quark masses because the sizes of the EW corrections are enhanced by the ratio of the pole and running quark masses as shown in Eq. (V.11). Although the size of the EW corrections for the total decay width also depends on the treatment of the quark masses, we have found that the results for $A \rightarrow \tau\bar{\tau}$, $A \rightarrow Zh$ and $A \rightarrow ZH$ are consistent with Ref. [39].

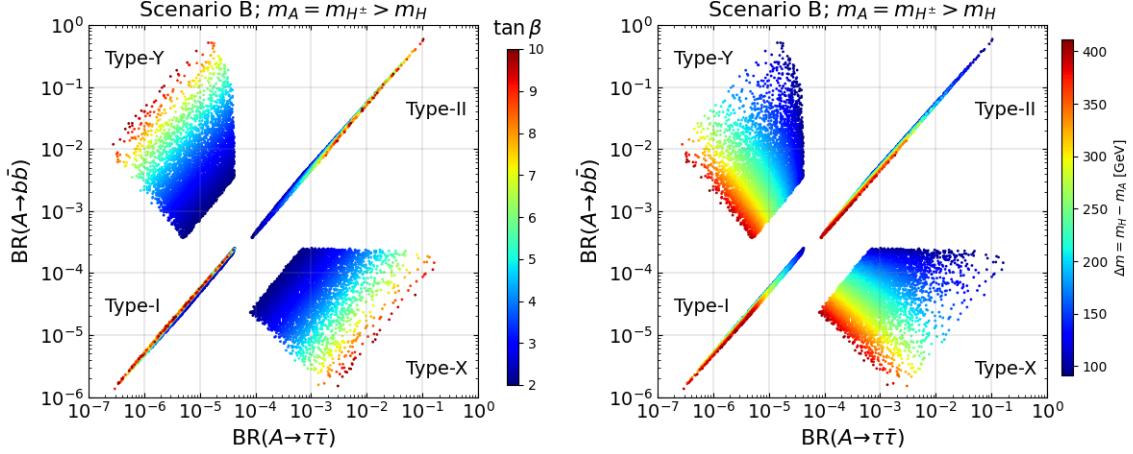


FIG. 17: Correlation between $BR(A \rightarrow \tau\bar{\tau})$ and $BR(A \rightarrow b\bar{b})$ in Type-I, Type-II, Type-X and Type-Y for Scenario B. The color differences correspond to the values of $\tan\beta$ and Δm in the left and the right panels, respectively.

C. Discrimination of Types of the Yukawa interaction in the 2HDMs

In this subsection, we discuss the discrimination of the types of 2HDMs by the decays of the CP-odd Higgs boson. Since $\Gamma_{Af\bar{f}}^{P,\text{tree}}$ is proportional to ζ_f , we can discriminate the types of 2HDMs by the correlations among $BR(A \rightarrow f\bar{f})$. We study the correlation between $BR(A \rightarrow \tau\bar{\tau})$ and $BR(A \rightarrow b\bar{b})$ including the NLO EW and higher-order QCD corrections in Type-I, Type-II, Type-X and Type-Y in Scenario B.

In Fig. 17, we show the correlation between $BR(A \rightarrow \tau\bar{\tau})$ and $BR(A \rightarrow b\bar{b})$ in Scenario B. The color differences correspond to the values of $\tan\beta$ and Δm in the left and right panels, respectively. In Scenario B, there is $A \rightarrow ZH$, and it can be dominant depending on Δm . From the left panel of Fig. 17, we can see that both $BR(A \rightarrow \tau\bar{\tau})$ and $BR(A \rightarrow b\bar{b})$ become small in Type-I, while both of them can take several dozens of percent due to the $\tan\beta$ enhancement in Type-II. On the other hand, $BR(A \rightarrow \tau\bar{\tau})$ can be large in Type-X, while $BR(A \rightarrow b\bar{b})$ becomes large in Type-Y. From the right panel of Fig. 17, we can see that both of $BR(A \rightarrow \tau\bar{\tau})$ and $BR(A \rightarrow b\bar{b})$ can be several dozens of percent if $\Delta m \lesssim 150$ GeV, while they are below 1% when $\Delta m \simeq 400$ GeV. Therefore, we can discriminate the types of 2HDMs by examining the decay pattern of the CP-odd Higgs boson if Δm is not so large. We note that $A \rightarrow b\bar{b}$ and $A \rightarrow \tau\bar{\tau}$ can be dominant when $c_{\beta-\alpha} \approx 0$. Therefore, the types of Yukawa interactions can be discriminated by examining the decay pattern of the CP-odd Higgs boson even in the case with $c_{\beta-\alpha} \simeq 0$, where it would be difficult to measure the deviation in the SM-like Higgs boson couplings. When Δm is large, we have sizable deviations

in the SM-like Higgs boson couplings as discussed in Sec. VB, and the measurement of SM-like Higgs boson couplings can be used to study the types of 2HDMs [16, 28]. Therefore, the decay pattern of the CP-odd Higgs boson and the deviation in the SM-like Higgs boson couplings play a comprehensive role, and we can determine the types of 2HDMs by using them.

VI. DISCUSSIONS AND CONCLUSIONS

We have discussed the impact of the NLO EW corrections on the decay rates of the CP-odd Higgs boson in the 2HDMs with the softly broken discrete Z_2 symmetry. We have calculated the decay rates of the CP-odd Higgs boson based on the improved on-shell renormalization scheme [23]. The decay rates of the CP-odd Higgs boson decays into a pair of quarks and leptons, Z and the neutral Higgs bosons, and W^\pm and the charged Higgs bosons have been calculated including the NLO EW corrections. On the other hand, the one-loop induced decays, $A \rightarrow W^\pm W^\mp$, ZZ , $\gamma\gamma$, $Z\gamma$ and gg , have been calculated at LO EW. We have presented the explicit formulae for the decay rates including the NLO EW corrections and higher-order QCD corrections. The NLO EW corrections have been written in terms of the renormalized vertex functions, and the analytical formulae have been presented.

The size of the NLO EW corrections on the partial decay widths, total decay widths and the decay branching ratios have been comprehensively studied in the near alignment scenario, where the couplings constants of the discovered Higgs boson are close to those in the SM. We have found that the decay branching ratio of $A \rightarrow Zh$ can be negative in the near alignment scenario. This is because the tree-level vertex becomes quite small, and the NLO correction can be larger than the LO contribution. In this paper, we have solved this problem by introducing the square of the NLO amplitude. However, we should include the contributions from the tree-level amplitude times the two-loop amplitude since the square of the one-loop amplitude corresponds to the NNLO. In the alignment limit, this contribution vanishes due to the multiplication of the tree-level amplitude. Therefore, we expect that the contribution from two-loop diagrams is also sub-leading in the nearly alignment scenario. For other decay processes such as $A \rightarrow f\bar{f}$, we have IR divergences in the one-loop amplitudes. Therefore, we need to take into account higher-order QED corrections in order to include partial NNLO contributions. Since the partial decay widths do not become negative except for $A \rightarrow Zh$ in the nearly alignment case, we include the partial NNLO contribution only for $A \rightarrow Zh$ in this paper.

We have discussed the behavior of the NLO EW corrections to the partial decay widths in detail.

The NLO EW corrections to $A \rightarrow b\bar{b}$ and the total decay width depend on the types of 2HDMs. On the other hand, those for the other decay modes are almost independent of the types of 2HDMs. We have also analyzed the correlations between the branching ratios of A and the scaling factor of the hZZ coupling including higher-order corrections. We have found that the NLO EW corrections sizably modify theoretical predictions at LO. For example, it is expected that $\text{BR}(A \rightarrow Zh)$ and $\Delta\kappa_Z$ become large at the same time because both of them are promotional to $|c_{\beta-\alpha}|$ at LO. However, $\Delta\kappa_Z$ can be sizable even when $\text{BR}(A \rightarrow Zh)$ is small due to the non-decoupling effect. We have shown that the NLO EW corrections sizably modify the decay branching ratio, and those behaviors have been discussed in detail.

We have shown that there are characteristic predictions in the decay pattern of the CP-odd Higgs boson depending on the types of the 2HDMs. We can discriminate the types of the 2HDMs by the correlations between $A \rightarrow b\bar{b}$ and $A \rightarrow \tau\bar{\tau}$ if the size of these decay branching ratios is enough large. When the decay branching ratios of $A \rightarrow b\bar{b}$ and $A \rightarrow \tau\bar{\tau}$ are small, the CP-odd Higgs boson mainly decays into $t\bar{t}$, Zh and ZH in our scenario, and we would be able to determine the types of 2HDMs through the decay patterns of the additional CP-even Higgs boson and the deviations in the SM-like Higgs boson couplings.

Acknowledgments

We would like to thank Mariko Kikuchi and Kei Yagyu for their useful comments. This work is supported in part by JSPS KAKENHI Grant No. 20H00160, No. 21F21324 [S.K.], No. 20H01894, No. 21K20363 [K.S.], and No. 22J01147 [M.A.].

Input parameter	Symbol	Value
fine-structure constant at the Thomson limit	$\alpha_{\text{em}}^{-1}(0)$	137.035999084
Z boson mass	m_Z [GeV]	91.1876
Fermi constant	G_F [GeV $^{-2}$]	1.1663787×10^{-5}
strong coupling constant at m_Z	$\alpha_s(m_Z)$	0.1179
Higgs boson mass	m_h [GeV]	125.1
top-quark pole mass	m_t [GeV]	172.5
bottom-quark pole mass	m_b [GeV]	4.78
charm-quark pole mass	m_c [GeV]	1.67
bottom-quark running mass	$\bar{m}_b(\bar{m}_b)$ [GeV]	4.18
charm-quark running mass	$\bar{m}_c(\bar{m}_c)$ [GeV]	1.27
tauon mass	m_τ [GeV]	1.77686
muon mass	m_μ [GeV]	0.1056583745
electron mass	m_e [GeV]	$5.109989461 \times 10^{-4}$
Total decay width of the top quark	Γ_t [GeV]	1.42
Total decay width of the W^\pm bosons	Γ_W [GeV]	2.085
Total decay width of the Z boson	Γ_Z [GeV]	2.4952

TABLE II: SM input parameters. The values are taken from Ref. [107].

Appendix A: Input parameters

We work in the scheme where $\alpha_{\text{em}}(0)$, G_F and m_Z are input parameters following the H-COUP program [40, 41]. In Table II, we list the SM input parameters. The values of input parameters are taken from Ref. [107]. The expressions for the running parameters such as $\alpha_s(\mu)$ and $\bar{m}_q(\mu)$ are given in Ref. [7].

Appendix B: Scalar couplings

We list the expression of the scalar trilinear couplings in terms of the coefficients of the Higgs potential on the Higgs basis given in Eq. (II.4). We use the following notation for these couplings,

$$\mathcal{L} = +\lambda_{\phi_i\phi_j\phi_k}\phi_i\phi_j\phi_k + \dots. \quad (\text{B.1})$$

In terms of the masses of Higgs bosons and mixing angles, the coefficients Z_1, \dots, Z_7 are given as [55, 108]

$$Z_1 v^2 = m_H^2 \cos^2(\beta - \alpha) + m_h^2 \sin^2(\beta - \alpha), \quad (\text{B.2})$$

$$Z_2 v^2 = m_H^2 \cos^2(\beta - \alpha) + m_h^2 \sin^2(\beta - \alpha) + 4(m_h^2 - m_H^2) \cos(\beta - \alpha) \sin(\beta - \alpha) \cot 2\beta \\ + 4[(m_H^2 - M^2) \sin^2(\beta - \alpha) + (m_h^2 - M^2) \cos^2(\beta - \alpha)] \cot^2 2\beta, \quad (\text{B.3})$$

$$Z_3 v^2 = m_H^2 \cos^2(\beta - \alpha) + m_h^2 \sin^2(\beta - \alpha) + 2(m_h^2 - m_H^2) \cos(\beta - \alpha) \sin(\beta - \alpha) \cot 2\beta \\ + 2(m_{H^\pm}^2 - M^2), \quad (\text{B.4})$$

$$Z_4 v^2 = m_H^2 \sin^2(\beta - \alpha) + m_h^2 \cos^2(\beta - \alpha) + m_A^2 - 2m_{H^\pm}^2, \quad (\text{B.5})$$

$$Z_5 v^2 = m_H^2 \sin^2(\beta - \alpha) + m_h^2 \cos^2(\beta - \alpha) - m_A^2, \quad (\text{B.6})$$

$$Z_6 v^2 = (m_h^2 - m_H^2) \cos(\beta - \alpha) \sin(\beta - \alpha), \quad (\text{B.7})$$

$$Z_7 v^2 = 2[(m_H^2 - M^2) \sin^2(\beta - \alpha) + (m_h^2 - M^2) \cos^2(\beta - \alpha)] \cot 2\beta \\ + (m_h^2 - m_H^2) \cos(\beta - \alpha) \sin(\beta - \alpha). \quad (\text{B.8})$$

The Higgs trilinear couplings relevant for the decays of the CP-odd Higgs boson are given by

$$\lambda_{AG^0 h} = -[Z_6 s_{\beta-\alpha} + Z_5 c_{\beta-\alpha}]v, \quad (\text{B.9})$$

$$\lambda_{AG^0 H} = -[Z_6 c_{\beta-\alpha} - Z_5 s_{\beta-\alpha}]v, \quad (\text{B.10})$$

$$\lambda_{hG^0 G^0} = -\frac{1}{2}(Z_1 s_{\beta-\alpha} + Z_6 c_{\beta-\alpha})v, \quad (\text{B.11})$$

$$\lambda_{HG^0 G^0} = -\frac{1}{2}(Z_1 c_{\beta-\alpha} - Z_6 s_{\beta-\alpha})v, \quad (\text{B.12})$$

$$\lambda_{AAh} = -\frac{1}{2}[Z_7 c_{\beta-\alpha} + (Z_3 + Z_4 - Z_5) s_{\beta-\alpha}]v, \quad (\text{B.13})$$

$$\lambda_{AAH} = -\frac{1}{2}[-Z_7 s_{\beta-\alpha} + (Z_3 + Z_4 - Z_5) c_{\beta-\alpha}]v, \quad (\text{B.14})$$

$$\lambda_{hhh} = -\frac{1}{2}[Z_1 s_{\beta-\alpha}^3 + Z_{345} c_{\beta-\alpha}^2 s_{\beta-\alpha} + 3Z_6 s_{\beta-\alpha}^2 c_{\beta-\alpha} + Z_7 c_{\beta-\alpha}^3]v, \quad (\text{B.15})$$

$$\lambda_{hhH} = -\frac{1}{2}[3Z_1 s_{\beta-\alpha}^2 c_{\beta-\alpha} + Z_{345}(c_{\beta-\alpha}^3 - 2s_{\beta-\alpha}^2 c_{\beta-\alpha}) \\ - 3Z_6(s_{\beta-\alpha}^3 - 2s_{\beta-\alpha} c_{\beta-\alpha}^2) - 3Z_7 c_{\beta-\alpha}^2 s_{\beta-\alpha}]v, \quad (\text{B.16})$$

$$\lambda_{hHH} = -\frac{1}{2}[3Z_1 c_{\beta-\alpha}^2 s_{\beta-\alpha} + Z_{345}(s_{\beta-\alpha}^3 - 2c_{\beta-\alpha}^2 s_{\beta-\alpha}) \\ + 3Z_6(c_{\beta-\alpha}^3 - 2c_{\beta-\alpha} s_{\beta-\alpha}^2) + 3Z_7 c_{\beta-\alpha} s_{\beta-\alpha}^2]v, \quad (\text{B.17})$$

$$\lambda_{HHH} = -\frac{1}{2}[Z_1 c_{\beta-\alpha}^3 + Z_{345} s_{\beta-\alpha}^2 c_{\beta-\alpha} - 3Z_6 c_{\beta-\alpha}^2 s_{\beta-\alpha} - Z_7 s_{\beta-\alpha}^3]v, \quad (\text{B.18})$$

$$\lambda_{H^\pm G^\mp A} = \pm \frac{i}{2}(Z_4 - Z_5)v, \quad (\text{B.19})$$

$$\lambda_{H^\pm G^\mp h} = -\left[Z_6 s_{\beta-\alpha} + \frac{1}{2}(Z_4 + Z_5) c_{\beta-\alpha}\right]v, \quad (\text{B.20})$$

$$\lambda_{H^\pm G^\mp H} = -\left[Z_6 c_{\beta-\alpha} - \frac{1}{2}(Z_4 + Z_5) s_{\beta-\alpha}\right]v, \quad (\text{B.21})$$

where $Z_{345} = Z_3 + Z_4 + Z_5$.

Appendix C: Three-body decays of the CP-odd Higgs boson

1. $A \rightarrow tt^* \rightarrow tbW$

When $m_t + m_W \leq m_A < 2m_t$, the CP-odd Higgs boson can decay into a pair of on-shell and off-shell top quarks, $A \rightarrow tt^* \rightarrow tbW$. The decay rate is given by [109, 110]

$$\Gamma(A \rightarrow tt^* \rightarrow tbW) = 2 \int_{y_t^-}^{y_t^+} dy_t \int_{y_b^-}^{y_b^+} dy_b \frac{d\Gamma}{dy_t dy_b}(A \rightarrow t\bar{b}W^-), \quad (\text{C.1})$$

with the scaling variables $y_{t(b)} = 1 - 2E_{t(b)}/m_A$. Since the charge conjugate $\bar{t}bW^+$ final state doubles the partial decay width, we multiply factor two. The kinematic boundaries are given by

$$y_t^+ = (1 - x_t)^2 - x_t^2, \quad (\text{C.2})$$

$$y_t^- = (x_b + x_W)^2 - x_t^2, \quad (\text{C.3})$$

$$y_b^\pm = x_t^2 - x_b^2 + x_W^2 + \frac{(1 - 2x_t^2 - y_t)(y_t + x_t^2 - x_b^2 + x_W^2)}{2(y_t + x_t^2)} \pm \frac{1}{2}\lambda^{1/2}(y_t + x_t^2, x_t^2)\lambda^{1/2}\left(\frac{x_b^2}{y_t + x_t^2}, \frac{x_W^2}{y_t + x_t^2}\right), \quad (\text{C.4})$$

where $x_i = m_i/m_A$ ($i = t, b, W$), and the kinematical factor $\lambda(x, y)$ is given in Eq. (III.21). The Dalitz density is given by

$$\frac{d\Gamma}{dy_t dy_b}(A \rightarrow t\bar{b}W^-) = 3 \frac{G_F^2 m_t^2 \zeta_u^2 m_A^3}{64\pi^3} \frac{\Gamma_0}{y_t^2 + \kappa_t \gamma_t}, \quad (\text{C.5})$$

with

$$\Gamma_0 = -y_t^3 + (1 - \kappa_t + \kappa_W - y_b)y_t^2 + [2\kappa_t - y_b(\kappa_t - 2\kappa_W)]y_t + (\kappa_t - \kappa_W)(\kappa_t + 2\kappa_W), \quad (\text{C.6})$$

and $\kappa_i = m_i^2/m_A^2$ ($i = t, b, W$). The reduced decay width for the virtual top quark is defined by $\gamma_t = \Gamma_t^2/m_A^2$ with the total decay width of the top quark Γ_t . In the numerical evaluation, we use the on-shell mass of the top quark in the Yukawa interaction.

2. $A \rightarrow \phi Z^* \rightarrow \phi f \bar{f}$

When $m_\phi \leq m_A < m_Z + m_\phi$, the CP-odd Higgs boson can decay into a pair of on-shell CP-even Higgs boson ϕ ($= h, H$) and off-shell Z boson, $A \rightarrow \phi Z^* \rightarrow \phi f \bar{f}$. The decay rate is given by [109]

$$\Gamma(A \rightarrow \phi Z^*) = \int_{x_f^-}^{x_f^+} dx_f \int_{x_{\bar{f}}^-}^{x_{\bar{f}}^+} dx_{\bar{f}} \frac{d\Gamma}{dx_f dx_{\bar{f}}}(A \rightarrow \phi Z^* \rightarrow \phi f \bar{f}), \quad (\text{C.7})$$

with the scaling variables $x_{f(\bar{f})} = 2E_{f(\bar{f})}/m_A$. We neglect the masses of the final-state fermions. The kinematic boundaries are given by

$$0 < x_f < 1 - \kappa_\phi, \quad (\text{C.8})$$

$$1 - x_f - \kappa_\phi < x_{\bar{f}} < 1 - \frac{\kappa_\phi}{1 - x_f}, \quad (\text{C.9})$$

with $\kappa_\phi = m_\phi^2/m_A^2$. The Dalitz density is given by

$$\begin{aligned} \frac{d\Gamma}{dx_f dx_{\bar{f}}} (A \rightarrow \phi Z^* \rightarrow \phi f \bar{f}) &= \frac{9G_F}{16\sqrt{2}\pi^3} |\Gamma_{AZ\phi}^{\text{tree}}|^2 m_Z^2 m_A \left(\frac{7}{12} - \frac{10}{9} s_W^2 + \frac{40}{27} s_W^4 \right) \\ &\times \frac{(1 - x_f)(1 - x_{\bar{f}}) - \kappa_\phi}{(1 - x_f - x_{\bar{f}} - \kappa_\phi + \kappa_Z)^2 + \kappa_Z \gamma_Z}, \end{aligned} \quad (\text{C.10})$$

where $\kappa_Z = m_Z^2/m_A^2$, and the tree-level couplings $\Gamma_{AZ\phi}^{\text{tree}}$ are given in Eq. (III.12). The reduced decay width for the virtual Z boson is defined by $\gamma_Z = \Gamma_Z^2/m_A^2$ with the total decay width of the Z boson Γ_Z .

3. $A \rightarrow H^\pm W^{\mp*} \rightarrow H^\pm f \bar{f}'$

When $m_{H^\pm} \leq m_A < m_W + m_{H^\pm}$, the CP-odd Higgs boson can decay into a pair of on-shell charged Higgs bosons H^\pm and off-shell W^\pm boson, $A \rightarrow H^\pm W^{\mp*} \rightarrow H^\pm f \bar{f}'$. The decay rate is given by

$$\Gamma(A \rightarrow H^\pm W^{\mp*}) = 2 \int_{x_f^-}^{x_f^+} dx_f \int_{x_{\bar{f}'}^-}^{x_{\bar{f}'}^+} dx_{\bar{f}'} \frac{d\Gamma}{dx_f dx_{\bar{f}'}} (A \rightarrow H^+ W^{-*} \rightarrow H^+ f \bar{f}'), \quad (\text{C.11})$$

with the scaling variables $x_{f(\bar{f}')} = 2E_{f(\bar{f}')}/m_A$. Since the charge conjugate $H^- \bar{f} f'$ final state doubles the partial decay width, we multiply factor two. We neglect the masses of the final state fermions. The kinematic boundaries are given by

$$0 < x_f < 1 - \kappa_{H^\pm}, \quad (\text{C.12})$$

$$1 - x_f - \kappa_{H^\pm} < x_{\bar{f}'} < 1 - \frac{\kappa_{H^\pm}}{1 - x_f}, \quad (\text{C.13})$$

with $\kappa_{H^\pm} = m_{H^\pm}^2/m_A^2$. The Dalitz density is given by

$$\begin{aligned} \frac{d\Gamma}{dx_f dx_{\bar{f}'}} (A \rightarrow H^+ W^{-*} \rightarrow H^+ f \bar{f}') &= \frac{9G_F}{16\sqrt{2}\pi^3} |\Gamma_{AW^\mp H^\pm}^{\text{tree}}|^2 m_W^2 m_A \\ &\times \frac{(1 - x_f)(1 - x_{\bar{f}'}) - \kappa_{H^\pm}}{(1 - x_f - x_{\bar{f}'} - \kappa_{H^\pm} + \kappa_W)^2 + \kappa_W \gamma_W}, \end{aligned} \quad (\text{C.14})$$

where $\kappa_W = m_W^2/m_A^2$, and the tree-level coupling $\Gamma_{AW^\mp H^\pm}^{\text{tree}}$ is given in Eq. (III.12). The reduced decay width for the virtual W boson is defined by $\gamma_W = \Gamma_W^2/m_A^2$ with the decay width of the W^\pm boson Γ_W .

Appendix D: QCD corrections for $A \rightarrow \gamma\gamma$ and $A \rightarrow gg$

1. $A \rightarrow \gamma\gamma$

The analytic expression for $I_F^A C_1^A(\tau)$ in Eq. (III.37) is given by [100]

$$\begin{aligned}
I_F^A(\tau)C_1^A(\tau) = & -\frac{\theta(1+\theta^2)}{(1-\theta)^3(1+\theta)} \left[72\text{Li}_4(\theta) + 96\text{Li}_4(-\theta) - \frac{128}{3}[\text{Li}_3(\theta) - \text{Li}_3(-\theta)] \ln \theta \right. \\
& + \frac{28}{3}\text{Li}_2(\theta) \ln^2 \theta + \frac{16}{3}\text{Li}_2(-\theta) \ln^2 \theta + \frac{1}{18} \ln^4 \theta + \frac{8}{3}\zeta(2) \ln^2 \theta + \frac{32}{3}\zeta(3) \ln \theta + 12\zeta(4) \Big] \\
& + \frac{\theta}{(1-\theta)^2} \left[-\frac{56}{3}\text{Li}_3(\theta) - \frac{64}{3}\text{Li}_3(-\theta) + 16\text{Li}_2(\theta) \ln \theta + \frac{32}{3}\text{Li}_2(-\theta) \ln \theta \right. \\
& + \frac{20}{3} \ln(1-\theta) \ln^2 \theta - \frac{8}{3}\zeta(2) \ln \theta + \frac{8}{3}\zeta(3) \Big] \\
& + \frac{2\theta(1+\theta)}{3(1-\theta)^3} \ln^3 \theta,
\end{aligned} \tag{D.1}$$

with

$$\theta \equiv \theta(\tau) = \frac{\sqrt{1-\tau^{-1}}-1}{\sqrt{1-\tau^{-1}}+1}. \tag{D.2}$$

For the evaluation of the polylog function $\text{Li}_n(x)$, we use CHAPLIN [111]. The analytic expression for $I_F^A C_2^A(\tau)$ in Eq. (III.37) is given by [100]

$$I_F^A(\tau)C_2^A(\tau) = \frac{2}{\tau} [f(\tau) - \tau f'(\tau)], \tag{D.3}$$

where $f(\tau)$ is given in Eq. (III.39).

2. $A \rightarrow gg$

The NLO QCD correction $E_A^{(1)}$ in (III.40) can be decomposed as [99]

$$E_A^{(1)} = E_A^{\text{virt}} \Big|_{m_t \rightarrow \infty} + E_A^{\text{real}} \Big|_{m_t \rightarrow \infty} + \Delta E_A. \tag{D.4}$$

The first and second terms on the right-hand side denote the contributions from virtual gluon loops and those from real gluon emissions in the large top-mass limit, respectively. At $\mu = m_A$, these are given by [99]

$$E_A^{\text{virt}} \Big|_{m_t \rightarrow \infty} = 6, \quad E_A^{\text{real}} \Big|_{m_t \rightarrow \infty} = \frac{73}{4} - \frac{7}{6} N_f. \tag{D.5}$$

The third term, ΔE_A , vanishes in the large top-mass limit. It can be decomposed as

$$\Delta E_A = \Delta E_A^{\text{virt}} + \Delta E_A^{ggg} + N_f \Delta E_A^{gq\bar{q}}. \tag{D.6}$$

The analytic expression for ΔE_A^{virt} is given by [100]

$$\Delta E_A^{\text{virt}} = \text{Re} \left\{ \frac{\sum_q 2I_f \zeta_f I_F^A(\tau_q) \left(B_1^A(\tau_q) + B_2^A(\tau_q) \ln \frac{m_A^2}{m_q^2} \right)}{\sum_q 2I_f \zeta_f I_F^A(\tau_q)} \right\} - 6, \quad (\text{D.7})$$

with

$$\begin{aligned} I_F^A(\tau) B_1^A(\tau) = & \frac{\theta}{(1-\theta)^2} \left[48H(1, 0, -1, -; \theta) + 4 \ln(1-\theta) \ln^3 \theta - 24\zeta(2) \text{Li}_2(\theta) - 24\zeta(2) \ln(1-\theta) \ln \theta \right. \\ & - 72\zeta(3) \ln(1-\theta) - \frac{220}{3} \text{Li}_3(\theta) - \frac{128}{3} \text{Li}_3(-\theta) + 68 \text{Li}_2(\theta) \ln \theta + \frac{64}{3} \text{Li}_2(-\theta) \ln \theta \\ & + \frac{94}{3} \ln(1-\theta) \ln^2 \theta - \frac{16}{3} \zeta(2) \ln \theta + \frac{124}{3} \zeta(3) + 3 \ln^2 \theta \left. \right] \\ & - \frac{24\theta(5+7\theta^2)}{(1-\theta)^3(1+\theta)} \text{Li}_4(\theta) - \frac{24\theta(5+11\theta^2)}{(1-\theta)^3(1+\theta)} \text{Li}_4(-\theta) \\ & + \frac{8\theta(23+41\theta^2)}{3(1-\theta)^3(1+\theta)} [\text{Li}_3(\theta) + \text{Li}_3(-\theta)] \ln \theta \\ & - \frac{4\theta(5+23\theta^2)}{3(1-\theta)^3(1+\theta)} \text{Li}_2(\theta) \ln^2 \theta - \frac{32\theta(1+\theta^2)}{3(1-\theta)^3(1+\theta)} \text{Li}_2(-\theta) \ln^2 \theta \\ & + \frac{\theta(5-13\theta^2)}{36(1-\theta)^3(1+\theta)} \ln^4 \theta + \frac{2\theta(1-17\theta^2)}{3(1-\theta)^3(1+\theta)} \zeta(2) \ln^2 \theta + \frac{4\theta(11-43\theta^2)}{3(1-\theta)^3(1+\theta)} \zeta(3) \ln \theta \\ & + \frac{24\theta(1-3\theta^2)}{(1-\theta)^3(1+\theta)} \zeta(4) + \frac{2\theta(2+11\theta)}{3(1-\theta)^3} \ln^3 \theta, \end{aligned} \quad (\text{D.8})$$

$$I_F^A(\tau) B_2^A(\tau) = \frac{4}{\tau} [f(\tau) - \tau f'(\tau)], \quad (\text{D.9})$$

where θ is given in Eq. (D.2), and $f(\tau)$ is given in Eq. (III.39). For the evaluation of the Harmonic Polylogarithm function $H(1, 0, -1, -; \theta)$, we use CHAPLIN [111]. According to Ref. [99], ΔE_A is dominantly determined by ΔE_A^{virt} . Therefore, we neglect the contributions from the real emissions ΔE_A^{ggg} and $\Delta E_A^{gq\bar{q}}$ in our calculation.

The NNLO QCD correction $E_A^{(2)}$ in (III.40) is evaluated in the large top-mass limit. It is given by [101]

$$\begin{aligned} E_A^{(2)} = & \frac{51959}{96} - \frac{363}{8} \zeta(2) - \frac{495}{8} \zeta(3) + N_f \left[-\frac{473}{8} + \frac{11}{2} \zeta(2) + \frac{5}{4} \zeta(3) - \ln \frac{\bar{m}_t^2(m_A)}{m_A^2} \right] \\ & + N_f^2 \left(\frac{251}{216} - \frac{1}{6} \zeta(2) \right). \end{aligned} \quad (\text{D.10})$$

Appendix E: 1PI diagram contributions for $Af\bar{f}$ and $AV\phi$ vertices

We give the analytic expressions for the 1PI diagram contributions in terms of the Passarino-Veltman functions [81]. We calculate 1PI diagrams in the 't Hooft-Feynman gauge with $\xi = 1$.

The coefficients of vector and axial-vector couplings of Z boson are given by

$$v_f = \frac{1}{2}I_f - Q_f s_W^2, \quad a_f = \frac{1}{2}I_f. \quad (\text{E.1})$$

1. $Af\bar{f}$ vertex

The 1PI contributions to the form factor of $Af\bar{f}$ vertex are given by

$$\begin{aligned} (16\pi^2)\Gamma_{Af\bar{f}}^{S,1\text{PI}} &= 2I_f \lambda_{H^+G^-A} \frac{m_f m_{f'}^2}{v^2} (\zeta_f + \zeta_{f'}) [C_0(H^\pm, f', G^\pm) - C_0(G^\pm, f', H^\pm)] \\ &\quad + i \frac{g_Z^2}{2} c_{\beta-\alpha} v_f \frac{m_f \zeta_{hff}}{v} [C_{Aff}^{SFV}(h, f, Z) - C_{Aff}^{VFS}(Z, f, h)] \\ &\quad - i \frac{g_Z^2}{2} s_{\beta-\alpha} v_f \frac{m_f \zeta_{Hff}}{v} [C_{Aff}^{SFV}(H, f, Z) - C_{Aff}^{VFS}(Z, f, H)] \\ &\quad + i \frac{g^2}{2} \frac{I_f m_f \zeta_f}{v} [C_{Aff}^{SFV}(H^\pm, f', W^\pm) - C_{Aff}^{VFS}(W^\pm, f', H^\pm)], \end{aligned} \quad (\text{E.2})$$

$$\begin{aligned} (16\pi^2)\Gamma_{Af\bar{f}}^{P,1\text{PI}} &= i \frac{2I_f m_f \zeta_f}{v} [g_Z^2 (v_f^2 - a_f^2) C_{Aff}^{FVF}(f, Z, f) + e^2 Q_f^2 C_{Aff}^{FVF}(f, \gamma, f)] \\ &\quad + i \frac{2I_f m_f^3 \zeta_f}{v^2} [\zeta_{hff}^2 C_{Aff}^{FSF}(f, h, f) + \zeta_{Hff}^2 C_{Aff}^{FSF}(f, H, f) - C_{Aff}^{FSF}(f, G^0, f) - \zeta_f^2 C_{Aff}^{FSF}(f, A, f)] \\ &\quad - i \frac{4I_{f'} m_f m_{f'}^2 \zeta_{f'}}{v^3} [C_{Aff}^{FSF}(f', G^\pm, f') + \zeta_f \zeta_{f'} C_{Aff}^{FSF}(f', H^\pm, f')] \\ &\quad + i \lambda_{AG^0h} \frac{m_f \zeta_{hff}}{v} \frac{2I_f m_f^2}{v} [C_0(h, f, G^0) + C_0(G^0, f, h)] \\ &\quad + i \lambda_{AG^0H} \frac{m_f \zeta_{Hff}}{v} \frac{2I_f m_f^2}{v} [C_0(H, f, G^0) + C_0(G^0, f, H)] \\ &\quad + i 2\lambda_{AAh} \frac{m_f \zeta_{hff}}{v} \frac{2I_f m_f^2 \zeta_f}{v} [C_0(h, f, A) + C_0(A, f, h)] \\ &\quad + i 2\lambda_{AAH} \frac{m_f \zeta_{Hff}}{v} \frac{2I_f m_f^2 \zeta_f}{v} [C_0(H, f, A) + C_0(A, f, H)] \\ &\quad + 2I_f \lambda_{H^+G^-A} \frac{m_f m_{f'}^2}{v^2} (\zeta_f - \zeta_{f'}) [C_0(H^\pm, f', G^\pm) + C_0(G^\pm, f', H^\pm)] \\ &\quad + i \frac{g_Z^2}{2} c_{\beta-\alpha} a_f \frac{m_f \zeta_{hff}}{v} [C_{Aff}^{SFV}(h, f, Z) + C_{Aff}^{VFS}(Z, f, h)] \\ &\quad - i \frac{g_Z^2}{2} s_{\beta-\alpha} a_f \frac{m_f \zeta_{Hff}}{v} [C_{Aff}^{SFV}(H, f, Z) + C_{Aff}^{VFS}(Z, f, H)] \\ &\quad + i \frac{g^2}{2} \frac{I_f m_f \zeta_f}{v} [C_{Aff}^{SFV}(H^\pm, f', W^\pm) + C_{Aff}^{VFS}(W^\pm, f', H^\pm)], \end{aligned} \quad (\text{E.3})$$

$$\begin{aligned}
& (16\pi^2)\Gamma_{Af\bar{f}}^{V_1,1\text{PI}} \\
&= i4g_Z^2 v_f a_f \frac{2I_f m_f^2 \zeta_f}{v} C_0(f, Z, f) + i\frac{g^2}{2} \frac{2I_{f'} m_{f'}^2 \zeta_{f'}}{v} C_0(f', W, f') \\
&+ i\frac{2I_{f'} m_{f'}^2 \zeta_{f'}}{v} \left[\frac{m_f^2 - m_{f'}^2}{v^2} C_0(f', G^\pm, f') + \frac{m_f^2 \zeta_f^2 - m_{f'}^2 \zeta_{f'}^2}{v^2} C_0(f', H^\pm, f') \right] \\
&- 2I_f \lambda_{H^+ G^- A} \frac{m_f^2 \zeta_f + m_{f'}^2 \zeta_{f'}}{v^2} [(C_0 + C_{11})(H^\pm, f', G^\pm) - (C_0 + C_{11})(G^\pm, f', H^\pm)] \\
&+ i\frac{g_Z^2}{2} c_{\beta-\alpha} v_f \frac{m_f^2 \zeta_{hff}}{v} [(C_{11} - C_0)(h, f, Z) - (C_{11} + 2C_0)(Z, f, h)] \\
&- i\frac{g_Z^2}{2} s_{\beta-\alpha} v_f \frac{m_f^2 \zeta_{Hff}}{v} [(C_{11} - C_0)(H, f, Z) - (C_{11} + 2C_0)(Z, f, H)] \\
&+ i\frac{g^2}{2} \frac{I_{f'} m_{f'}^2 \zeta_{f'}}{v} [(C_{11} - C_0)(H^\pm, f', W^\pm) - (C_{11} + 2C_0)(W^\pm, f', H^\pm)], \tag{E.4}
\end{aligned}$$

$$\begin{aligned}
& (16\pi^2)\Gamma_{Af\bar{f}}^{V_2,1\text{PI}} \\
&= i4g_Z^2 v_f a_f \frac{2I_f m_f^2 \zeta_f}{v} C_0(f, Z, f) + i\frac{g^2}{2} \frac{2I_{f'} m_{f'}^2 \zeta_{f'}}{v} C_0(f', W, f') \\
&+ i\frac{2I_{f'} m_{f'}^2 \zeta_{f'}}{v} \left[\frac{m_f^2 - m_{f'}^2}{v^2} C_0(f', G^\pm, f') + \frac{m_f^2 \zeta_f^2 - m_{f'}^2 \zeta_{f'}^2}{v^2} C_0(f', H^\pm, f') \right] \\
&- 2I_f \lambda_{H^+ G^- A} \frac{m_f^2 \zeta_f + m_{f'}^2 \zeta_{f'}}{v^2} [C_{12}(H^\pm, f', G^\pm) - C_{12}(G^\pm, f', H^\pm)] \\
&+ i\frac{g_Z^2}{2} c_{\beta-\alpha} v_f \frac{m_f^2 \zeta_{hff}}{v} [(C_{12} - C_0)(h, f, Z) - (C_{12} + 2C_0)(Z, f, h)] \\
&- i\frac{g_Z^2}{2} s_{\beta-\alpha} v_f \frac{m_f^2 \zeta_{Hff}}{v} [(C_{12} - C_0)(H, f, Z) - (C_{12} + 2C_0)(Z, f, H)] \\
&- i\frac{g^2}{2} \frac{I_{f'} m_{f'}^2 \zeta_{f'}}{v} [(C_{12} - C_0)(H^\pm, f', W^\pm) - (C_{12} + 2C_0)(W^\pm, f', H^\pm)], \tag{E.5}
\end{aligned}$$

$$\begin{aligned}
& (16\pi^2)\Gamma_{Af\bar{f}}^{A_1,1\text{PI}} \\
&= -i\frac{2I_f m_f^2 \zeta_f}{v} [2g_Z^2(v_f^2 + a_f^2)C_0(f, Z, f) + 2e^2 Q_f^2 C_0(f, \gamma, f)] - i\frac{g^2}{2} \frac{2I_{f'} m_{f'}^2 \zeta_{f'}}{v} C_0(f', W, f') \\
&+ i\frac{2I_f m_f^4 \zeta_f}{v^3} \left[\zeta_{hff}^2 C_0(f, h, f) + \zeta_{Hff}^2 C_0(f, H, f) + C_0(f, G^0, f) + \zeta_f^2 C_0(f, A, f) \right] \\
&+ i\frac{2I_{f'} m_{f'}^2 \zeta_{f'}}{v} \left[\frac{m_f^2 + m_{f'}^2}{v^2} C_0(f', G^\pm, f') + \frac{m_f^2 \zeta_f^2 + m_{f'}^2 \zeta_{f'}^2}{v^2} C_0(f', H^\pm, f') \right] \\
&- i\lambda_{AG^0 h} \frac{m_f \zeta_{hff}}{v} \frac{2I_f m_f}{v} [(C_0 + C_{11})(h, f, G^0) - (C_0 + C_{11})(G^0, f, h)] \\
&- i\lambda_{AG^0 H} \frac{m_f \zeta_{Hff}}{v} \frac{2I_f m_f}{v} [(C_0 + C_{11})(H, f, G^0) - (C_0 + C_{11})(G^0, f, H)] \\
&- i2\lambda_{AAh} \frac{m_f \zeta_{hff}}{v} \frac{2I_f m_f \zeta_f}{v} [(C_0 + C_{11})(h, f, A) - (C_0 + C_{11})(A, f, h)]
\end{aligned}$$

$$\begin{aligned}
& -i2\lambda_{AAH}\frac{m_f\zeta_{Hff}}{v}\frac{2I_fm_f\zeta_f}{v}[(C_0+C_{11})(H,f,A)-(C_0+C_{11})(A,f,H)] \\
& -2I_f\lambda_{H^+G^-A}\frac{m_f^2\zeta_f-m_{f'}^2\zeta_{f'}}{v^2}[(C_0+C_{11})(H^\pm,f',G^\pm)-(C_0+C_{11})(G^\pm,f',H^\pm)] \\
& +i\frac{g_Z^2}{2}c_{\beta-\alpha}a_f\frac{m_f^2\zeta_{hff}}{v}[(-C_{11}+C_0)(h,f,Z)+(C_{11}+2C_0)(Z,f,h)] \\
& -i\frac{g_Z^2}{2}s_{\beta-\alpha}a_f\frac{m_f^2\zeta_{Hff}}{v}[(-C_{11}+C_0)(H,f,Z)+(C_{11}+2C_0)(Z,f,H)] \\
& +i\frac{g^2}{2}\frac{I_{f'}m_{f'}^2\zeta_{f'}}{v}[(-C_{11}+C_0)(H^\pm,f',W^\pm)+(C_{11}+2C_0)(W^\pm,f',H^\pm)], \tag{E.6}
\end{aligned}$$

$$\begin{aligned}
& (16\pi^2)\Gamma_{Af\bar{f}}^{A_2,1PI} \\
& = -i\frac{2I_fm_f^2\zeta_f}{v}[2g_Z^2(v_f^2+a_f^2)C_0(f,Z,f)+2e^2Q_f^2C_0(f,\gamma,f)]-i\frac{g^2}{2}\frac{2I_{f'}m_{f'}^2\zeta_{f'}}{v}C_0(f',W,f') \\
& +i\frac{2I_fm_f^4\zeta_f}{v^3}\left[\zeta_{hff}^2C_0(f,h,f)+\zeta_{Hff}^2C_0(f,H,f)+C_0(f,G^0,f)+\zeta_f^2C_0(f,A,f)\right] \\
& +i\frac{2I_{f'}m_{f'}^2\zeta_{f'}}{v}\left[\frac{m_f^2+m_{f'}^2}{v^2}C_0(f',G^\pm,f')+\frac{m_f^2\zeta_f^2+m_{f'}^2\zeta_{f'}^2}{v^2}C_0(f',H^\pm,f')\right] \\
& -i\lambda_{AG^0h}\frac{m_f\zeta_{hff}}{v}\frac{2I_fm_f}{v}[C_{12}(h,f,G^0)-C_{12}(G^0,f,h)] \\
& -i\lambda_{AG^0H}\frac{m_f\zeta_{Hff}}{v}\frac{2I_fm_f}{v}[C_{12}(H,f,G^0)-C_{12}(G^0,f,H)] \\
& -i2\lambda_{AAh}\frac{m_f\zeta_{hff}}{v}\frac{2I_fm_f\zeta_f}{v}[C_{12}(h,f,A)-C_{12}(A,f,h)] \\
& -i2\lambda_{AAH}\frac{m_f\zeta_{Hff}}{v}\frac{2I_fm_f\zeta_f}{v}[C_{12}(H,f,A)-C_{12}(A,f,H)] \\
& -2I_f\lambda_{H^+G^-A}\frac{m_f^2\zeta_f-m_{f'}^2\zeta_{f'}}{v^2}[C_{12}(H^\pm,f',G^\pm)-C_{12}(G^\pm,f',H^\pm)] \\
& +i\frac{g_Z^2}{2}c_{\beta-\alpha}a_f\frac{m_f^2\zeta_{hff}}{v}[(-C_{12}+C_0)(h,f,Z)+(C_{12}+2C_0)(Z,f,h)] \\
& -i\frac{g_Z^2}{2}s_{\beta-\alpha}a_f\frac{m_f^2\zeta_{Hff}}{v}[(-C_{12}+C_0)(H,f,Z)+(C_{12}+2C_0)(Z,f,H)] \\
& -i\frac{g^2}{2}\frac{I_{f'}m_{f'}^2\zeta_{f'}}{v}[(-C_{12}+C_0)(H^\pm,f',W^\pm)+(C_{12}+2C_0)(W^\pm,f',H^\pm)], \tag{E.7}
\end{aligned}$$

$$\begin{aligned}
& (16\pi^2)\Gamma_{Af\bar{f}}^{T,1PI} \\
& = i\frac{g_Z^2}{2}c_{\beta-\alpha}v_f\frac{m_f\zeta_{hff}}{v}[(C_0+C_{11}-2C_{12})(h,f,Z)-(2C_0+2C_{11}-C_{12})(Z,f,h)] \\
& -i\frac{g_Z^2}{2}s_{\beta-\alpha}v_f\frac{m_f\zeta_{Hff}}{v}[(C_0+C_{11}-2C_{12})(H,f,Z)-(2C_0+2C_{11}-C_{12})(Z,f,H)] \\
& +i\frac{g^2}{2}\frac{I_fm_f\zeta_f}{v}[(C_0+C_{11}-2C_{12})(H^\pm,f',W^\pm)-(2C_0+2C_{11}-C_{12})(W^\pm,f',H^\pm)], \tag{E.8}
\end{aligned}$$

$$\begin{aligned}
& (16\pi^2)\Gamma_{Aff}^{PT,1PI} \\
& = i \frac{2I_f m_f^3 \zeta_f}{v^3} \left[\zeta_{hff}^2 (-C_{11} + C_{12})(f, h, f) + \zeta_{Hff}^2 (-C_{11} + C_{12})(f, H, f) \right. \\
& \quad \left. - (-C_{11} + C_{12})(f, G^0, f) - \zeta_f^2 (-C_{11} + C_{12})(f, A, f) \right] \\
& \quad - i \frac{4I_{f'} m_f m_{f'}^2 \zeta_{f'}}{v^3} \left[(-C_{11} + C_{12})(f', G^\pm, f') + \zeta_f \zeta_{f'} (-C_{11} + C_{12})(f', H^\pm, f') \right] \\
& \quad + i \frac{g_Z^2}{2} c_{\beta-\alpha} a_f \frac{m_f \zeta_{hff}}{v} [(C_0 + C_{11} - 2C_{12})(h, f, Z) + (2C_0 + 2C_{11} - C_{12})(Z, f, h)] \\
& \quad - i \frac{g_Z^2}{2} s_{\beta-\alpha} a_f \frac{m_f \zeta_{Hff}}{v} [(C_0 + C_{11} - 2C_{12})(H, f, Z) + (2C_0 + 2C_{11} - C_{12})(Z, f, H)] \\
& \quad + i \frac{g^2}{2} \frac{I_f m_f \zeta_f}{v} [(C_0 + C_{11} - 2C_{12})(H^\pm, f', W^\pm) + (2C_0 + 2C_{11} - C_{12})(W^\pm, f', H^\pm)]. \quad (E.9)
\end{aligned}$$

where

$$\begin{aligned}
C_{Aff}^{SFV}(X, Y, Z) &= B_0(p_2^2; Y, Z) \\
&+ \left[(m_X^2 - q^2 + p_2^2)C_0 - (q^2 - p_1^2 - p_2^2)C_{11} + (q^2 - p_1^2 - 2p_2^2)C_{12} \right] (p_1^2, p_2^2, q^2; X, Y, Z), \quad (E.10)
\end{aligned}$$

$$\begin{aligned}
C_{Aff}^{VFS}(X, Y, Z) &= B_0(p_2^2; Y, Z) \\
&+ \left[(m_X^2 + 2p_1^2)C_0 + 3p_1^2 C_{11} + 2(q^2 - p_1^2)C_{12} \right] (p_1^2, p_2^2, q^2; X, Y, Z), \quad (E.11)
\end{aligned}$$

$$\begin{aligned}
C_{Aff}^{FVF}(X, Y, Z) &= 4B_0(p_2^2; Y, Z) - 2 \\
&+ \left[4m_X(m_X - m_Z)C_0 + 2(q^2 + p_1^2 - p_2^2)C_{11} + 2(q^2 - p_1^2 + p_2^2)C_{12} \right] (p_1^2, p_2^2, q^2; X, Y, Z), \quad (E.12)
\end{aligned}$$

$$\begin{aligned}
C_{Aff}^{FSF}(X, Y, Z) &= B_0(p_2^2; Y, Z) \\
&+ \left[m_X(m_X - m_Z)C_0 + (q^2 - p_2^2)C_{11} + p_2^2 C_{12} \right] (p_1^2, p_2^2, q^2; X, Y, Z). \quad (E.13)
\end{aligned}$$

The loop functions satisfy following relations

$$C_{Aff}^{SFV}(X, Y, Z) = C_{hff}^{SFV}(X, Y, Z), \quad (E.14)$$

$$C_{Aff}^{VFS}(X, Y, Z) = C_{hff}^{VFS}(X, Y, Z), \quad (E.15)$$

$$C_{Aff}^{FVF}(X, Y, Z) = C_-^{FVF}(X, Y, Z), \quad (E.16)$$

$$C_{Aff}^{FSF}(X, Y, Z) = C_P^{FSF}(X, Y, Z), \quad (E.17)$$

where C_{hff}^{SFV} and C_{hff}^{VFS} are given in Eq. (C.44) in Ref. [19], while C_-^{FVF} and C_P^{FSF} are given in Eqs. (B.23) and (B.22) in Ref. [44].

2. $AV\phi$ vertex

The 1PI contributions to the form factor of AZh vertex are given by

$$(16\pi^2)\Gamma_{AZh}^{\text{1PI}}(p_1^2, p_2^2, q^2)_F$$

$$= i \sum_f 8I_f N_c^f g_Z a_f \frac{m_f^2 \zeta_f \zeta_{hff}}{v^2} \left[B_0(p_2^2; f, f) + 2m_f^2 C_0 + p_1^2 C_{11} + (q^2 - p_1^2) C_{12} \right] (f, f, f), \quad (\text{E.18})$$

$$(16\pi^2)\Gamma_{AZh}^{\text{1PI}}(p_1^2, p_2^2, q^2)_B$$

$$= i \frac{g^3}{2} c_{\beta-\alpha} c_W C_{AZ\phi}^{SVV}(H^\pm, W^\pm, W^\pm)$$

$$+ i \frac{g_Z^3}{8} c_{\beta-\alpha} \left[c_{\beta-\alpha}^2 C_{AZ\phi}^{VSS}(Z, A, h) + s_{\beta-\alpha}^2 C_{AZ\phi}^{VSS}(Z, A, H) \right.$$

$$+ s_{\beta-\alpha}^2 C_{AZ\phi}^{VSS}(Z, G^0, h) - s_{\beta-\alpha}^2 C_{AZ\phi}^{VSS}(Z, G^0, H) - 2c_W^2 (c_W^2 - s_W^2) C_{AZ\phi}^{VSS}(W^\pm, H^\pm, H^\pm) \left. \right]$$

$$- i \frac{g_Z^3}{8} c_{\beta-\alpha} \left[(B_0 - B_1)(q^2; h, Z) + 2s_W^2 c_W^2 (B_0 - B_1)(q^2; H^\pm, W^\pm) \right.$$

$$+ (B_0 - B_1)(p_1^2; A, Z) + 2s_W^2 c_W^2 (B_0 - B_1)(p_1^2; H^\pm, W^\pm) \left. \right]$$

$$- i \frac{g_Z^3 m_Z^2}{4} s_{\beta-\alpha}^2 c_{\beta-\alpha} \left[(2C_0 + C_{11})(Z, Z, h) - (2C_0 + C_{11})(Z, Z, H) \right]$$

$$+ i \frac{g_Z^2 m_Z}{4} \left[6\lambda_{hhh} s_{\beta-\alpha} c_{\beta-\alpha} (C_0 - C_{11})(h, h, Z) + 2\lambda_{hhH} c_{\beta-\alpha}^2 (C_0 - C_{11})(h, H, Z) \right.$$

$$- 2\lambda_{hHh} s_{\beta-\alpha}^2 (C_0 - C_{11})(H, h, Z) - 2\lambda_{HHH} s_{\beta-\alpha} c_{\beta-\alpha} (C_0 - C_{11})(H, H, Z) \left. \right]$$

$$+ 2s_W^2 c_W^2 \lambda_{hH+G^-} (C_0 - C_{11})(H^\pm, G^\pm, W^\pm) \left. \right]$$

$$+ i \frac{g_Z^2 m_Z}{4} \left[2\lambda_{AAh} s_{\beta-\alpha} c_{\beta-\alpha} (C_0 - C_{11})(A, Z, h) + 2\lambda_{AAH} c_{\beta-\alpha}^2 (C_0 - C_{11})(A, Z, H) \right.$$

$$+ \lambda_{AG^0h} s_{\beta-\alpha}^2 (C_0 - C_{11})(G^0, Z, h) + \lambda_{AG^0H} s_{\beta-\alpha} c_{\beta-\alpha} (C_0 - C_{11})(G^0, Z, H) \left. \right]$$

$$- i s_W^2 c_W^2 \lambda_{AG^+H^-} c_{\beta-\alpha} (C_0 - C_{11})(H^\pm, W^\pm, G^\pm)$$

$$+ i s_W^2 c_W^2 \lambda_{AG^-H^+} c_W^2 c_{\beta-\alpha}^2 (C_0 - C_{11})(H^\pm, W^\pm, G^\pm) \left. \right]$$

$$+ i \frac{g_Z}{2} \left[-12\lambda_{AhA} \lambda_{hhh} c_{\beta-\alpha} (C_0 + C_{11})(h, h, A) + 4\lambda_{AhA} \lambda_{hhH} s_{\beta-\alpha} (C_0 + C_{11})(h, H, A) \right.$$

$$- 4\lambda_{AHA} \lambda_{hHh} c_{\beta-\alpha} (C_0 + C_{11})(H, h, A) - 4\lambda_{AHA} \lambda_{HHh} s_{\beta-\alpha} (C_0 + C_{11})(H, H, A) \left. \right]$$

$$+ 4\lambda_{AAh}^2 c_{\beta-\alpha} (C_0 + C_{11})(A, A, h) - 4\lambda_{AAH} \lambda_{hAA} s_{\beta-\alpha} (C_0 + C_{11})(A, A, H)$$

$$- 6\lambda_{AhG^0} \lambda_{hhh} s_{\beta-\alpha} (C_0 + C_{11})(h, h, G^0) - 2\lambda_{AhG^0} \lambda_{hhH} c_{\beta-\alpha} (C_0 + C_{11})(h, H, G^0)$$

$$- 2\lambda_{AHG^0} \lambda_{hHh} s_{\beta-\alpha} (C_0 + C_{11})(H, h, G^0) - 2\lambda_{AHG^0} \lambda_{HHh} c_{\beta-\alpha} (C_0 + C_{11})(H, H, G^0)$$

$$+ 2\lambda_{AAh} \lambda_{hAG^0} s_{\beta-\alpha} (C_0 + C_{11})(A, G^0, h) + \lambda_{AG^0h}^2 c_{\beta-\alpha} (C_0 + C_{11})(G^0, A, h)$$

$$\begin{aligned}
& + 2\lambda_{AAH}\lambda_{hAG^0}c_{\beta-\alpha}(C_0 + C_{11})(A, G^0, H) - \lambda_{AG^0H}\lambda_{hG^0A}s_{\beta-\alpha}(C_0 + C_{11})(G^0, A, H) \\
& + 2\lambda_{AG^0h}\lambda_{hG^0G^0}s_{\beta-\alpha}(C_0 + C_{11})(G^0, G^0, h) + 2\lambda_{AG^0H}\lambda_{hG^0G^0}c_{\beta-\alpha}(C_0 + C_{11})(G^0, G^0, H) \\
& + i(c_W^2 - s_W^2)\lambda_{AG^-H^+}\lambda_{hG^+H^-}(C_0 + C_{11})(G^\pm, H^\pm, H^\pm) \\
& - i(c_W^2 - s_W^2)\lambda_{AG^+H^-}\lambda_{hG^-H^+}(C_0 + C_{11})(G^\pm, H^\pm, H^\pm) \\
& + i(c_W^2 - s_W^2)\lambda_{AH^-G^+}\lambda_{hH^+G^-}(C_0 + C_{11})(H^\pm, G^\pm, G^\pm) \\
& - i(c_W^2 - s_W^2)\lambda_{AH^+G^-}\lambda_{hH^-G^+}(C_0 + C_{11})(H^\pm, G^\pm, G^\pm) \Big]. \tag{E.19}
\end{aligned}$$

where

$$\begin{aligned}
C_{AZ\phi}^{SVV}(X, Y, Z) = & 2B_0(p_2^2; Y, Z) + \left[-\frac{1}{2}(3p_1^2 - p_2^2 + q^2)C_{21} + (p_1^2 - q^2)C_{23} - 2C_{24} \right. \\
& \left. + \frac{1}{2}(-p_1^2 - 2p_2^2 + q^2)C_{11} + (p_1^2 - q^2)C_{12} + \frac{1}{2}(p_2^2 + 4m_X^2)C_0 \right] (p_1^2, p_2^2, q^2; X, Y, Z), \tag{E.20}
\end{aligned}$$

$$\begin{aligned}
C_{AZ\phi}^{VSS}(X, Y, Z) = & \left[(q^2 + 3p_1^2 - p_2^2)C_{21} + 2(q^2 - p_1^2)C_{23} + 4C_{24} + (3q^2 + 5p_1^2 - 3p_2^2 + m_X^2)C_{11} \right. \\
& \left. + 2(q^2 - p_1^2)C_{12} + (2q^2 + 2p_1^2 - 2p_2^2 + m_X^2)C_0 \right] (p_1^2, p_2^2, q^2; X, Y, Z). \tag{E.21}
\end{aligned}$$

The 1PI contributions to the form factor of AZH vertex are given by

$$\begin{aligned}
& (16\pi^2)\Gamma_{AZH}^{1PI}(p_1^2, p_2^2, q^2)_F \\
& = i \sum_f 8I_f N_c^f g_Z a_f \frac{m_f^2 \zeta_f \zeta_{Hff}}{v^2} \left[B_0(p_2^2; f, f) + 2m_f^2 C_0 + p_1^2 C_{11} + (q^2 - p_1^2)C_{12} \right] (f, f, f), \tag{E.22}
\end{aligned}$$

$$\begin{aligned}
& (16\pi^2)\Gamma_{AZH}^{1PI}(p_1^2, p_2^2, q^2)_B \\
& = -i \frac{g^3}{2} c_W s_{\beta-\alpha} C_{AZ\phi}^{SVV}(H^\pm, W^\pm, W^\pm) \\
& + i \frac{g_Z^3}{8} s_{\beta-\alpha} \left[-c_{\beta-\alpha}^2 C_{AZ\phi}^{VSS}(Z, A, h) - s_{\beta-\alpha}^2 C_{AZ\phi}^{VSS}(Z, A, H) \right. \\
& + c_{\beta-\alpha}^2 C_{AZ\phi}^{VSS}(Z, G^0, h) - c_{\beta-\alpha}^2 C_{AZ\phi}^{VSS}(Z, G^0, H) + 2c_W^2 (c_W^2 - s_W^2) C_{AZ\phi}^{VSS}(W^\pm, H^\pm, H^\pm) \Big] \\
& + i \frac{g_Z^3}{8} s_{\beta-\alpha} \left[(B_0 - B_1)(q^2; H, Z) + 2s_W^2 c_W^2 (B_0 - B_1)(q^2; H^\pm, W^\pm) \right. \\
& + (B_0 - B_1)(p_1^2; A, Z) + 2s_W^2 c_W^2 (B_0 - B_1)(p_1^2; H^\pm, W^\pm) \Big] \\
& - i \frac{g_Z^3 m_Z^2}{4} s_{\beta-\alpha} c_{\beta-\alpha}^2 \left[(2C_0 + C_{11})(Z, Z, h) - (2C_0 + C_{11})(Z, Z, H) \right] \\
& + i \frac{g_Z^2 m_Z}{4} \left[2\lambda_{Hhh}s_{\beta-\alpha}c_{\beta-\alpha}(C_0 - C_{11})(h, h, Z) + 2\lambda_{HhH}c_{\beta-\alpha}^2(C_0 - C_{11})(h, H, Z) \right. \\
& - 2\lambda_{HHh}s_{\beta-\alpha}^2(C_0 - C_{11})(H, h, Z) - 6\lambda_{HHH}s_{\beta-\alpha}c_{\beta-\alpha}(C_0 - C_{11})(H, H, Z) \\
& \left. + 2s_W^2 c_W^2 \lambda_{HH^+G^-}(C_0 - C_{11})(H^\pm, G^\pm, W^\pm) \right]
\end{aligned}$$

$$\begin{aligned}
& -i\frac{g_Z^2 m_Z}{4} \left[2\lambda_{AAh}s_{\beta-\alpha}^2(C_0 - C_{11})(A, Z, h) + 2\lambda_{AAH}c_{\beta-\alpha}s_{\beta-\alpha}(C_0 - C_{11})(A, Z, H) \right. \\
& - \lambda_{AG^0h}c_{\beta-\alpha}s_{\beta-\alpha}(C_0 - C_{11})(G^0, Z, h) - \lambda_{AG^0H}c_{\beta-\alpha}^2(C_0 - C_{11})(G^0, Z, H) \\
& - is_W^2c_W^2\lambda_{AG^+H^-}s_{\beta-\alpha}(C_0 - C_{11})(H^\pm, W^\pm, G^\pm) \\
& \left. + is_W^2c_W^2\lambda_{AG^-H^+}s_{\beta-\alpha}(C_0 - C_{11})(H^\pm, W^\pm, G^\pm) \right] \\
& + i\frac{g_Z}{2} \left[-4\lambda_{AhA}\lambda_{Hhh}c_{\beta-\alpha}(C_0 + C_{11})(h, h, A) + 4\lambda_{AhA}\lambda_{HhH}s_{\beta-\alpha}(C_0 + C_{11})(h, H, A) \right. \\
& - 4\lambda_{AHA}\lambda_{HHh}c_{\beta-\alpha}(C_0 + C_{11})(H, h, A) + 12\lambda_{AHA}\lambda_{HHH}s_{\beta-\alpha}(C_0 + C_{11})(H, H, A) \\
& + 4\lambda_{AAh}\lambda_{HAAC}\beta-\alpha(C_0 + C_{11})(A, A, h) - 4\lambda_{AAH}^2s_{\beta-\alpha}(C_0 + C_{11})(A, A, H) \\
& - 2\lambda_{AhG^0}\lambda_{Hhh}s_{\beta-\alpha}(C_0 + C_{11})(h, h, G^0) - 2\lambda_{AhG^0}\lambda_{HhH}c_{\beta-\alpha}(C_0 + C_{11})(h, H, G^0) \\
& - 2\lambda_{AHG^0}\lambda_{HHh}s_{\beta-\alpha}(C_0 + C_{11})(H, h, G^0) - 6\lambda_{AHG^0}\lambda_{HHH}c_{\beta-\alpha}(C_0 + C_{11})(H, H, G^0) \\
& + 2\lambda_{AAh}\lambda_{HAG^0}s_{\beta-\alpha}(C_0 + C_{11})(A, G^0, h) + \lambda_{AG^0h}\lambda_{HG^0A}c_{\beta-\alpha}(C_0 + C_{11})(G^0, A, h) \\
& + 2\lambda_{AAH}\lambda_{HAG^0}c_{\beta-\alpha}(C_0 + C_{11})(A, G^0, H) - \lambda_{AG^0H}^2s_{\beta-\alpha}(C_0 + C_{11})(G^0, A, H) \\
& + 2\lambda_{AG^0h}\lambda_{HG^0G^0}s_{\beta-\alpha}(C_0 + C_{11})(G^0, G^0, h) + 2\lambda_{AG^0H}\lambda_{HG^0G^0}c_{\beta-\alpha}(C_0 + C_{11})(G^0, G^0, H) \\
& + i(c_W^2 - s_W^2)\lambda_{AG^-H^+}\lambda_{HG^+H^-}(C_0 + C_{11})(G^\pm, H^\pm, H^\pm) \\
& - i(c_W^2 - s_W^2)\lambda_{AG^+H^-}\lambda_{HG^-H^+}(C_0 + C_{11})(G^\pm, H^\pm, H^\pm) \\
& + i(c_W^2 - s_W^2)\lambda_{AH-G^+}\lambda_{HH^+G^-}(C_0 + C_{11})(H^\pm, G^\pm, G^\pm) \\
& \left. - i(c_W^2 - s_W^2)\lambda_{AH+G^-}\lambda_{HH^-G^+}(C_0 + C_{11})(H^\pm, G^\pm, G^\pm) \right]. \tag{E.23}
\end{aligned}$$

3. AV_1V_2 vertex

The 1PI contributions to the form factor of AW^+W^- vertex are given by

$$(16\pi^2)\Gamma_{AW^+W^-}^{3,1\text{PI}}(p_1^2, p_2^2, q^2)_F = ig^2 \sum_f N_c^f \frac{2I_f m_f^2 \zeta_f}{v} \left[C_0 + C_{11} - C_{12} \right] (f, f', f) + (f \leftrightarrow f'), \tag{E.24}$$

where f' is the $SU(2)_L$ partner of f .

The 1PI contributions to the form factor of AZZ vertex are given by

$$(16\pi^2)\Gamma_{AZZ}^{3,1\text{PI}}(p_1^2, p_2^2, q^2)_F = ig_Z^2 \sum_f N_c^f \frac{16I_f m_f^2 \zeta_f}{v} \left[v_f^2 C_0 + a_f^2 (C_0 + 2C_{11} - 2C_{12}) \right] (f, f, f). \tag{E.25}$$

The 1PI contributions to the form factor of $AZ\gamma$ vertex are given by

$$(16\pi^2)\Gamma_{AZ\gamma}^{3,1\text{PI}}(p_1^2, p_2^2, q^2)_F = ieg_Z \sum_f N_c^f Q_f \frac{16I_f m_f^2 \zeta_f}{v} v_f C_0 (f, f, f). \tag{E.26}$$

The 1PI contributions to the form factor of $A\gamma\gamma$ vertex are given by

$$(16\pi^2)\Gamma_{A\gamma\gamma}^{3,1\text{PI}}(p_1^2, p_2^2, q^2)_F = ie^2 \sum_f N_c^f Q_f^2 \frac{16I_f m_f^2 \zeta_f}{v} C_0(f, f, f). \quad (\text{E.27})$$

Our results are consistent with Ref. [84].³

Appendix F: Formulae for the real photon emissions

We here give the decay rate of a massive particle with $p_0^2 = m_0^2$ into two massive particles with $p_1^2 = m_1^2$ and $p_2^2 = m_2^2$ and a photon with $q^2 = \mu^2$, where we introduce the small photon mass as an IR regulator. We need to evaluate the following phase space integrals,

$$I_{i_1, \dots, i_n}^{j_1, \dots, j_m}(m_0, m_1, m_2) = 32\pi^3 \int d\Phi_3 \frac{(\pm 2q \cdot p_{j_1}) \cdots (\pm 2q \cdot p_{j_m})}{(\pm 2q \cdot p_{i_1}) \cdots (\pm 2q \cdot p_{i_n})}, \quad (\text{F.1})$$

where $j_k, i_\ell = 0, 1, 2$ and the plus signs belong to p_1, p_2 , the minus signs to p_0 . The analytic formulae for $I_{i_1, \dots, i_n}^{j_1, \dots, j_m}(m_0, m_1, m_2)$ are listed in Ref. [91].

1. Decay rates of $A \rightarrow f\bar{f}\gamma$

The decay rate for $A \rightarrow f\bar{f}\gamma$ is given by [112]

$$\Gamma(A \rightarrow f\bar{f}\gamma) = N_c^f \frac{2\alpha_{\text{em}} Q_f^2}{16\pi^2 m_A} \left(\frac{2I_f m_f \zeta_f}{v} \right)^2 [\Omega_{11} + \Omega_{22} + \Omega_{12}], \quad (\text{F.2})$$

where the functions Ω_{ij} are given by

$$\Omega_{11} = -2I + 2m_A^2 I_1 - 4m_f^2 m_A^2 I_{11}, \quad (\text{F.3})$$

$$\Omega_{22} = -2I + 2m_A^2 I_2 - 4m_f^2 m_A^2 I_{22}, \quad (\text{F.4})$$

$$\Omega_{12} = 8I + 2(I_1^2 + I_2^2) - 6m_A^2(I_1 + I_2) + 4m_A^2(m_A^2 - 2m_f^2)I_{12}. \quad (\text{F.5})$$

These expressions can be obtained from the decay rate of $H^\pm \rightarrow f\bar{f}'\gamma$ given in Eq. (C.2) in Ref. [44] by replacing

$$c_L \rightarrow -i \frac{2I_f m_f \zeta_f}{v}, \quad c_R \rightarrow i \frac{2I_f m_f \zeta_f}{v}, \quad (\text{F.6})$$

and $H^\pm \rightarrow A, f' \rightarrow f$. The functions Ω_{ij} are defined by

$$\Omega_{ij} = \Omega_{ij}^{LL} - \Omega_{ij}^{LR}, \quad (\text{F.7})$$

where the functions Ω_{ij}^{LL} and Ω_{ij}^{LR} are given in Eqs. (C.3) to (C.14) in Ref. [44].

³ Difference in the overall sign comes from the notation of $\epsilon^{\mu\nu\rho\sigma}$. We take $\epsilon^{0123} = +1$, while $\epsilon^{0123} = -1$ in Ref. [84].

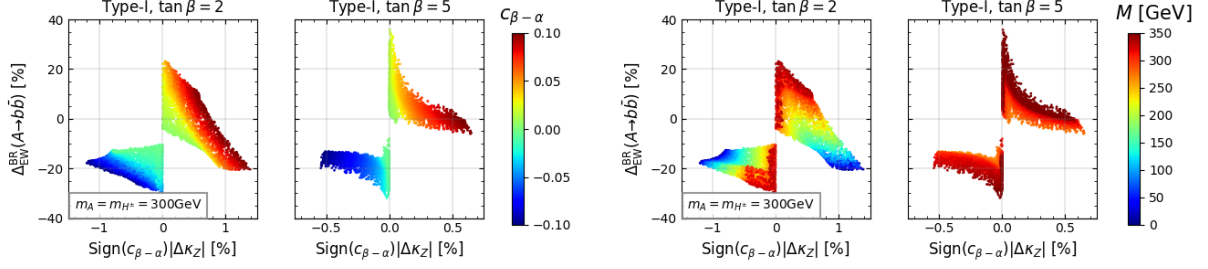


FIG. 18: NLO corrections to the decay branching ratios of the CP-odd Higgs boson in Type-I 2HDM in Scenario A. The color differences correspond to the values of $c_{\beta-\alpha}$ and $\sqrt{M^2}$, in the left and right panels, respectively.

2. Decay rate of $A \rightarrow H^\pm W^\mp \gamma$

The decay rate of $A \rightarrow H^\pm W^\mp \gamma$ is given by [112]

$$\Gamma(A \rightarrow H^\pm W^\mp \gamma) = -\frac{\alpha_{\text{em}} \sqrt{2} G_F m_W^2 m_A^3}{2\pi^2} \left\{ \lambda \left(\frac{m_{H^\pm}^2}{m_A^2}, \frac{m_W^2}{m_A^2} \right) \left[I_{22} + \frac{m_{H^\pm}^2}{m_W^2} I_{11} \right] + \left(1 + \frac{m_{H^\pm}^2 - m_A^2}{m_W^2} \right) I_{12} + \frac{1}{m_W^2} (I_1 + I_2) \right] - \frac{2}{m_A^4} [I + 2I_2^1 + I_{22}^{11}] \right\}. \quad (\text{F.8})$$

Appendix G: Size of next-to-leading order electroweak corrections for fermionic decays

In this section, we discuss the size of NLO EW corrections to the decay branching ratios $\Delta_{\text{EW}}^{\text{BR}}(A \rightarrow f\bar{f})$ in Scenario A and Scenario B.

1. Scenario A

In Fig. 18, we show the size of NLO EW corrections to the decay branching ratios $\Delta_{\text{EW}}^{\text{BR}}(A \rightarrow b\bar{b})$ in Scenario A. The color differences correspond to the values of $c_{\beta-\alpha}$ and $\sqrt{M^2}$, in the left and right panels, respectively. $\Delta_{\text{EW}}^{\text{BR}}(A \rightarrow b\bar{b})$ can reach +20% (−30%) at most when $c_{\beta-\alpha} > 0$ ($c_{\beta-\alpha} < 0$) with $\tan \beta = 2$, while it can reach +40% (−30%) at most when $c_{\beta-\alpha} > 0$ ($c_{\beta-\alpha} < 0$) with $\tan \beta = 5$. We note that $\Delta_{\text{EW}}^{\text{BR}}(A \rightarrow b\bar{b})$ takes non-zero value even if $c_{\beta-\alpha} \simeq 0$ because $\text{BR}_{\text{LO}}(A \rightarrow b\bar{b})$ does not become 100%, and $\overline{\Delta}_{\text{EW}}(A \rightarrow b\bar{b})$ and $\overline{\Delta}_{\text{EW}}^{\text{tot}}$ are not cancelled.

2. Scenario B

In Fig. 19, we show the size of $\Delta_{\text{EW}}^{\text{BR}}(A \rightarrow f\bar{f})$ as a function of Δm . The color differences

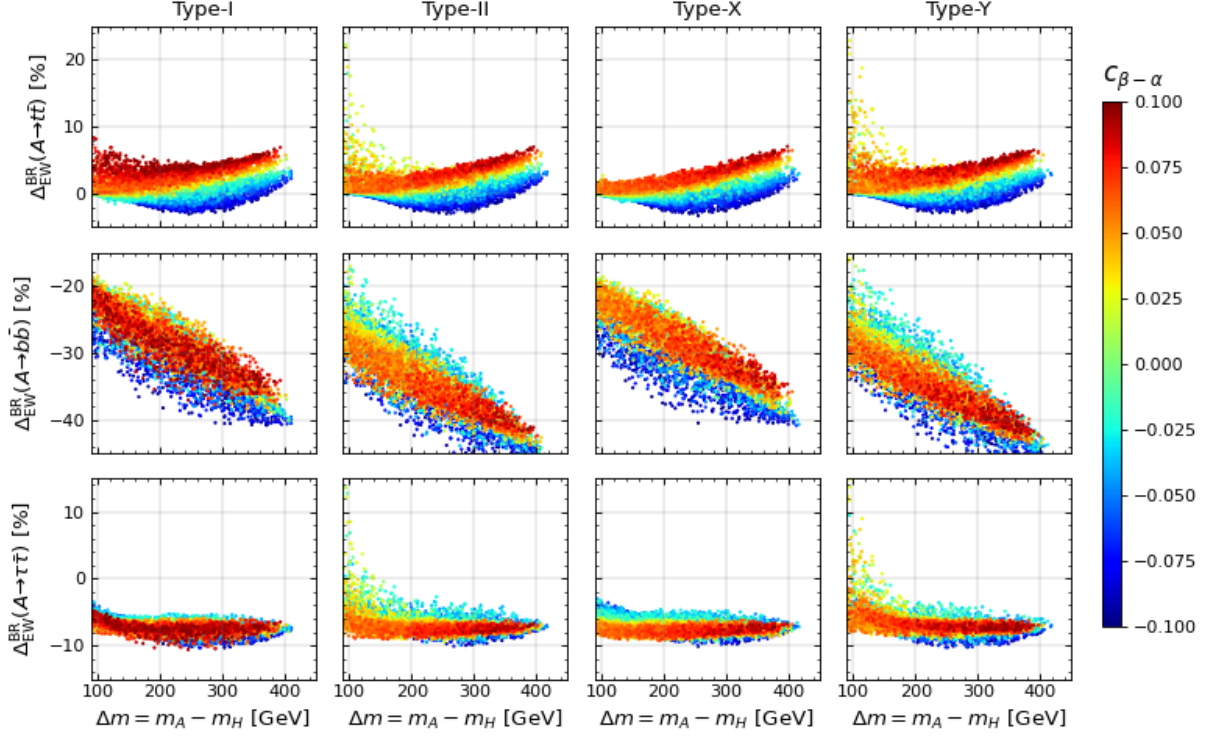


FIG. 19: NLO corrections to the decay branching ratios for the CP-odd Higgs boson as a function of $m_A - m_H$ in Scenario B. Predictions on Type-I, Type-II, Type-X and Type-Y are shown from the left to the right panels in order. The color differences correspond to the values of $c_{\beta-\alpha}$.

correspond to the values of $c_{\beta-\alpha}$. $\Delta_{\text{EW}}^{\text{BR}}(A \rightarrow t\bar{t})$ tends to be positive, while $\overline{\Delta}_{\text{EW}}(A \rightarrow t\bar{t})$ is negative in most case. This is because $\overline{\Delta}_{\text{EW}}^{\text{tot}}$ is negative, and it gives positive contribution for $\Delta_{\text{EW}}^{\text{BR}}(A \rightarrow XY)$, as shown in Eq. (V.8). On the other hand, both $\Delta_{\text{EW}}^{\text{BR}}(A \rightarrow b\bar{b})$ and $\overline{\Delta}_{\text{EW}}(A \rightarrow b\bar{b})$ are negative because the magnitude of $\overline{\Delta}_{\text{EW}}(A \rightarrow b\bar{b})$ is larger than that of $\overline{\Delta}_{\text{EW}}^{\text{tot}}$. As similar to $\Delta_{\text{EW}}^{\text{BR}}(A \rightarrow b\bar{b})$, $\Delta_{\text{EW}}^{\text{BR}}(A \rightarrow \tau\bar{\tau})$ is negative except for the parameter regions with $\Delta m \lesssim 150$ GeV and $c_{\beta-\alpha} \simeq 0$ in Type-II and Type-Y, where $\tan\beta$ enhancement in $\overline{\Delta}_{\text{EW}}^{\text{tot}}$ gives large positive contribution.

-
- [1] Georges Aad, et al. Observation of a new particle in the search for the Standard Model Higgs boson with the ATLAS detector at the LHC. *Phys. Lett. B*, Vol. 716, pp. 1–29, 2012.
 - [2] Serguei Chatrchyan, et al. Observation of a New Boson at a Mass of 125 GeV with the CMS Experiment at the LHC. *Phys. Lett. B*, Vol. 716, pp. 30–61, 2012.
 - [3] Georges Aad, et al. Combined measurements of Higgs boson production and decay using up to 80 fb⁻¹ of proton-proton collision data at $\sqrt{s} = 13$ TeV collected with the ATLAS experiment. *Phys.*

- Rev. D*, Vol. 101, No. 1, p. 012002, 2020.
- [4] Combined Higgs boson production and decay measurements with up to 137 fb⁻¹ of proton-proton collision data at $\sqrt{s} = 13$ TeV. 2020.
 - [5] John F. Gunion and Howard E. Haber. The CP conserving two Higgs doublet model: The Approach to the decoupling limit. *Phys. Rev. D*, Vol. 67, p. 075019, 2003.
 - [6] Marcela Carena, Ian Low, Nausheen R. Shah, and Carlos E. M. Wagner. Impersonating the Standard Model Higgs Boson: Alignment without Decoupling. *JHEP*, Vol. 04, p. 015, 2014.
 - [7] Masashi Aiko, Shinya Kanemura, Mariko Kikuchi, Kentarou Mawatari, Kodai Sakurai, and Kei Yagyu. Probing extended Higgs sectors by the synergy between direct searches at the LHC and precision tests at future lepton colliders. *Nucl. Phys. B*, Vol. 966, p. 115375, 2021.
 - [8] High-Luminosity Large Hadron Collider (HL-LHC): Technical Design Report V. 0.1. Vol. 4/2017, , 2017.
 - [9] The International Linear Collider Technical Design Report - Volume 2: Physics. 6 2013.
 - [10] Keisuke Fujii, et al. Physics Case for the 250 GeV Stage of the International Linear Collider. 10 2017.
 - [11] Shoji Asai, Junichi Tanaka, Yutaka Ushiroda, Mikihiro Nakao, Junping Tian, Shinya Kanemura, Shigeki Matsumoto, Satoshi Shirai, Motoi Endo, and Mitsuru Kakizaki. Report by the Committee on the Scientific Case of the ILC Operating at 250 GeV as a Higgs Factory. 10 2017.
 - [12] Keisuke Fujii, et al. Tests of the Standard Model at the International Linear Collider. 8 2019.
 - [13] M. Bicer, et al. First Look at the Physics Case of TLEP. *JHEP*, Vol. 01, p. 164, 2014.
 - [14] Muhammd Ahmad, et al. CEPC-SPPC Preliminary Conceptual Design Report. 1. Physics and Detector. 3 2015.
 - [15] Mayumi Aoki, Shinya Kanemura, Koji Tsumura, and Kei Yagyu. Models of Yukawa interaction in the two Higgs doublet model, and their collider phenomenology. *Phys. Rev. D*, Vol. 80, p. 015017, 2009.
 - [16] Shinya Kanemura, Koji Tsumura, Kei Yagyu, and Hiroshi Yokoya. Fingerprinting nonminimal Higgs sectors. *Phys. Rev. D*, Vol. 90, p. 075001, 2014.
 - [17] Shinya Kanemura, Yasuhiro Okada, Eibun Senaha, and C. P. Yuan. Higgs coupling constants as a probe of new physics. *Phys. Rev. D*, Vol. 70, p. 115002, 2004.
 - [18] Shinya Kanemura, Mariko Kikuchi, and Kei Yagyu. Radiative corrections to the Yukawa coupling constants in two Higgs doublet models. *Phys. Lett. B*, Vol. 731, pp. 27–35, 2014.
 - [19] Shinya Kanemura, Mariko Kikuchi, and Kei Yagyu. Fingerprinting the extended Higgs sector using one-loop corrected Higgs boson couplings and future precision measurements. *Nucl. Phys. B*, Vol. 896, pp. 80–137, 2015.
 - [20] Shinya Kanemura, Mariko Kikuchi, and Kei Yagyu. Radiative corrections to the Higgs boson couplings in the model with an additional real singlet scalar field. *Nucl. Phys. B*, Vol. 907, pp. 286–322, 2016.
 - [21] Shinya Kanemura, Mariko Kikuchi, and Kei Yagyu. One-loop corrections to the Higgs self-couplings in the singlet extension. *Nucl. Phys. B*, Vol. 917, pp. 154–177, 2017.
 - [22] Shinya Kanemura, Mariko Kikuchi, and Kodai Sakurai. Testing the dark matter scenario in the inert

- doublet model by future precision measurements of the Higgs boson couplings. *Phys. Rev. D*, Vol. 94, No. 11, p. 115011, 2016.
- [23] Shinya Kanemura, Mariko Kikuchi, Kodai Sakurai, and Kei Yagyu. Gauge invariant one-loop corrections to Higgs boson couplings in non-minimal Higgs models. *Phys. Rev. D*, Vol. 96, No. 3, p. 035014, 2017.
 - [24] Masashi Aiko, Shinya Kanemura, and Kentarou Mawatari. Next-to-leading-order corrections to the Higgs strahlung process from electron–positron collisions in extended Higgs models. *Eur. Phys. J. C*, Vol. 81, No. 11, p. 1000, 2021.
 - [25] A. Arhrib, M. Capdequi Peyranere, W. Hollik, and S. Penaranda. Higgs decays in the two Higgs doublet model: Large quantum effects in the decoupling regime. *Phys. Lett. B*, Vol. 579, pp. 361–370, 2004.
 - [26] A. Arhrib, R. Benbrik, J. El Falaki, and W. Hollik. Triple Higgs coupling effect on $h^0 \rightarrow b\bar{b}$ and $h^0 \rightarrow \tau^+\tau^-$ in the 2HDM. *Phys. Lett. B*, Vol. 774, pp. 195–204, 2017.
 - [27] Shinya Kanemura, Mariko Kikuchi, Kentarou Mawatari, Kodai Sakurai, and Kei Yagyu. Loop effects on the Higgs decay widths in extended Higgs models. *Phys. Lett. B*, Vol. 783, pp. 140–149, 2018.
 - [28] Shinya Kanemura, Mariko Kikuchi, Kentarou Mawatari, Kodai Sakurai, and Kei Yagyu. Full next-to-leading-order calculations of Higgs boson decay rates in models with non-minimal scalar sectors. *Nucl. Phys. B*, Vol. 949, p. 114791, 2019.
 - [29] Jiayin Gu, Honglei Li, Zhen Liu, Shufang Su, and Wei Su. Learning from Higgs Physics at Future Higgs Factories. *JHEP*, Vol. 12, p. 153, 2017.
 - [30] Ning Chen, Tao Han, Shufang Su, Wei Su, and Yongcheng Wu. Type-II 2HDM under the Precision Measurements at the Z -pole and a Higgs Factory. *JHEP*, Vol. 03, p. 023, 2019.
 - [31] Tao Han, Shuailong Li, Shufang Su, Wei Su, and Yongcheng Wu. Comparative Studies of 2HDMs under the Higgs Boson Precision Measurements. *JHEP*, Vol. 01, p. 045, 2021.
 - [32] David Lopez-Val, Joan Sola, and Nicolas Bernal. Quantum effects on Higgs-strahlung events at Linear Colliders within the general 2HDM. *Phys. Rev. D*, Vol. 81, p. 113005, 2010.
 - [33] H. Castilla-Valdez, A. Moyotl, M. A. Perez, and C. G. Honorato. Sensitivity of the decay $h \rightarrow ZZ^* \rightarrow Zl + l-$ to the Higgs self-coupling through radiative corrections. *Phys. Rev. D*, Vol. 93, No. 5, p. 055001, 2016.
 - [34] Wenhai Xie, R. Benbrik, Abdeljalil Habjia, Souad Taj, Bin Gong, and Qi-Shu Yan. Signature of 2HDM at Higgs Factories. *Phys. Rev. D*, Vol. 103, No. 9, p. 095030, 2021.
 - [35] Lukas Altenkamp, Stefan Dittmaier, and Heidi Rzehak. Renormalization schemes for the Two-Higgs-Doublet Model and applications to $h \rightarrow WW/ZZ \rightarrow 4$ fermions. *JHEP*, Vol. 09, p. 134, 2017.
 - [36] Lukas Altenkamp, Stefan Dittmaier, and Heidi Rzehak. Precision calculations for $h \rightarrow WW/ZZ \rightarrow 4$ fermions in the Two-Higgs-Doublet Model with Prophecy4f. *JHEP*, Vol. 03, p. 110, 2018.
 - [37] Lukas Altenkamp, Michele Boggia, and Stefan Dittmaier. Precision calculations for $h \rightarrow WW/ZZ \rightarrow 4$ fermions in a Singlet Extension of the Standard Model with Prophecy4f. *JHEP*, Vol. 04, p. 062, 2018.

- [38] Abdesslam Arhrib, Rachid Benbrik, Jaouad El Falaki, and Adil Jueid. Radiative corrections to the Triple Higgs Coupling in the Inert Higgs Doublet Model. *JHEP*, Vol. 12, p. 007, 2015.
- [39] Marcel Krause and Margarete Mühlleitner. Impact of Electroweak Corrections on Neutral Higgs Boson Decays in Extended Higgs Sectors. *JHEP*, Vol. 04, p. 083, 2020.
- [40] Shinya Kanemura, Mariko Kikuchi, Kodai Sakurai, and Kei Yagyu. H-COUP: a program for one-loop corrected Higgs boson couplings in non-minimal Higgs sectors. *Comput. Phys. Commun.*, Vol. 233, pp. 134–144, 2018.
- [41] Shinya Kanemura, Mariko Kikuchi, Kentarou Mawatari, Kodai Sakurai, and Kei Yagyu. H-COUP Version 2: a program for one-loop corrected Higgs boson decays in non-minimal Higgs sectors. *Comput. Phys. Commun.*, Vol. 257, p. 107512, 2020.
- [42] Marcel Krause, Margarete Mühlleitner, and Michael Spira. 2HDECAY —A program for the calculation of electroweak one-loop corrections to Higgs decays in the Two-Higgs-Doublet Model including state-of-the-art QCD corrections. *Comput. Phys. Commun.*, Vol. 246, p. 106852, 2020.
- [43] Ansgar Denner, Stefan Dittmaier, and Alexander Mück. PROPHECY4F 3.0: A Monte Carlo program for Higgs-boson decays into four-fermion final states in and beyond the Standard Model. *Comput. Phys. Commun.*, Vol. 254, p. 107336, 2020.
- [44] Masashi Aiko, Shinya Kanemura, and Kodai Sakurai. Radiative corrections to decays of charged Higgs bosons in two Higgs doublet models. *Nucl. Phys. B*, Vol. 973, p. 115581, 2021.
- [45] Shinya Kanemura, Mariko Kikuchi, and Kei Yagyu. Next-to-leading order corrections to decays of the heavier CP-even Higgs boson in the two Higgs doublet model. 3 2022.
- [46] Masashi Aiko, Shinya Kanemura, Mariko Kikuchi, Kodai Sakurai, and Kei Yagyu. in preparation.
- [47] R. Santos, A. Barroso, and L. Brucher. Top quark loop corrections to the decay $H^+ \rightarrow h^0 W^+$ in the two Higgs doublet model. *Phys. Lett. B*, Vol. 391, pp. 429–433, 1997.
- [48] Andrew G. Akeroyd, Abdesslam Arhrib, and El-Mokhtar Naimi. Yukawa coupling corrections to the decay $H^+ \rightarrow W^+ A^0$. *Eur. Phys. J. C*, Vol. 12, pp. 451–460, 2000. [Erratum: *Eur.Phys.J.C* 14, 371 (2000)].
- [49] A. G. Akeroyd, A. Arhrib, and E. Naimi. Radiative corrections to the decay $H^+ \rightarrow W^+ A^0$. *Eur. Phys. J. C*, Vol. 20, pp. 51–62, 2001.
- [50] Marcel Krause, Robin Lorenz, Margarete Muhlleitner, Rui Santos, and Hanna Ziesche. Gauge-independent Renormalization of the 2-Higgs-Doublet Model. *JHEP*, Vol. 09, p. 143, 2016.
- [51] Marcel Krause, Margarete Muhlleitner, Rui Santos, and Hanna Ziesche. Higgs-to-Higgs boson decays in a 2HDM at next-to-leading order. *Phys. Rev. D*, Vol. 95, No. 7, p. 075019, 2017.
- [52] Wei Su, Martin White, Anthony G. Williams, and Yongcheng Wu. Exploring the low $\tan \beta$ region of two Higgs doublet models at the LHC. *Eur. Phys. J. C*, Vol. 81, No. 9, p. 810, 2021.
- [53] Sheldon L. Glashow and Steven Weinberg. Natural Conservation Laws for Neutral Currents. *Phys. Rev. D*, Vol. 15, p. 1958, 1977.
- [54] E. A. Paschos. Diagonal Neutral Currents. *Phys. Rev. D*, Vol. 15, p. 1966, 1977.

- [55] Sacha Davidson and Howard E. Haber. Basis-independent methods for the two-Higgs-doublet model. *Phys. Rev. D*, Vol. 72, p. 035004, 2005. [Erratum: *Phys.Rev.D* 72, 099902 (2005)].
- [56] Shinya Kanemura, Takahiro Kubota, and Eiichi Takasugi. Lee-Quigg-Thacker bounds for Higgs boson masses in a two doublet model. *Phys. Lett. B*, Vol. 313, pp. 155–160, 1993.
- [57] Andrew G. Akeroyd, Abdesslam Arhrib, and El-Mokhtar Naimi. Note on tree level unitarity in the general two Higgs doublet model. *Phys. Lett. B*, Vol. 490, pp. 119–124, 2000.
- [58] I. F. Ginzburg and I. P. Ivanov. Tree-level unitarity constraints in the most general 2HDM. *Phys. Rev. D*, Vol. 72, p. 115010, 2005.
- [59] Shinya Kanemura and Kei Yagyu. Unitarity bound in the most general two Higgs doublet model. *Phys. Lett. B*, Vol. 751, pp. 289–296, 2015.
- [60] Nilendra G. Deshpande and Ernest Ma. Pattern of Symmetry Breaking with Two Higgs Doublets. *Phys. Rev. D*, Vol. 18, p. 2574, 1978.
- [61] K. G. Klimenko. On Necessary and Sufficient Conditions for Some Higgs Potentials to Be Bounded From Below. *Theor. Math. Phys.*, Vol. 62, pp. 58–65, 1985.
- [62] Marc Sher. Electroweak Higgs Potentials and Vacuum Stability. *Phys. Rept.*, Vol. 179, pp. 273–418, 1989.
- [63] Shuquan Nie and Marc Sher. Vacuum stability bounds in the two Higgs doublet model. *Phys. Lett. B*, Vol. 449, pp. 89–92, 1999.
- [64] Shinya Kanemura, Takashi Kasai, and Yasuhiro Okada. Mass bounds of the lightest CP even Higgs boson in the two Higgs doublet model. *Phys. Lett. B*, Vol. 471, pp. 182–190, 1999.
- [65] A. Barroso, P. M. Ferreira, I. P. Ivanov, and Rui Santos. Metastability bounds on the two Higgs doublet model. *JHEP*, Vol. 06, p. 045, 2013.
- [66] V. Branchina, F. Contino, and P. M. Ferreira. Electroweak vacuum lifetime in two Higgs doublet models. *JHEP*, Vol. 11, p. 107, 2018.
- [67] Vernon D. Barger, J. L. Hewett, and R. J. N. Phillips. New Constraints on the Charged Higgs Sector in Two Higgs Doublet Models. *Phys. Rev. D*, Vol. 41, pp. 3421–3441, 1990.
- [68] Michael E. Peskin and Tatsu Takeuchi. A New constraint on a strongly interacting Higgs sector. *Phys. Rev. Lett.*, Vol. 65, pp. 964–967, 1990.
- [69] Michael E. Peskin and Tatsu Takeuchi. Estimation of oblique electroweak corrections. *Phys. Rev. D*, Vol. 46, pp. 381–409, 1992.
- [70] Stefano Bertolini. Quantum Effects in a Two Higgs Doublet Model of the Electroweak Interactions. *Nucl. Phys. B*, Vol. 272, pp. 77–98, 1986.
- [71] W. Grimus, L. Lavoura, O. M. Ogreid, and P. Osland. The Oblique parameters in multi-Higgs-doublet models. *Nucl. Phys. B*, Vol. 801, pp. 81–96, 2008.
- [72] Shinya Kanemura, Yasuhiro Okada, Hiroyuki Taniguchi, and Koji Tsumura. Indirect bounds on heavy scalar masses of the two-Higgs-doublet model in light of recent Higgs boson searches. *Phys. Lett. B*, Vol. 704, pp. 303–307, 2011.

- [73] Johannes Haller, Andreas Hoecker, Roman Kogler, Klaus Mönig, Thomas Peiffer, and Jörg Stelzer. Update of the global electroweak fit and constraints on two-Higgs-doublet models. *Eur. Phys. J. C*, Vol. 78, No. 8, p. 675, 2018.
- [74] Mikolaj Misiak and Matthias Steinhauser. Weak radiative decays of the B meson and bounds on M_{H^\pm} in the Two-Higgs-Doublet Model. *Eur. Phys. J. C*, Vol. 77, No. 3, p. 201, 2017.
- [75] M. Misiak, Abdur Rehman, and Matthias Steinhauser. Towards $\bar{B} \rightarrow X_s \gamma$ at the NNLO in QCD without interpolation in m_c . *JHEP*, Vol. 06, p. 175, 2020.
- [76] Xiao-Dong Cheng, Ya-Dong Yang, and Xing-Bo Yuan. Revisiting $B_s \rightarrow \mu^+ \mu^-$ in the two-Higgs doublet models with Z_2 symmetry. *Eur. Phys. J. C*, Vol. 76, No. 3, p. 151, 2016.
- [77] Tetsuya Enomoto and Ryoutaro Watanabe. Flavor constraints on the Two Higgs Doublet Models of Z_2 symmetric and aligned types. *JHEP*, Vol. 05, p. 002, 2016.
- [78] M. Bohm, H. Spiesberger, and W. Hollik. On the One Loop Renormalization of the Electroweak Standard Model and Its Application to Leptonic Processes. *Fortsch. Phys.*, Vol. 34, pp. 687–751, 1986.
- [79] W. F. L. Hollik. Radiative Corrections in the Standard Model and their Role for Precision Tests of the Electroweak Theory. *Fortsch. Phys.*, Vol. 38, pp. 165–260, 1990.
- [80] Youichi Yamada. Gauge dependence of the on-shell renormalized mixing matrices. *Phys. Rev. D*, Vol. 64, p. 036008, 2001.
- [81] G. Passarino and M. J. G. Veltman. One Loop Corrections for $e^+ e^-$ Annihilation Into $\mu^+ \mu^-$ in the Weinberg Model. *Nucl. Phys. B*, Vol. 160, pp. 151–207, 1979.
- [82] T. Hahn and M. Perez-Victoria. Automatized one loop calculations in four-dimensions and D-dimensions. *Comput. Phys. Commun.*, Vol. 118, pp. 153–165, 1999.
- [83] Karina E. Williams, Heidi Rzehak, and Georg Weiglein. Higher order corrections to Higgs boson decays in the MSSM with complex parameters. *Eur. Phys. J. C*, Vol. 71, p. 1669, 2011.
- [84] John F. Gunion, Howard E. Haber, and Chung Kao. Searching for the CP odd Higgs boson of the minimal supersymmetric model at hadron supercolliders. *Phys. Rev. D*, Vol. 46, pp. 2907–2917, 1992.
- [85] J. F. Gunion and Howard E. Haber. Higgs Bosons in Supersymmetric Models. 2. Implications for Phenomenology. *Nucl. Phys. B*, Vol. 278, p. 449, 1986. [Erratum: Nucl.Phys.B 402, 569–569 (1993)].
- [86] E. Braaten and J. P. Leveille. Higgs Boson Decay and the Running Mass. *Phys. Rev. D*, Vol. 22, p. 715, 1980.
- [87] N. Sakai. Perturbative QCD Corrections to the Hadronic Decay Width of the Higgs Boson. *Phys. Rev. D*, Vol. 22, p. 2220, 1980.
- [88] Takeo Inami and Takahiro Kubota. Renormalization Group Estimate of the Hadronic Decay Width of the Higgs Boson. *Nucl. Phys. B*, Vol. 179, pp. 171–188, 1981.
- [89] Manuel Drees and Ken-ichi Hikasa. NOTE ON QCD CORRECTIONS TO HADRONIC HIGGS DECAY. *Phys. Lett. B*, Vol. 240, p. 455, 1990. [Erratum: Phys.Lett.B 262, 497 (1991)].
- [90] A. Sirlin. Radiative Corrections in the $SU(2)\text{-}L \times U(1)$ Theory: A Simple Renormalization Framework.

- Phys. Rev. D*, Vol. 22, pp. 971–981, 1980.
- [91] Ansgar Denner. Techniques for calculation of electroweak radiative corrections at the one loop level and results for W physics at LEP-200. *Fortsch. Phys.*, Vol. 41, pp. 307–420, 1993.
 - [92] S.G. Gorishnii, A.L. Kataev, S.A. Larin, and L.R. Surguladze. Corrected Three Loop QCD Correction to the Correlator of the Quark Scalar Currents and γ (Tot) ($H^0 \rightarrow$ Hadrons). *Mod. Phys. Lett. A*, Vol. 5, pp. 2703–2712, 1990.
 - [93] S. G. Gorishnii, A. L. Kataev, S. A. Larin, and L. R. Surguladze. Scheme dependence of the next to next-to-leading QCD corrections to Gamma(tot) ($H^0 \rightarrow$ hadrons) and the spurious QCD infrared fixed point. *Phys. Rev. D*, Vol. 43, pp. 1633–1640, 1991.
 - [94] K. G. Chetyrkin and A. Kwiatkowski. Second order QCD corrections to scalar and pseudoscalar Higgs decays into massive bottom quarks. *Nucl. Phys. B*, Vol. 461, pp. 3–18, 1996.
 - [95] S. A. Larin, T. van Ritbergen, and J. A. M. Vermaseren. The Large top quark mass expansion for Higgs boson decays into bottom quarks and into gluons. *Phys. Lett. B*, Vol. 362, pp. 134–140, 1995.
 - [96] Manuel Drees and Ken-ichi Hikasa. Heavy Quark Thresholds in Higgs Physics. *Phys. Rev. D*, Vol. 41, p. 1547, 1990.
 - [97] A. Djouadi and P. Gambino. QCD corrections to Higgs boson selfenergies and fermionic decay widths. *Phys. Rev. D*, Vol. 51, pp. 218–228, 1995. [Erratum: *Phys.Rev.D* 53, 4111 (1996)].
 - [98] A. Djouadi, J. Kalinowski, and M. Spira. HDECAY: A Program for Higgs boson decays in the standard model and its supersymmetric extension. *Comput. Phys. Commun.*, Vol. 108, pp. 56–74, 1998.
 - [99] M. Spira, A. Djouadi, D. Graudenz, and P. M. Zerwas. Higgs boson production at the LHC. *Nucl. Phys. B*, Vol. 453, pp. 17–82, 1995.
 - [100] Robert Harlander and Philipp Kant. Higgs production and decay: Analytic results at next-to-leading order QCD. *JHEP*, Vol. 12, p. 015, 2005.
 - [101] K. G. Chetyrkin, Bernd A. Kniehl, M. Steinhauser, and William A. Bardeen. Effective QCD interactions of CP odd Higgs bosons at three loops. *Nucl. Phys. B*, Vol. 535, pp. 3–18, 1998.
 - [102] J. M. Gerard and M. Herquet. A Twisted custodial symmetry in the two-Higgs-doublet model. *Phys. Rev. Lett.*, Vol. 98, p. 251802, 2007.
 - [103] Howard E. Haber and Deva O’Neil. Basis-independent methods for the two-Higgs-doublet model III: The CP-conserving limit, custodial symmetry, and the oblique parameters S, T, U. *Phys. Rev. D*, Vol. 83, p. 055017, 2011.
 - [104] Masashi Aiko and Shinya Kanemura. New scenario for aligned Higgs couplings originated from the twisted custodial symmetry at high energies. *JHEP*, Vol. 02, p. 046, 2021.
 - [105] Alex Pomarol and Roberto Vega. Constraints on CP violation in the Higgs sector from the rho parameter. *Nucl. Phys. B*, Vol. 413, pp. 3–15, 1994.
 - [106] Tim Barklow, Keisuke Fujii, Sunghoon Jung, Robert Karl, Jenny List, Tomohisa Ogawa, Michael E. Peskin, and Junping Tian. Improved Formalism for Precision Higgs Coupling Fits. *Phys. Rev. D*, Vol. 97, No. 5, p. 053003, 2018.

- [107] P. A. Zyla, et al. Review of Particle Physics. *PTEP*, Vol. 2020, No. 8, p. 083C01, 2020.
- [108] J  r  my Bernon, John F. Gunion, Howard E. Haber, Yun Jiang, and Sabine Kraml. Scrutinizing the alignment limit in two-Higgs-doublet models: $m_h=125$ GeV. *Phys. Rev. D*, Vol. 92, No. 7, p. 075004, 2015.
- [109] A. Djouadi, J. Kalinowski, and P. M. Zerwas. Two and three-body decay modes of SUSY Higgs particles. *Z. Phys. C*, Vol. 70, pp. 435–448, 1996.
- [110] E. Barradas, J. L. Diaz-Cruz, A. Gutierrez, and A. Rosado. Three body decays of Higgs bosons in the MSSM. *Phys. Rev. D*, Vol. 53, pp. 1678–1683, 1996.
- [111] Stephan Buehler and Claude Duhr. CHAPLIN - Complex Harmonic Polylogarithms in Fortran. *Comput. Phys. Commun.*, Vol. 185, pp. 2703–2713, 2014.
- [112] Mark D. Goodsell, Stefan Liebler, and Florian Staub. Generic calculation of two-body partial decay widths at the full one-loop level. *Eur. Phys. J. C*, Vol. 77, No. 11, p. 758, 2017.